Turbulence Modeling for CFD

Third Edition

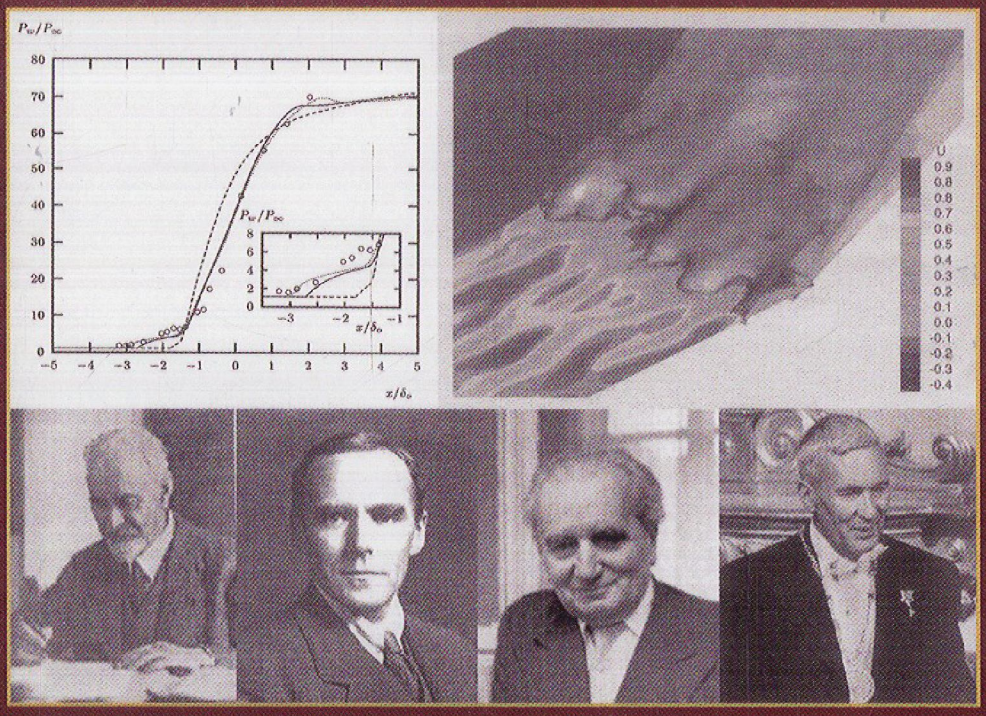

David C. Wilcox

Contents

Turbulence Modeling for CFD

Third Edition

by

David C. Wilcox

DCW Industries

Turbulence Modeling for CFD

First Printing: November, 2006

DCW Industries, Inc.
5354 Palm Drive, La Cañada, California 91011
818/790-3844 (FAX) 818/952-1272
World Wide Web: http://www.dcwindustries.com

This book was prepared with LaTeX as implemented by Personal TeX, Inc. of Mill Valley, California. It was printed and bound in the United States of America by Birmingham Press, Inc., San Diego, California.

Library of Congress Cataloging in Publication Data

Wilcox, David C.
Turbulence Modeling for CFD / David C. Wilcox—3rd edition
Includes bibliography, index and Compact Disk.
1. Turbulence–Mathematical Models.
2. Fluid Dynamics–Mathematical Models.
Catalog Card Number 2006908990

ISBN 978-1-928729-08-2 (1-928729-08-8)

Dedicated to my Wife

BARBARA

my Children

KINLEY and BOB

and my Dad

About the Author

Dr. David C. Wilcox, was born in Wilmington, Delaware. He did his undergraduate studies from 1963 to 1966 at the Massachusetts Institute of Technology, graduating with a Bachelor of Science degree in Aeronautics and Astronautics. From 1966 to 1967, he was employed by the McDonnell Douglas Aircraft Division in Long Beach, California, and began his professional career under the guidance of A. M. O. Smith. His experience with McDonnell Douglas focused on subsonic and transonic flow calculations. From 1967 to 1970, he attended the California Institute of Technology, graduating with a Ph.D. in Aeronautics. In 1970 he joined TRW Systems, Inc. in Redondo Beach, California, where he performed studies of both high- and low-speed fluid-mechanical and heat-transfer problems, such as turbulent hypersonic flow and thermal radiation from a flame. From 1972 to 1973, he was a staff scientist for Applied Theory, Inc., in Los Angeles, California. He participated in many research efforts involving numerical computation and analysis of fluid flows such as separated turbulent flow, transitional flow and hypersonic plume-body interaction.

In 1973, he founded DCW Industries, Inc., a La Cañada, California firm engaged in engineering research and book publishing, for which he is currently President. He has taught several fluid mechanics and applied mathematics courses at the University of Southern California and at the University of California, Los Angeles.

Dr. Wilcox has numerous publications on turbulence modeling, computational fluid dynamics, boundary-layer separation, boundary-layer transition, thermal radiation, and rapidly-rotating fluids. His book publications include texts entitled *Elements of Fluid Mechanics*, *Basic Fluid Mechanics* and *Perturbation Methods in the Computer Age*.

He is an Associate Fellow of the American Institute of Aeronautics and Astronautics (AIAA) and has served as an Associate Editor for the AIAA Journal.

Contents

Notation

This section includes the most commonly used notation in this book. In order to avoid departing too much from conventions normally used in literature on turbulence modeling and general fluid mechanics, a few symbols denote more than one quantity.

English Symbols

Symbol	Definition
a	Speed of sound; strain rate
a_{ijkl}	Tensor in rapid-pressure-strain term
A_n, B_n, C_n, D_n	Coefficients in tridiagonal matrix equation
A^+	Van Driest damping coefficient
A_{ij}	Slow pressure-strain tensor
b_{ij}	Dimensionless Reynolds-stress anisotropy tensor
c_f	Skin friction based on edge velocity, $\tau_w/(\frac{1}{2}\rho U_e^2)$
c_{f_∞}	Skin friction based on freestream velocity, $\tau_w/(\frac{1}{2}\rho U_\infty^2)$
c_p, c_v	Specific heat for constant pressure, volume
C	Additive constant in the law of the wall
C_κ	Kolmogorov constant
C_p	Pressure coefficient, $(P - P_\infty)/(\frac{1}{2}\rho U_\infty^2)$
C_s	Smagorinsky constant
C_{ij}	LES cross-term stress tensor
C_{ijk}	Turbulent transport tensor
C_{lim}	Stress-limiter strength
d	Distance from closest surface
D	Drag per unit body width; diameter
D_{ij}	The tensor $\tau_{im}\partial U_m/\partial x_j + \tau_{jm}\partial U_m/\partial x_i$
e	Specific internal energy
E	Total energy
$E(\kappa)$	Energy spectral density

$E(\eta)$	Dimensionless self-similar dissipation rate
E_h	Discretization error
$f(x;r)$	Longitudinal correlation function
f_β	Vortex-stretching function
$\mathbf{f}$, $\mathbf{f}_v$	Turbulence-flux vectors
$F(\eta)$	Dimensionless self-similar streamfunction
$F_{Kleb}(y;\delta)$	Klebanoff intermittency function
$\mathbf{F}$, $\mathbf{F}_v$	Mean-flow flux vectors
G	Amplitude factor in von Neumann stability analysis
$G(\mathbf{x}-\boldsymbol{\xi})$	LES filter
h	Specific enthalpy
H	Total enthalpy; channel height; shape factor, δ^*/θ
$\mathcal{H}(x)$	Heaviside step function
$\mathbf{i}$, $\mathbf{j}$, $\mathbf{k}$	Unit vectors in x, y, z directions
I	Unit (identity) matrix
II, III	Stress-tensor invariants
j	Two-dimensional ($j=0$), axisymmetric ($j=1$) index
J	Specific momentum flux (flux per unit mass)
k	Kinetic energy of turbulent fluctuations per unit mass
k_g	Geometric progression ratio
k_s	Surface roughness height
K	Distortion parameter
$K(\eta)$	Dimensionless self-similar turbulence kinetic energy
Kn	Knudsen number
ℓ	Turbulence length scale; characteristic eddy size
ℓ_{mfp}	Mean free path
ℓ_{mix}	Mixing length
ℓ_μ	von Kármán length scale
L	Characteristic length scale
L_a	Reattachment length
L_{ij}	Leonard-stress tensor
m	Molecular mass; round/radial jet index
M	Mach number
M_{ijkl}	Tensor in rapid-pressure-strain term
M_c	Convective Mach number
M_t	Turbulence Mach number, $\sqrt{2k}/a$
M_τ	Turbulence Mach number, u_τ/a_w
n	Normal distance; number density
$N(\eta)$	Dimensionless self-similar eddy viscosity
N_{CFL}	CFL number
$\mathcal{N}(u_i)$	Navier-Stokes operator
p	Instantaneous static pressure

p_{ij}	Instantaneous momentum-flux tensor
P	Mean static pressure; turbulence-energy production, $\frac{1}{2}P_{ii}$
P_{ij}	Production tensor, $\tau_{im}\partial U_j/\partial x_m + \tau_{jm}\partial U_i/\partial x_m$
P_k, P_ω, P_ϵ	Net production per unit dissipation of k, ω, ϵ
Pr_L, Pr_T	Laminar, turbulent Prandtl number
P^+	Dimensionless pressure-gradient parameter, $(\nu_w/\rho u_\tau^3)dP/dx$
q_j	Heat-flux vector
q_w	Surface heat flux
q_{L_j}, q_{T_j}	Laminar, turbulent mean heat-flux vector
Q_{ij}	LES stress tensor, $C_{ij} + R_{ij}$
q, **Q**	Dependent-variable vectors
r, θ, x	Cylindrical polar coordinates
R	Pipe radius; channel half height; perfect-gas constant
R_{ij}	SGS Reynolds stress tensor
R_{ij}(**x**,t;**r**)	Two-point velocity correlation tensor
$\mathcal{R}$	Radius of curvature
$\mathcal{R}_E(\mathbf{x};t')$	Eulerian time-correlation coefficient
$\mathcal{R}_{ij}(\mathbf{x},t;t')$	Autocorrelation tensor
R^+	Sublayer scaled radius or half height, $u_\tau R/\nu$
Re_L	Reynolds number based on length L
Re_T	Turbulence Reynolds number, $k^{1/2}\ell/\nu$
Re_τ	Sublayer scaled radius or half height, R^+
Ri_T	Turbulence Richardson number
R_y	Near-wall turbulence Reynolds number, $k^{1/2}y/\nu$
s	Arc length
s_{ij}	Instantaneous strain-rate tensor
s, **S**	Source-term vectors
S	Source term; shear rate
S_{ij}	Mean strain-rate tensor
$\mathring{S}_{ij}$	Oldroyd derivative of S_{ij}
S_e, S_k, S_u, S_w	Source terms in a similarity solution
S_B	Dimensionless surface mass-injection function
S_R	Dimensionless surface-roughness function
t	Time
t_{ij}	Instantaneous viscous stress tensor
T	Temperature; characteristic time scale
T'	Freestream turbulence intensity
u, v, w	Instantaneous velocity components in x, y, z directions
u_i	Instantaneous velocity in tensor notation
u	Instantaneous velocity in vector notation
u', v', w'	Fluctuating velocity components in x, y, z directions
u_i'	Fluctuating velocity in tensor notation

$\mathbf{u}'$	Fluctuating velocity in vector notation
$\hat{u}$, $\hat{v}$, $\hat{w}$	Relative turbulence intensity, $\sqrt{u'^2}/U_e$, $\sqrt{v'^2}/U_e$, $\sqrt{w'^2}/U_e$
$\tilde{u}$, $\tilde{v}$, $\tilde{w}$	Favre-averaged velocity components in x, y, z directions
$\tilde{u}_i$	Favre-averaged velocity in tensor notation
$\tilde{\mathbf{u}}$	Favre-averaged velocity in vector notation
u'', v'', w''	Favre fluctuating velocity components in x, y, z directions
u_i''	Favre fluctuating velocity in tensor notation
$\mathbf{u}''$	Favre fluctuating velocity; fluctuating molecular velocity
u_{rms}, v_{rms}	RMS fluctuating velocity components in x, y directions
$\overline{u_i'u_j'}$	Temporal average of fluctuating velocities
u_τ	Friction velocity, $\sqrt{\tau_w/\rho_w}$
$\hat{\mathbf{u}}$	Velocity perturbation vector
u^*	Van Driest scaled velocity
U, V, W	Mean velocity components in x, y, z directions
$\mathbf{U}$	Mean velocity in vector notation
U_e	Shear-layer edge velocity
U_i	Mean velocity in tensor notation
U_∞	Freestream velocity
U^+	Dimensionless, sublayer-scaled, velocity, U/u_τ
U_m	Maximum or centerline velocity
$\mathcal{U}(\eta)$	Dimensionless self-similar streamwise velocity
v_{mix}	Mixing velocity
v_{th}	Thermal velocity
v_w	Surface injection velocity
$\mathcal{V}(\eta)$	Dimensionless self-similar normal velocity
$W(\eta)$	Dimensionless self-similar specific dissipation rate
x, y, z	Rectangular Cartesian coordinates
x_i	Position vector in tensor notation
$\mathbf{x}$	Position vector in vector notation
y^+	Dimensionless, sublayer-scaled, distance, $u_\tau y/\nu$
y_2^+	y^+ at first grid point above surface
y_m	Inner/outer layer matching point

Greek Symbols

Symbol	Definition
α_T, σ_T, ω_T	Defect-layer similarity parameters
β_r	Bradshaw's constant
β_T	Equilibrium parameter, $(\delta^*/\tau_w)dP/dx$
γ	Specific-heat ratio, c_p/c_v
δ	Boundary-layer or shear-layer thickness

δ_{vi}	Viscous-interface layer thickness
δ'	Free shear layer spreading rate
δ^*	Displacement thickness, $\int_0^\delta \left(1 - \frac{\rho}{\rho_e}\frac{U}{U_e}\right) dy$
δ_v^*	Velocity thickness, $\int_0^\delta \left(1 - \frac{U}{U_e}\right) dy$
δ_x	Finite-difference matrix operator
δ_{ij}	Kronecker delta
Δ	LES filter width
$\Delta(x)$	Clauser thickness, $U_e\delta^*/u_\tau$
$\Delta\mathbf{q}$, $\Delta\mathbf{Q}$	Incremental change in $\mathbf{q}$, $\mathbf{Q}$
Δx, Δy	Incremental change in x, y
Δt	Timestep
ϵ	Dissipation per unit mass
ϵ_d	Dilatation dissipation
ϵ_s	Solenoidal dissipation
ϵ_{ij}	Dissipation tensor
ϵ_{ijk}	Permutation tensor
ζ	Second viscosity coefficient; enstrophy
η	Kolmogorov length scale; similarity variable
θ	Momentum thickness, $\int_0^\delta \frac{\rho}{\rho_e}\frac{U}{U_e}\left(1 - \frac{U}{U_e}\right) dy$
κ	Kármán constant; wavenumber; thermal conductivity
κ_v	Effective Kármán constant for flows with mass injection
κ_ϵ, κ_ω	Effective Kármán constants for compressible flows
λ	Taylor microscale; RNG k-ϵ model parameter
λ_{max}	Largest eigenvalue
μ	Molecular viscosity
μ_T	Eddy viscosity
μ_{T_i}	Inner-layer eddy viscosity
μ_{T_o}	Outer-layer eddy viscosity
ν	Kinematic molecular viscosity, μ/ρ
ν_T	Kinematic eddy viscosity, μ_T/ρ
ν_{T_i}	Inner-layer kinematic eddy viscosity
ν_{T_o}	Outer-layer kinematic eddy viscosity
ξ	Dimensionless streamwise distance
Π	Coles' wake-strength parameter
Π_{ij}	Pressure-strain correlation tensor
$\Pi_{ij}^{(w)}$	Wall-reflection (pressure-echo) term
ρ	Mass density
$\sigma(x)$	Nonequilibrium parameter
τ	Kolmogorov time scale; turbulence dissipation time
τ_E	Micro-time scale

τ_{ij}	Specific Reynolds stress tensor, $-\overline{u_i' u_j'}$
$\tau_{turnover}$	Eddy turnover time
τ_{xy}	Specific Reynolds shear stress, $-\overline{u'v'}$
τ_{xx}, τ_{yy}, τ_{zz}	Specific normal Reynolds stresses, $-\overline{u'^2}$, $-\overline{v'^2}$, $-\overline{w'^2}$
τ_w	Surface shear stress
υ	Kolmogorov velocity scale
χ_p, χ_ω	Dimensionless vortex-stretching parameter
ψ	Streamfunction
ψ_k, ψ_ϵ, ψ_ω	Parabolic marching scheme coefficients
ω	Specific dissipation rate; vorticity-vector magnitude
Ω_{ij}	Mean-rotation tensor

Other

Symbol	Definition
$\partial \mathbf{f}/\partial \mathbf{q}$	Turbulence flux-Jacobian matrix
$\partial \mathbf{F}/\partial \mathbf{Q}$	Mean-flow flux-Jacobian matrix
$\partial \mathbf{s}/\partial \mathbf{q}$	Source-Jacobian matrix

Subscripts

Symbol	Definition
aw	Adiabatic wall
DES	Detached Eddy Simulation
DNS	Direct Numerical Simulation
e	Boundary-layer-edge value
eq	Equilibrium value
LES	Large Eddy Simulation
o	Centerline value
sep	Separation
t	Transition
v	Viscous
w	Wall (surface) value
∞	Freestream value

Superscripts

Symbol	Definition
$+$	Sublayer-scaled value

Preface

"How do you think you would do if you tried a shock-wave/boundary-layer interaction with a stronger shock?"

The question came from one of the hardy souls who had endured the July heat of Palm Springs to attend the Open Forum session tagged on at the end of the 1973 AIAA summer meeting. Although my memory is a bit sketchy, I believe he preceded his question by identifying himself as Robert MacCormack of the NASA Ames Research Center and the conversation went like this.

"Well, this case causes the pressure to rise by a factor of about three and I have a case running now that has a pressure rise of around five," I replied. "I'll be able to tell you a week from now how things turn out." Such computations took about 40 hours of CPU time on a UNIVAC 1108 in those days.

"I was thinking of a shock that increases static pressure by a factor of seventy," MacCormack responded.

"Oh wow!" I was really intrigued. "These are first-of-a-kind computations, and I really don't know. Tackling that tough a problem would require some contract support from NASA Ames and a lot of CDC 7600 time. Perhaps we can talk about it after the session ends."

That exchange indeed led to a series of contracts from NASA Ames and helped me achieve a goal I had set for myself in high school, namely, to found my own business before my thirtieth birthday. However, while my research efforts under NASA Ames sponsorship produced useful results, I was unsuccessful in obtaining a satisfactory solution for that factor-of-seventy pressure rise case. That awaited a key improvement to the k-ω model and the arrival of the extremely-fast, and very inexpensive, personal computer that rests on my desktop today.

I mention that meeting of 33 summers ago to explain why writing the third edition of *Turbulence Modeling for CFD* has been one of the greatest joys of my life. This edition represents, for me, a mission accomplished. It's a mission I scoped out for myself three decades ago when I was fresh out of Caltech and bound for that fateful 1973 AIAA meeting. What was that mission? To develop a set of turbulence-model equations that, with an absolute minimum of complexity, would accurately compute properties of a series of roughly 100 test cases.

Over the years I have assembled a set of test cases that I deem essential for validating a turbulence model. The set includes attached boundary layers, free shear flows, backward-facing steps and shock-separated flows to mention a few, most dealing with Mach numbers from incompressible speeds to hypersonic. Over the years my list of test cases has expanded, but the core cases were established long ago. One of those cases is the Mach 11 shock-wave/boundary-layer interaction that Bob MacCormack cited at that 1973 AIAA meeting.

As time has passed, I have improved the k-ω model that I inherited from my PhD thesis adviser, Philip Saffman. With the publishing of the second edition of the book, the model was quite suitable for all but shock-separated flows and was demonstrably superior to all models of comparable complexity. As a result, the model has gained wide acceptance in the Computational Fluid Mechanics community. As an added benefit, other researchers have begun to address some of the model's shortcomings. Two key papers have appeared since I published the second edition that had a major impact on my research efforts.

The first is by Johan Kok who demonstrated that cross diffusion can be added to the model with no serious degradation of accuracy for attached boundary layers. Most important, he did it without doubling the number of closure coefficients by introducing complicated "blending functions." I had dabbled with cross diffusion in the early 1990s but abandoned it for a variety of reasons, one of which was concern about its adverse impact on boundary layers.

The second is a paper by a longtime friend, George Huang, who showed me how profound the effect of a stress limiter is, and how it could resolve the model's shortcomings for shock-separated flows at all Mach numbers. Again, I had tried it about a decade ago, achieved some success for a transonic airfoil, but never formally integrated a limiter into the model. With the formal integration of cross diffusion and a stress limiter into the k-ω model, my 100-or-so test case mission has been accomplished — with just 6 closure coefficients and no compressibility modifications!

And, oh yes, the model now does a nice job computing properties of that flow my friend Bob MacCormack asked about way back in 1973. It's taken me an awful lot longer than I could have ever predicted, but I suppose that's the nature of scientific research and — even more significantly — the erratic nature of funds available for basic research.

Of course, more research and validation needs to be done in order to arrive at a general-purpose turbulence model. None of my test cases are for three-dimensional flows, for example, and only a couple involve heat transfer. Applying any empirical model beyond the types of applications for which it has been validated is an adventure that may or may not yield satisfactory results. So, while I have now accomplished the research task I laid out for myself way back in the 1970s, I would be the first to say that we can still aim even higher. Many of today's turbulence researchers are indeed doing precisely that.

In addition to my desire to document my personal contributions to the field, the third edition of *Turbulence Modeling for CFD* has been motivated by its continuing popularity. It has been adopted for course use in universities all around the world and I have presented a short course based on the book many times in the United States and beyond since I first published it in 1993. Demand for the book continues to exceed all of my expectations, and I am very grateful to the turbulence-research and CFD communities. While new developments in the field have come far less frequently since the book first appeared, a few useful advances, such as the two noted above, have been made. I have been as diligent as possible in integrating new developments into the third edition.

The most noteworthy development in turbulence modeling since publication of the second edition has been the detached-eddy simulation (DES) concept. Consequently, I have added a major section to Chapter 8 addressing this promising technique. Other revisions the reader will find in the third edition of the text are as follows.

- I have made significant improvements to the k-ω and Stress-ω models that have been the focus of my own research, most notably with regard to the proper role of cross diffusion in such models and a stress limiter for the k-ω model. I have also revised and improved the boundary conditions for surfaces that are rough and/or have mass transfer.

- As with previous editions, the book comes with a companion Compact Disk (CD) that contains source code and documentation for several useful computer programs. In addition to the software provided with the first and second editions, the CD includes a two-dimensional/axisymmetric Navier-Stokes program and some simple grid-generation software. The CD also contains input-data files for most of the test cases used in this book to test and validate turbulence models.

- The software on the CD has been modernized and optimized for personal computers running the Microsoft Windows operating system. All programs have menu-driven input-data preparation and plotting utilities, written entirely in Visual C++, that provide a user-friendly environment.

- I have added some new homework problems to enhance the book's utility in the classroom.

Turbulence Modeling for CFD maintains its basic theme, which is description of and development tools for engineering models of turbulence. While it is currently fashionable for turbulence researchers to focus their efforts on Direct Numerical Simulation, Large Eddy Simulation, Detached Eddy Simulation, etc., these models are not yet suitable for day-to-day engineering design and analysis. As in earlier editions of *Turbulence Modeling for CFD*, Chapter 8 provides a brief

introduction with suitable references to provide the reader with a good starting point for further study. However, such methods are worthy of a complete text. Further expansion of this text's coverage of these topics would run counter to the overall theme of the book, which would dilute its quality.

This book originated from the lecture notes that I used in presenting a graduate course on turbulence modeling at the University of Southern California. While several computational fluid dynamics (CFD) texts include some information about turbulence modeling, very few texts dealing exclusively with turbulence modeling have been written. As a consequence, turbulence modeling is regarded by many CFD researchers as "black magic," lacking in rigor and physical foundation. This book has been written to show that turbulence modeling can be done in a systematic and physically-sound manner. This is not to say all turbulence modeling has been done in such a manner, for indeed many ill-conceived and ill-fated turbulence models have appeared in engineering journals. However, with judicious use of relatively simple mathematical tools, systematic construction of a well-founded turbulence model is not only possible but can be an exciting and challenging research project.

Thus, the primary goal of this book is to provide a systematic approach to developing a set of constitutive equations suitable for computation of turbulent flows. The engineer who feels no existing turbulence model is suitable for his or her needs and wishes to modify an existing model or to devise a new model will benefit from this feature of the text. A methodology is presented in Chapters 3 and 4 for devising and testing such equations. The methodology is illustrated in great detail for two-equation turbulence models. However, it is by no means limited to such models and is used again in Chapter 6 for a full stress-transport model, but with less detail.

A secondary goal of this book is to provide a rational way for deciding how complex a model is required for a given problem. The engineer who wishes to select an existing model that is sufficient for his or her needs will benefit most from this feature of the text. Chapter 3 begins with the simplest turbulence models and subsequent chapters chart a course leading to some of the most complex models that have been applied to a nontrivial turbulent-flow problem. Two things are done at each level of complexity. First, the range of applicability of the model is estimated. Second, many of the models are applied to the same flows, including comparisons with measurements, to illustrate how accuracy changes with complexity.

The methodology makes extensive use of tensor analysis, similarity solutions, singular-perturbation methods, and numerical procedures. The text assumes the user has limited prior knowledge of these mathematical concepts and provides what is needed in the main text or in the Appendices. For example, Appendix A introduces Cartesian tensor analysis to facilitate manipulation of the Navier-Stokes equation, which is done extensively in Chapter 2. Chapter 3 shows, in

detail, the way a similarity solution is generated. Similarity solutions are then obtained for the turbulent mixing layer, jet and far wake. Appendix B presents elements of singular-perturbation theory. Chapters 4, 5 and 6 use these tools to dissect model-predicted features of the turbulent boundary layer.

No book on turbulence-model equations is complete without a discussion of numerical-solution methods. Anyone who has ever tried to obtain a numerical solution to a set of turbulence-transport equations can attest to this. Often, standard numerical procedures just won't work and alternative methods must be found to obtain accurate converged solutions. Chapter 7 focuses on numerical methods and elucidates some of the commonly encountered problems such as stiffness, sharp turbulent-nonturbulent interfaces, and difficulties attending turbulence related time scales.

The concluding chapter presents a brief overview of new horizons, including direct numerical simulation (DNS), large-eddy simulation (LES), detached-eddy simulation (DES) and the interesting mathematical theory of chaos.

Since turbulence modeling is a key CFD ingredient, the text would be incomplete without companion software implementing numerical solutions to standard turbulence-model equations. The book's companion CD includes several programs with Fortran source code and detailed user's information. The programs all have similar structure and can be easily modified to include new models.

The material presented in this book is appropriate for a one-semester, first or second year graduate course, or as a reference text for a CFD course. Successful study of this material requires an understanding of viscous-flow and boundary-layer theory. Some degree of proficiency in solving partial differential equations is also needed. A working knowledge of computer programming, preferably in FORTRAN, the most common programming language in engineering, will help the reader gain maximum benefit from the software on the companion CD.

I have been blessed over the years with a series of colleagues and friends who have contributed to the quality and accuracy of the material contained in *Turbulence Modeling for CFD*. Their contributions are as follows.

Third Edition: Drs. T. Coakley and M. Olsen were extremely helpful in their review of the manuscript. Their close attention to detail and extensive knowledge of turbulence modeling made them outstanding reviewers. Drs. J. Forsythe, P. J. Roache and G. Huang provided several figures and valuable research papers.

Second Edition: Prof. P. Bradshaw reviewed the entire manuscript as I wrote it, and taught me a lot through numerous discussions, comments and suggestions that greatly improved the final draft. Prof. Bradshaw also assisted in preparation of key material in Chapters 5 and 8, adding physical insight and state-of-the-art information. One of my best graduate students, Patrick Yee, was very thorough in reviewing the second edition, including the solutions manual. Dr. C. G. Speziale also provided an excellent review.

First Edition: Prof. P. Bradshaw and Dr. C. G. Speziale reviewed the manuscript and offered a great deal of insight in the process. Dr. D. D. Knight helped me understand why I had to write this book, reviewed the entire text and assisted in its preparation by introducing me to LaTeX. My favorite Caltech mathematics teacher, Dr. D. S. Cohen, made sure I omitted the dot over every $\imath$ and crossed every z in Appendix B. Drs. F. R. Menter, C. C. Horstman and P. R. Spalart were kind enough to provide results of several of their computations in digital form. Thanks are also due for the support and help of several other friends, most notably Dr. P. J. Roache, Dr. J. A. Domaradzki and Prof. R. M. C. So.

I extend my thanks to Dr. L. G. Redekopp of USC for encouraging and supporting development of the course for which this book was originally intended. I also thank the nine students who were the first to take the course that this book was written for. Their patience was especially noteworthy, particularly in regard to typographical errors in the homework problems! That outstanding group of young engineers is D. Foley, R. T. Holbrook, N. Kale, T.-S. Leu, H. Lin, T. Magee, S. Tadepalli, P. Taniguchi and D. Hammond.

Finally, I owe a lifelong debt to my loving wife Barbara for tolerating the hectic pace first in college and then in the business world. Without her, this book would not have been possible.

David C. Wilcox

NOTE: We have taken great pains to assure the accuracy of this manuscript. However, if you find errors, please report them to DCW Industries' Home Page on the Worldwide Web at **http://dcwindustries.com**. As long as we maintain a WWW page, we will provide an updated list of known typographical errors.

Chapter 1

Introduction

This book has been described by many writers as the "how-to guide for engineers interested in computing turbulent flows." This description is consistent with the contents of the book in the following sense. While the text provides some discussion of the physics of turbulent flows, it is by no means a thorough treatise on the complexities of the phenomenon. Rather, the discussion focuses on the most significant aspects of turbulence that underlie the engineering approximations introduced over the decades to facilitate affordable numerical computations.

In other words, the book presents as much of the physics of turbulence as necessary to understand why existing modeling approximations have been made—but no more. This is true because the theme of the book is the modeling of turbulence, which begins with understanding the physics involved. However, it also involves correlation of measurements, engineering judgment, a healthy dose of mathematics and a lot of trial and error.

The field is, to some extent, a throwback to the days of Prandtl, Taylor, von Kármán and all the many other clever engineers who spent a good portion of their time devising engineering approximations and models describing complicated

Figure 1.1: *Pioneers of turbulence modeling; from left Ludwig Prandtl (1875-1953), Geoffrey Taylor (1886-1975) and Theodore von Kármán (1881-1963).*

physical flows. The best efforts in turbulence modeling have been an attempt to develop a set of constitutive equations suitable for application to general turbulent flows, and to do it in as elegant and physically sound a manner as possible. These three fluid mechanics pioneers helped establish a solid framework for several generations of engineers to work in.

Turbulence modeling is one of three key elements in Computational Fluid Dynamics (CFD). Very precise mathematical theories have evolved for the other two key elements, viz., grid generation and algorithm development. By its nature — in creating a mathematical model that approximates the physical behavior of turbulent flows — far less precision has been achieved in turbulence modeling. This is not really a surprising event since our objective has been to approximate an extremely complicated phenomenon. Two key questions we must ask at the outset are the following. What constitutes the ideal turbulence model and how complex must it be?

1.1 Definition of an Ideal Turbulence Model

Simplicity combined with physical insight seems to have been a common denominator of the work of great men like Prandtl, Taylor and von Kármán. Using their work as a gauge, **an ideal model should introduce the minimum amount of complexity while capturing the essence of the relevant physics**. This description of an ideal model serves as the keystone of this text.

1.2 How Complex Must a Turbulence Model Be?

Aside from any physical considerations, turbulence is inherently three dimensional and time dependent. Thus, an enormous amount of information is required to completely describe a turbulent flow. Fortunately, we usually require something less than a complete time history over all spatial coordinates for every flow property. Thus, for a given turbulent-flow application, we must pose the following question. Given a set of initial and/or boundary conditions, how do we predict the relevant properties of the flow? What properties of a given flow are relevant is generally dictated by the application. For the simplest applications, we may require only the skin-friction and heat-transfer coefficients. More esoteric applications may require detailed knowledge of energy spectra, turbulence fluctuation magnitudes and scales.

Certainly, we should expect the complexity of the mathematics required for a given application to increase as the amount of required flowfield detail increases. On the one hand, if all we require is skin friction for an attached flow, a simple mixing-length model (Chapter 3) may suffice. Such models are well developed

and can be implemented with very little specialized knowledge. On the other hand, if we desire a complete time history of every aspect of a turbulent flow, only a solution to the complete Navier-Stokes equation will suffice. Such a solution requires an extremely accurate numerical solver and may require use of subtle transform techniques, not to mention vast computer resources. Most engineering problems fall somewhere between these two extremes.

Thus, once the question of how much detail we need is answered, the level of complexity of the model follows, qualitatively speaking.[1] In the spirit of Prandtl, Taylor and von Kármán, the conscientious engineer will strive to use as conceptually simple an approach as possible to achieve his ends. Overkill is often accompanied by unexpected difficulties that, in CFD applications, almost always manifest themselves as numerical difficulties!

1.3 Comments on the Physics of Turbulence

Before plunging into the mathematics of turbulence, it is worthwhile to first discuss physical aspects of the phenomenon. The following discussion is not intended as a complete description of this complex topic. Rather, we focus upon a few features of interest in engineering applications, and in construction of a mathematical model. For a more complete introduction, refer to basic texts on the physics of turbulence such as those by Hinze (1975), Tennekes and Lumley (1983), Landahl and Mollo-Christensen (1992), Libby (1996) or Durbin and Pettersson Reif (2001).

1.3.1 Importance of Turbulence in Practical Situations

For "small enough" scales and "low enough" velocities, in the sense that the Reynolds number is not too large, the equations of motion for a viscous fluid have well-behaved, steady solutions. Such flows are controlled by viscous diffusion of vorticity and momentum. The motion is termed laminar and can be observed experimentally and in nature.

At larger Reynolds numbers, the fluid's inertia overcomes the viscous stresses, and the laminar motion becomes unstable. Rapid velocity and pressure fluctuations appear and the motion becomes inherently three dimensional and unsteady. When this occurs, we describe the motion as being turbulent. In the cases of fully-developed Couette flow and pipe flow, for example, laminar flow is assured only if the Reynolds number based on maximum velocity and channel height or pipe radius is less than 1500 and 2300, respectively.

[1] This is not a foolproof criterion, however. For example, a complicated model may be required to predict even the simplest properties of a very complex flow.

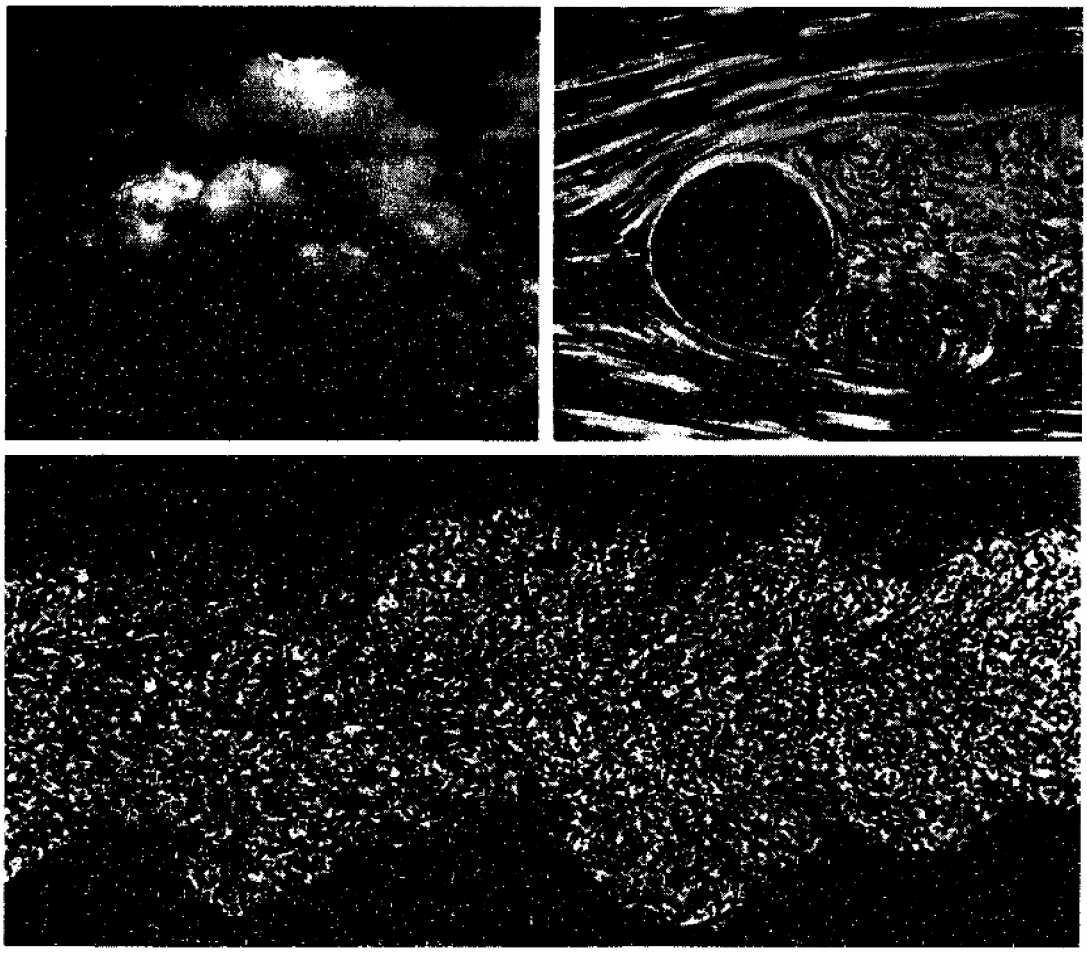

Figure 1.2: *Examples of turbulent motion. Upper left: a cumulus cloud; Upper right: flow in the wake of a cylinder; Bottom: flow in the wake of a bullet [Bottom photograph courtesy of Corrsin and Kistler (1954)].*

Virtually all flows of practical engineering interest are turbulent. Flow past vehicles such as rockets, airplanes, ships and automobiles, for example, is always turbulent. Turbulence dominates in geophysical applications such as river currents, the planetary boundary layer and the motion of clouds (Figure 1.2). Turbulence even plays a role at the breakfast table, greatly enhancing the rate at which sugar and cream mix in a cup of coffee!

Turbulence matters even in applications that normally involve purely laminar flow. For example, blood flow is laminar in the arteries and veins of a healthy human. However, the presence of turbulence generally corresponds to a health problem such as a defective heart valve.

Turbulent flow always occurs when the Reynolds number is large. For slightly viscous fluids such as water and air, "large" Reynolds number corresponds to

anything stronger than a tiny swirl, a small breeze or a puff of wind. Thus, to analyze fluid motion for general applications, we must deal with turbulence. Although vigorous research has been conducted to help discover the mysteries of turbulence, it has been called the major unsolved problem of classical physics! In the following subsections, we will explore some of the most important aspects of turbulence.

1.3.2 General Properties of Turbulence

- **Basic Definition.** In 1937, von Kármán defined turbulence in a presentation at the Twenty-Fifth Wilbur Wright Memorial Lecture entitled "Turbulence." He quoted G. I. Taylor as follows [see von Kármán (1937)]:

  > *"Turbulence is an irregular motion which in general makes its appearance in fluids, gaseous or liquid, when they flow past solid surfaces or even when neighboring streams of the same fluid flow past or over one another."*

  As the understanding of turbulence has progressed, researchers have found the term "irregular motion" to be too imprecise. Simply stated, an irregular motion is one that is typically aperiodic and that cannot be described as a straightforward function of time and space coordinates. An irregular motion might also depend strongly and sensitively upon initial conditions. The problem with the Taylor-von Kármán definition of turbulence lies in the fact that there are nonturbulent flows that can be described as irregular.

  Turbulent motion is indeed irregular in the sense that it can be described by the laws of probability. Even though instantaneous properties in a turbulent flow are extremely sensitive to initial conditions, statistical averages of the instantaneous properties are not. To provide a sharper definition of turbulence, Hinze (1975) offers the following revised definition:

  > *"Turbulent fluid motion is an irregular condition of flow in which the various quantities show a random variation with time and space coordinates, so that statistically distinct average values can be discerned."*

  To complete the definition of turbulence, Bradshaw [cf. Cebeci and Smith (1974)] adds the statement that *turbulence has a wide range of scales*. Time and length scales of turbulence are represented by frequencies and wavelengths that are revealed by a Fourier analysis of a turbulent-flow time history.

  The irregular nature of turbulence stands in contrast to laminar motion, so called historically because the fluid was imagined to flow in smooth

laminae, or layers. In describing turbulence, many researchers refer to **eddying motion**, which is a local swirling motion where the vorticity can often be very intense. **Turbulent eddies** of a wide range of sizes appear and give rise to vigorous mixing and effective turbulent stresses (a consequence of the "mixing" of momentum) that can be enormous compared to laminar values.

- **Instability and Nonlinearity.** Analysis of solutions to the Navier-Stokes equation, or more typically to its boundary-layer form, shows that turbulence develops as an instability of laminar flow. To analyze the stability of laminar flows, classical methods begin by linearizing the equations of motion. Although linear theories achieve some degree of success in predicting the onset of instabilities that ultimately lead to turbulence, the inherent nonlinearity of the Navier-Stokes equation precludes a complete analytical description of the actual transition process, let alone the fully-turbulent state. For a real (i.e., viscous) fluid, mathematically speaking, the instabilities result mainly[2] from interaction between the Navier-Stokes equation's nonlinear inertial terms and viscous terms. The interaction is very complex because it is rotational, fully three dimensional and time dependent.

  As an overview, the nonlinearity of the Navier-Stokes equation leads to interactions between fluctuations of differing wavelengths and directions. As discussed below, the wavelengths of the motion usually extend all the way from a maximum comparable to the width of the flow to a minimum fixed by viscous dissipation of energy. The main physical process that spreads the motion over a wide range of wavelengths is vortex stretching. The turbulence gains energy if the vortex elements are primarily oriented in a direction in which the mean velocity gradients can stretch them. Most importantly, wavelengths that are not too small compared to the mean-flow width interact most strongly with the mean flow. **Consequently, the larger-scale turbulent motion carries most of the energy and is mainly responsible for the enhanced diffusivity and attending stresses.** In turn, the larger eddies randomly stretch the vortex elements that comprise the smaller eddies, cascading energy to them. Energy is dissipated by viscosity in the shortest wavelengths, although the *rate* of dissipation of energy is set by the long-wavelength motion at the start of the cascade. The shortest wavelengths simply adjust accordingly.

- **Statistical Aspects.** The time-dependent nature of turbulence also contributes to its intractability. The additional complexity goes beyond the introduction of an additional dimension. Turbulence is characterized by

[2] Inviscid instabilities, such as the Kelvin-Helmholtz instability, also play a role.

random fluctuations thus mandating the use of statistical methods to analyze it. On the one hand, this aspect is not really a problem from the engineer's viewpoint. Even if we had a complete time history of a turbulent flow, we would usually integrate the flow properties of interest over time to extract **time averages**, or **mean values**. On the other hand, as we will see in Chapter 2, time-averaging operations lead to terms in the equations of motion that cannot be determined a priori.

- **Turbulence is a Continuum Phenomenon.** In principle, we know that the time-dependent, three-dimensional continuity and Navier-Stokes equations contain all of the physics of a given turbulent flow. That this is true follows from the fact that turbulence is a continuum phenomenon. As noted by Tennekes and Lumley (1983),

  > *"Even the smallest scales occurring in a turbulent flow are ordinarily far larger than any molecular length scale."*

  Nevertheless, the smallest scales of turbulence are still extremely small (we will see just how small in the next subsection). They are generally many orders of magnitude smaller than the largest scales of turbulence, the latter often being of the same order of magnitude as the dimension of the object about which the fluid is flowing. Furthermore, the ratio of smallest to largest scales decreases rapidly as the Reynolds number increases. To make an accurate numerical simulation (i.e., a fully time-dependent three-dimensional solution) of a turbulent flow, all physically relevant scales must be resolved.

  While more and more progress is being made with such simulations, computers of the early twenty-first century have insufficient memory and speed to solve any turbulent-flow problem of practical interest. To underscore the magnitude of the problem, Speziale (1985) notes that a numerical simulation of turbulent pipe flow at a Reynolds number of 500,000 would require a computer 10 million times faster than a Cray Y/MP. While standard personal computers are comparable in speed to a vintage 1985 Cray Y/MP, modern mainframe computers are still confined to simple geometries at low Reynolds numbers. This is true because, as discussed in Chapter 8, the number of numerical operations in such a computation is proportional to $Re^{9/4}$, where Re is a characteristic Reynolds number. However, the results are very useful in developing and testing approximate methods.

- **Vortex Stretching.** The strongly rotational nature of turbulence goes hand-in-hand with its three dimensionality. The vorticity in a turbulent flow is itself three dimensional so that vortex lines in the flow are non-parallel. The resulting vigorous stretching of vortex lines maintains the

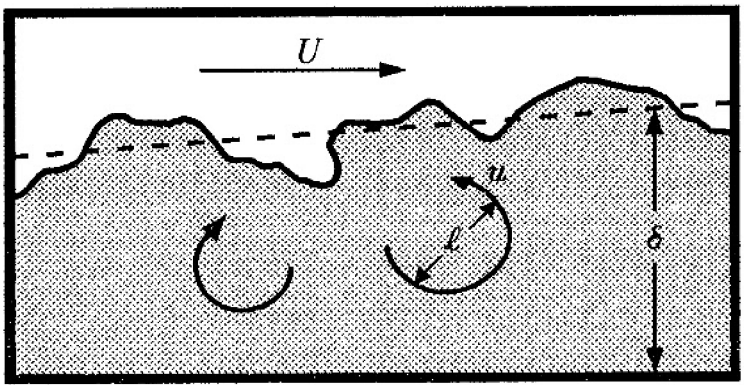

Figure 1.3: *Schematic of large eddies in a turbulent boundary layer. The flow above the boundary layer has a steady velocity U; the eddies move at randomly-fluctuating velocities of the order of a tenth of U. The largest eddy size (ℓ) is comparable to the boundary-layer thickness (δ). The interface and the flow above the boundary is quite sharp [Corrsin and Kistler (1954)].*

ever-present fluctuating vorticity in a turbulent flow. Vortex stretching is absent in two-dimensional flows so that turbulence must be three dimensional. This inherent three dimensionality means there are no satisfactory two-dimensional approximations for determining fine details of turbulent flows. This is true even when the average motion is two dimensional. The induced velocity field attending these skewed vortex lines further increases three dimensionality and, at all but very low Reynolds numbers, the vorticity is drawn out into a tangle of thin tubes or sheets. Therefore, **most of the vorticity in a turbulent flow resides in the smallest eddies**.

- **Turbulence Scales and the Cascade.** Turbulence consists of a continuous spectrum of scales ranging from largest to smallest, as opposed to a discrete set of scales. In order to visualize a turbulent flow with a spectrum of scales we often cast the discussion in terms of eddies. As noted above, a turbulent eddy can be thought of as a local swirling motion whose characteristic dimension is the local turbulence scale (Figure 1.3). Alternatively, from a more mathematical point of view, we sometimes speak in terms of wavelengths. When we think in terms of wavelength, we imagine we have done a Fourier analysis of the fluctuating flow properties.

  We observe that eddies overlap in space, large ones carrying smaller ones. Turbulence features a **cascade process** whereby, as the turbulence decays, its kinetic energy transfers from larger eddies to smaller eddies. Ultimately, the smallest eddies dissipate into heat through the action of molecular viscosity. Thus, we observe that, like any viscous flow, **turbulent flows are always dissipative**.

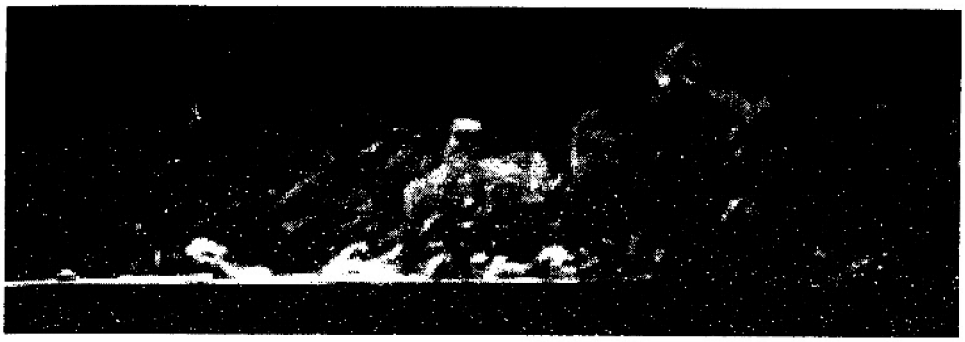

Figure 1.4: *Laser-induced fluorescence image of an incompressible turbulent boundary layer. Flow is from left to right and has been visualized with disodium fluorescein dye in water. Reynolds number based on momentum thickness is 700. [From C. Delo—Used with permission.]*

- **Large Eddies and Turbulent Mixing.** An especially striking feature of a turbulent flow is the way large eddies migrate across the flow, carrying smaller-scale disturbances with them. The arrival of these large eddies near the interface between the turbulent region and nonturbulent fluid distorts the interface into a highly convoluted shape (Figures 1.3 and 1.4). In addition to migrating across the flow, they have a lifetime so long that they persist for distances as much as 30 times the width of the flow [Bradshaw (1972)]. **Hence, the state of a turbulent flow at a given position depends upon upstream history and cannot be uniquely specified in terms of the local strain-rate tensor as in laminar flow.**

- **Enhanced Diffusivity.** Perhaps the most important feature of turbulence from an engineering point of view is its enhanced diffusivity. Turbulent diffusion greatly enhances the transfer of mass, momentum and energy. Apparent stresses in turbulent flows are often several orders of magnitude larger than in corresponding laminar flows.

In summary, turbulence is dominated by the large, energy-bearing, eddies. The large eddies are primarily responsible for the enhanced diffusivity and stresses observed in turbulent flows. Because large eddies persist for long distances, the diffusivity and stresses are dependent upon flow history, and cannot necessarily be expressed as functions of local flow properties. Also, while the small eddies ultimately dissipate turbulence energy through viscous action, the rate at which they dissipate is controlled by the rate at which they receive energy from the largest eddies. These observations must play an important role in the formulation of any rational turbulence model. As we progress through the following chapters, we will introduce more specific details of turbulence properties for common flows on an as-needed basis.

1.3.3 The Smallest Scales of Turbulence

As stated in the preceding subsection, we regard turbulence as a continuum phenomenon because the smallest scales of turbulence are much larger than any molecular length scale. We can estimate the magnitude of the smallest scales by appealing to dimensional analysis, and thereby confirm this claim. Of course, to establish the relevant dimensional quantities, we must first consider the physics of turbulence at very small length scales.

We begin by noting that the cascade process present in all turbulent flows involves a transfer of **turbulence kinetic energy** (per unit mass), k, from larger eddies to smaller eddies. Dissipation of kinetic energy to heat through the action of molecular viscosity occurs at the scale of the smallest eddies. Because small-scale motion tends to occur on a short time scale, we can reasonably assume that such motion is independent of the relatively slow dynamics of the large eddies and of the mean flow. Hence, the smaller eddies should be in a state where the rate of receiving energy from the larger eddies is very nearly equal to the rate at which the smallest eddies dissipate the energy to heat. This is one of the premises of Kolmogorov's (1941) **universal equilibrium theory**. Hence, the motion at the smallest scales should depend only upon: (a) the rate at which the larger eddies supply energy, $\epsilon = -dk/dt$, and (b) the kinematic viscosity, ν.

Having established ϵ (whose dimensions are length^2/time^3) and ν (whose dimensions are length^2/time) as the appropriate dimensional quantities, it is a simple matter to form the following length (η), time (τ) and velocity (υ) scales.

$$\eta \equiv \left(\nu^3/\epsilon\right)^{1/4}, \qquad \tau \equiv \left(\nu/\epsilon\right)^{1/2}, \qquad \upsilon \equiv \left(\nu\epsilon\right)^{1/4} \tag{1.1}$$

These are the **Kolmogorov scales** of length, time and velocity.

Figure 1.5: *Andrei Nikolaevich Kolmogorov (1903-1987), whose classic 1941 paper on the universal equilibrium theory of turbulence provided an early foundation for an understanding of turbulent fluid motion.*

To appreciate how small the Kolmogorov length scale is, for example, estimates based on properties of typical turbulent boundary layers indicate the following. For an automobile moving at 65 mph, the Kolmogorov length scale near the driver's window is about $\eta \approx 1.8 \cdot 10^{-4}$ inch. Also, on a day when the temperature is 68° F, the mean free path of air, i.e., the average distance traveled by a molecule between collisions, is $\ell_{mfp} \approx 2.5 \cdot 10^{-6}$ inch. Therefore,

$$\frac{\eta}{\ell_{mfp}} \approx 72 \tag{1.2}$$

so that the Kolmogorov length is indeed much larger than the mean free path of air, which, in turn, is typically 10 times the molecular diameter.

1.3.4 Spectral Representation and the Kolmogorov -5/3 Law

To provide further insight into the description of turbulence presented above, it is worthwhile to cast the discussion in a bit more quantitative form. Since turbulence contains a continuous spectrum of scales, it is often convenient to do our analysis in terms of the **spectral distribution** of energy. In general, a spectral representation is a Fourier decomposition into wavenumbers, κ, or, equivalently, wavelengths, $\lambda = 2\pi/\kappa$. While this text, by design, makes only modest use of Fourier-transform methods, there are a few interesting observations we can make now without considering all of the complexities involved in the mathematics of Fourier transforms. In the present context, we think of the reciprocal of κ as the eddy size.

If $E(\kappa)d\kappa$ is the turbulence kinetic energy contained between wavenumbers κ and $\kappa + d\kappa$, we can say

$$k = \int_0^\infty E(\kappa)\, d\kappa \tag{1.3}$$

Recall that k is the kinetic energy per unit mass of the fluctuating turbulent velocity. Correspondingly, the **energy spectral density** or **energy spectrum function**, $E(\kappa)$, is related to the Fourier transform of k.

Observing that turbulence is so strongly driven by the large eddies, we expect $E(\kappa)$ to be a function of a length characteristic of the larger eddies, ℓ, and the mean strain rate, S, which feeds the turbulence through direct interaction of the mean flow and the large eddies. Additionally, since turbulence is always dissipative, we expect $E(\kappa)$ to depend upon ν and ϵ. By definition, it also must depend upon κ. For high Reynolds number turbulence, dimensional analysis suggests, and measurements confirm, that k can be expressed in terms of ϵ and ℓ according to [Taylor (1935)]

$$\epsilon \sim \frac{k^{3/2}}{\ell} \quad \Longrightarrow \quad k \sim (\epsilon\ell)^{2/3} \tag{1.4}$$

Although we have not yet quantified the length scale ℓ, it is the primary length scale most turbulence models are based on. In our discussion of two-point correlations in Chapter 2, an alternative to the spectral representation of turbulence, we will find that one measure of ℓ is known as the **integral length scale**. In most turbulence-modeling analysis, we assume there is a wide separation of scales, which means we implicitly assume ℓ is very large compared to the Kolmogorov length scale, viz.,

$$\ell \gg \eta \tag{1.5}$$

Substituting the estimate of ϵ from Equation (1.4) into the Kolmogorov length scale, we find

$$\frac{\ell}{\eta} = \frac{\ell}{(\nu^3/\epsilon)^{1/4}} \sim \frac{\ell\left(k^{3/2}/\ell\right)^{1/4}}{\nu^{3/4}} \sim Re_T^{3/4} \qquad \text{where} \qquad Re_T \equiv \frac{k^{1/2}\ell}{\nu} \tag{1.6}$$

The quantity Re_T is the **turbulence Reynolds number**. It is based on the velocity characteristic of the turbulent motions as represented by the square root of k, the turbulence length scale, ℓ, and the kinematic viscosity of the fluid, ν. Thus, the condition $\ell \gg \eta$ holds provided we have high Reynolds number turbulence in the sense that

$$Re_T \gg 1 \tag{1.7}$$

The existence of a wide separation of scales is a central assumption Kolmogorov made as part of his universal equilibrium theory. That is, he hypothesized that for very large Reynolds number, there is a range of eddy sizes between the largest and smallest for which the cascade process is independent of the statistics of the energy-containing eddies (so that S and ℓ can be ignored) and of the direct effects of molecular viscosity (so that ν can be ignored). The idea is that a range of wavenumbers exists in which the energy transferred by inertial effects dominates, wherefore $E(\kappa)$ depends only upon ϵ and κ. On dimensional grounds, he thus concluded that

$$E(\kappa) = C_K \epsilon^{2/3} \kappa^{-5/3}, \qquad \frac{1}{\ell} \ll \kappa \ll \frac{1}{\eta} \tag{1.8}$$

where C_K is the **Kolmogorov constant**. Because inertial transfer of energy dominates, Kolmogorov identified this range of wavenumbers as the **inertial subrange**. The existence of the inertial subrange has been verified by many experiments and numerical simulations, although many years passed before definitive data were available to confirm its existence. Figure 1.6 shows a typical energy spectrum for a turbulent flow.

While Equation (1.8) is indeed consistent with measurements, it is not the only form that can be deduced from dimensional analysis. Unfortunately, this

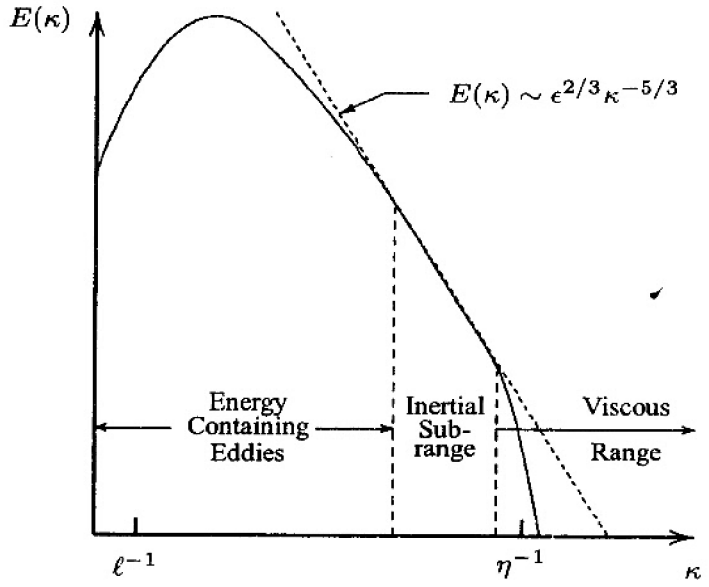

Figure 1.6: *Energy spectrum for a turbulent flow—log-log scales.*

is one of the shortcomings of dimensional analysis, i.e., the results we obtain are rarely unique. For example, lacking Kolmogorov's physical intuition, some researchers would retain ν as a dimensional quantity upon which $E(\kappa)$ depends as well as ϵ and κ. Then, a perfectly valid alternative to Equation (1.8) is

$$E(\kappa) = \epsilon^{1/4}\nu^{5/4} f(\kappa\eta), \qquad \eta = (\nu^3/\epsilon)^{1/4} \tag{1.9}$$

where $f(\kappa\eta)$ is an undetermined function. This form reveals nothing regarding the variation of $E(\kappa)$ with κ, which is a straightforward illustration of how dimensional analysis, although helpful, is insufficient to deduce physical laws.

Afzal and Narasimha (1976) use the more-powerful concepts from perturbation theory (Appendix B) to remove this ambiguity and determine the asymptotic variation of the function f in the inertial subrange. In their analysis, they assume that for small scales, corresponding to large wavenumbers, the energy spectrum function is given by Equation (1.9). This represents the *inner solution.*

Afzal and Narasimha also assume that viscous effects are unimportant for the largest eddies, and that if the only relevant scales are k and ℓ, the energy spectrum function is given by

$$E(\kappa) = k\ell g(\kappa\ell) \tag{1.10}$$

where k is the turbulence kinetic energy, ℓ is the large-eddy length scale discussed above, and $g(\kappa\ell)$ is a second undetermined function. Although we omit the details here for the sake of brevity, we can exclude explicit dependence of $E(\kappa)$ on strain rate, S, since it is proportional to $k^{1/2}/\ell$ for high Reynolds number boundary layers. This represents the *outer solution.*

Finally, they *match* the two solutions, which means they insist that the inner and outer solutions are identical when $\kappa\eta$ is small and $\kappa\ell$ is large, i.e.,

$$\epsilon^{1/4}\nu^{5/4}f(\kappa\eta) = k\ell g(\kappa\ell) \qquad \text{for} \qquad \kappa\eta \ll 1 \quad \text{and} \quad \kappa\ell \gg 1 \tag{1.11}$$

In words, this matching operation assumes that

> *"Between the viscous and the energetic scales in any turbulent flow exists an overlap domain over which the solutions [characterizing] the flow in the two corresponding limits must match as Reynolds number tends to infinity."*

The qualification regarding Reynolds number means it must be large enough to permit a wide separation of scales so that $\ell \gg \eta$. To complete the matching operation, Afzal and Narasimha proceed as follows. In the spirit of singular-perturbation theory, the matching operation presumes that the *functional forms* of the inner and outer solutions are the same in the overlap region. This is a much stronger condition than requiring the two solutions to have the same value at a given point. Hence, if their functional forms are the same, so are their first derivatives. Differentiating both sides of Equation (1.11) with respect to κ gives

$$\eta\epsilon^{1/4}\nu^{5/4}f'(\kappa\eta) = k\ell^2 g'(\kappa\ell) \qquad \text{for} \qquad \kappa\eta \ll 1 \quad \text{and} \quad \kappa\ell \gg 1 \tag{1.12}$$

Then, noting that the Kolmogorov length scale is $\eta = \nu^{3/4}\epsilon^{-1/4}$ while Equation (1.4) tells us $k = \epsilon^{2/3}\ell^{2/3}$, we can rewrite Equation (1.12) as

$$\nu^2 f'(\kappa\eta) = \epsilon^{2/3}\ell^{8/3}g'(\kappa\ell) \qquad \text{for} \qquad \kappa\eta \ll 1 \quad \text{and} \quad \kappa\ell \gg 1 \tag{1.13}$$

Finally, multiplying through by $\kappa^{8/3}\epsilon^{-2/3}$ and using the fact that $\nu^2\epsilon^{-2/3} = \eta^{8/3}$, we arrive at the following equation.

$$(\kappa\eta)^{8/3}f'(\kappa\eta) = (\kappa\ell)^{8/3}g'(\kappa\ell) \qquad \text{for} \qquad \kappa\eta \ll 1 \quad \text{and} \quad \kappa\ell \gg 1 \tag{1.14}$$

If there is a wide separation of scales, we can regard $\kappa\eta$ and $\kappa\ell$ as separate independent variables. Thus, Equation (1.14) says that a function of one independent variable, $\kappa\eta$, is equal to a function of a different independent variable, $\kappa\ell$. This can be true only if both functions tend to a constant value in the indicated limits. Thus, in the Afzal-Narasimha overlap domain, which is the inertial subrange,

$$(\kappa\eta)^{8/3}f'(\kappa\eta) = \text{constant} \quad \Longrightarrow \quad f(\kappa\eta) = C_\kappa(\kappa\eta)^{-5/3} \tag{1.15}$$

where C_κ is a constant. Combining Equations (1.9) and (1.15), we again arrive at the Kolmogorov inertial-subrange relation, viz.,

$$E(\kappa) = C_\kappa\epsilon^{2/3}\kappa^{-5/3} \tag{1.16}$$

which is identical to Equation (1.8).

Although the Kolmogorov $-5/3$ law is of minimal use in conventional turbulence models, it is of central importance in work on Direct Numerical Simulation (DNS), Large Eddy Simulation (LES), and Detached Eddy Simulation (DES), which we discuss in Chapter 8. The Kolmogorov $-5/3$ law is so well established that, as noted by Rogallo and Moin (1984), theoretical or numerical predictions are regarded with skepticism if they fail to reproduce it. Its standing is as important as the law of the wall, which we discuss in the next subsection.

1.3.5 The Law of the Wall

The **law of the wall** is one of the most famous empirically-determined relationships in turbulent flows near solid boundaries. Measurements show that, for both internal and external flows, the streamwise velocity in the flow near the wall varies logarithmically with distance from the surface. This behavior is known as the law of the wall. In this section, we use both dimensional analysis and matching arguments to infer this logarithmic variation.

Observation of high Reynolds number turbulent boundary layers reveals a useful, approximate description of the near-surface turbulence statistics. We find that effects of the fluid's inertia and the pressure gradient are small near the surface. Consequently, the statistics of the flow near the surface in a turbulent boundary layer are established by two primary mechanisms. The first is the rate at which momentum is transferred to the surface, per unit area per unit time, which is equal to the local shear stress, τ. The second is molecular diffusion of momentum, which plays an important role very close to the surface. Observations also indicate that the details of the eddies farther from the surface are of little importance to the near-wall flow statistics.

The validity of this approximate description improves with decreasing y/δ, where δ is the boundary-layer thickness. This is true because the ratio of typical eddy size far from the surface to eddy size close to the surface increases as y/δ decreases. In other words, since δ increases with Reynolds number, we find a wide separation of scales at high Reynolds numbers. The astute reader will note interesting parallels between this description of the turbulent boundary layer and the general description of turbulence presented in Subsection 1.3.2. Note, however, that the analogy is mathematical rather than physical. This analogy is discussed, for example, by Mellor (1972) and by Afzal and Narasimha (1976).

Although τ varies near the surface, the variation with distance from the surface, y, is fairly slow. Hence, for the dimensional-analysis arguments to follow, we can use the surface shear stress, τ_w, in place of the local shear stress. Also, we denote the molecular viscosity of the fluid by μ. Since turbulence behaves the same in gases as in liquids, it is reasonable to begin with τ_w/ρ and kinematic viscosity, $\nu = \mu/\rho$, as our primary dimensional quantities, effectively eliminating fluid density, ρ, as a primary dimensional quantity.

Since the dimensions of the quantity τ_w/ρ are length^2/time^2, while those of ν are length^2/time, clearly we can derive a velocity scale, u_τ, defined by

$$u_\tau \equiv \sqrt{\frac{\tau_w}{\rho}} \tag{1.17}$$

and a length scale, ν/u_τ. The quantity u_τ is known as the **friction velocity**, and is a velocity scale representative of velocities close to a solid boundary. If we now postulate that the mean velocity gradient, $\partial U/\partial y$, can be correlated as a function of u_τ, ν/u_τ and y, dimensional analysis yields

$$\frac{\partial U}{\partial y} = \frac{u_\tau}{y} F\left(u_\tau y/\nu\right) \tag{1.18}$$

where $F(u_\tau y/\nu)$ is presumed to be a universal function. Examination of experimental data for a wide range of boundary layers [see, for example, Coles and Hirst (1969)], indicates that, as a good leading-order approximation,

$$F\left(u_\tau y/\nu\right) \to \frac{1}{\kappa} \qquad \text{as} \qquad u_\tau y/\nu \to \infty \tag{1.19}$$

where κ is **Kármán's constant**. The function $F(u_\tau y/\nu)$ approaching a constant value is consistent with the notion that viscous effects cease to matter far from the surface, i.e., if it varies with $u_\tau y/\nu$ it would thus depend upon ν. Integrating over y, we arrive at the famous law of the wall, viz.,

$$\frac{U}{u_\tau} = \frac{1}{\kappa} \ell n \frac{u_\tau y}{\nu} + C \tag{1.20}$$

where C is a dimensionless integration constant. Correlation of measurements indicate $C \approx 5.0$ for smooth surfaces and $\kappa \approx 0.41$ for smooth and rough surfaces [see Kline et al. (1969)].

Figure 1.7 shows a typical velocity profile for a turbulent boundary layer. The graph displays the dimensionless velocity, u^+, and distance, y^+, defined as:

$$u^+ \equiv \frac{U}{u_\tau} \quad \text{and} \quad y^+ \equiv \frac{u_\tau y}{\nu} \tag{1.21}$$

The velocity profile matches the law of the wall for values of y^+ in excess of about 30. As Reynolds number increases, the maximum value of y^+ at which the law of the wall closely matches the actual velocity increases.

Observe that three distinct regions are discernible, viz., the **viscous sublayer**, the **log layer** and the **defect layer**. By definition, the log layer is the portion of the boundary layer where the sublayer and defect layer merge and the law of the wall accurately represents the velocity. It is not a distinct layer. Rather, it is

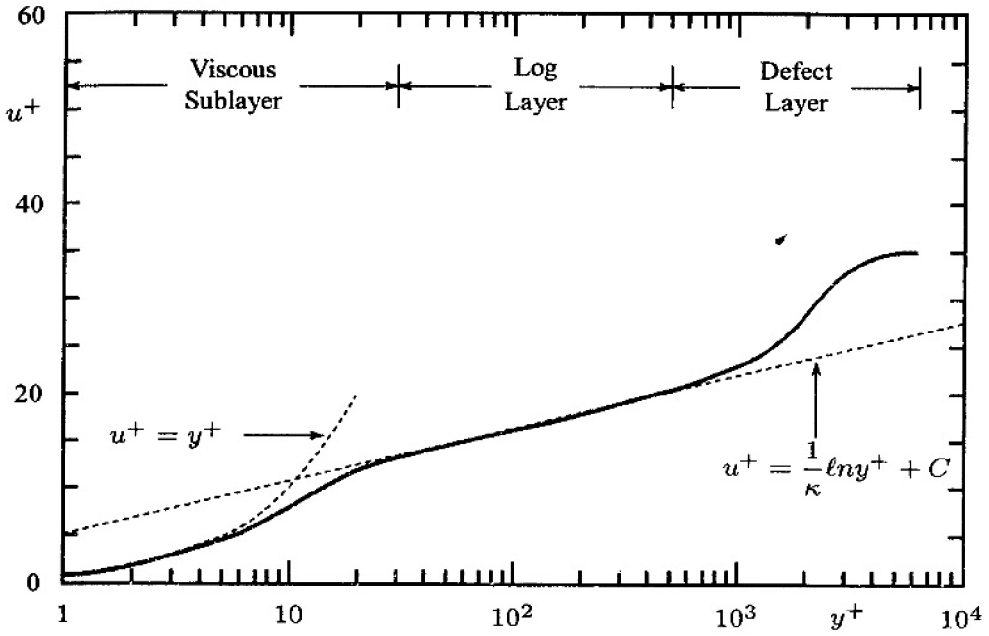

Figure 1.7: *Typical velocity profile for a turbulent boundary layer.*

an overlap region between the inner and outer parts of the boundary layer. As we will see in the following discussion, originally presented by Millikan (1938), it is an overlap domain similar to that of the Afzal-Narasimha analysis of the preceding subsection.

Assuming the velocity in the viscous sublayer should depend only upon u_τ, ν and y, we expect to have a relationship of the form

$$U = u_\tau f\left(y^+\right) \tag{1.22}$$

where $f(y^+)$ is a dimensionless function. This general functional form is often referred to as the **law of the wall**, and Equation (1.20) is simply a more explicit form. By contrast, in the defect layer, numerous experimenters including Darcy, von Kármán and Clauser found that velocity data correlate reasonably well with the so-called **velocity-defect law** or **Clauser defect law**:

$$U = U_e - u_\tau g(\eta), \qquad \eta \equiv \frac{y}{\Delta} \tag{1.23}$$

where U_e is the velocity at the boundary-layer edge and $g(\eta)$ is another dimensionless function. The quantity Δ is a thickness characteristic of the outer portion of the boundary layer.

Hence, we have an inner length scale ν/u_τ and an outer length scale Δ. Millikan's postulate is that if a wide separation of scales exists in the sense that

$$\frac{\nu}{u_\tau} \ll \Delta \tag{1.24}$$

then an overlap domain exists such that

$$u_\tau f\left(y^+\right) = U_e - u_\tau g(\eta) \qquad \text{for} \qquad y^+ \gg 1 \ \text{ and } \ \eta \ll 1 \tag{1.25}$$

We can complete the matching without explicit knowledge of the functions f and g by differentiating Equation (1.25) with respect to y. Hence,

$$\frac{u_\tau^2}{\nu} f'\left(y^+\right) = -\frac{u_\tau}{\Delta} g'(\eta) \qquad \text{for} \qquad y^+ \gg 1 \ \text{ and } \ \eta \ll 1 \tag{1.26}$$

Then, multiplying through by y/u_τ, we find

$$y^+ f'\left(y^+\right) = -\eta g'(\eta) \qquad \text{for} \qquad y^+ \gg 1 \ \text{ and } \ \eta \ll 1 \tag{1.27}$$

Thus, since a wide separation of scales means we can regard y^+ and η as independent variables, clearly the only way a function of y^+ can be equal to a function of η is for both to be equal to a constant. Therefore,

$$y^+ f'\left(y^+\right) = \text{constant} = \frac{1}{\kappa} \quad \Longrightarrow \quad f(y^+) = \frac{1}{\kappa} \ell n y^+ + C \tag{1.28}$$

which, when combined with Equation (1.22), yields Equation (1.20).

As noted earlier, the value of C for a perfectly-smooth surface is $C \approx 5.0$. For surfaces with roughness elements of average height k_s, the law of the wall still holds, although C is a function of k_s. Figure 1.8 illustrates how C varies as a function of the dimensionless roughness height given by

$$k_s^+ \equiv \frac{u_\tau k_s}{\nu} \tag{1.29}$$

As shown, as k_s increases, the value of C decreases. For large roughness height, measurements of Nikuradse [Schlichting-Gersten (1999)] show that

$$C \to 8.0 - \frac{1}{\kappa} \ell n k_s^+, \qquad k_s^+ \gg 1 \tag{1.30}$$

Substituting this value of C into the law of the wall as represented in Equation (1.20) yields:

$$\frac{U}{u_\tau} = \frac{1}{\kappa} \ell n \left(\frac{y}{k_s}\right) + 8.0 \qquad \text{(completely-rough wall)} \tag{1.31}$$

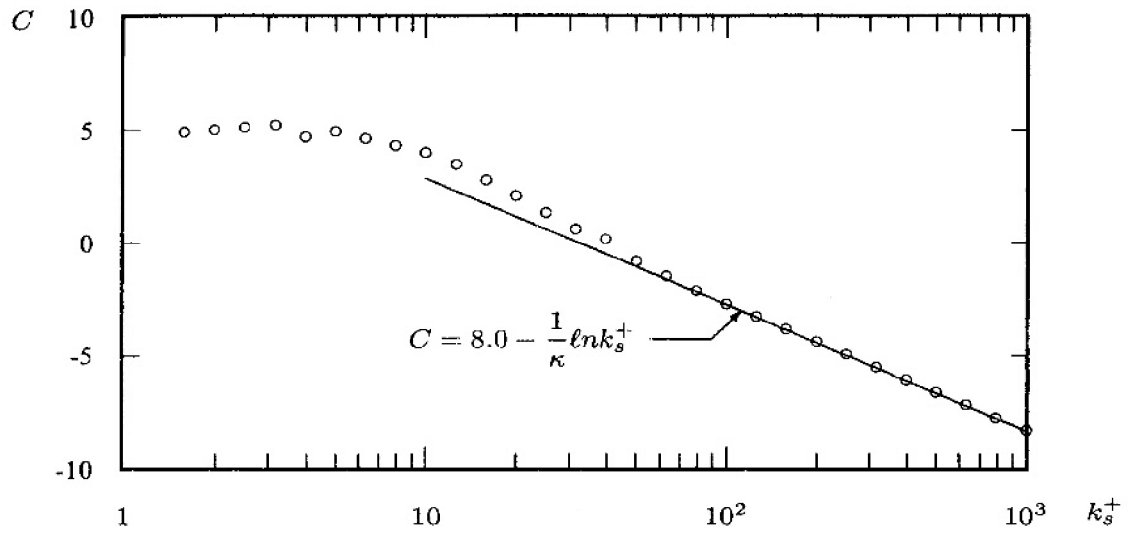

Figure 1.8: *Constant in the law of the wall, C, as a function of surface roughness; o based on measurements of Nikuradse [Schlichting-Gersten (1999)].*

The absence of viscosity in this equation is consistent with the notion that the surface "shear stress" is due to pressure drag on the roughness elements.

The defect layer lies between the log layer and the edge of the boundary layer. The velocity asymptotes to the law of the wall as $y/\delta \rightarrow 0$, and makes a noticeable departure from logarithmic behavior approaching the freestream. Again, from correlation of measurements, the velocity behaves as

$$U^+ = \frac{1}{\kappa}\ell n y^+ + C + \frac{2\Pi}{\kappa}\sin^2\left(\frac{\pi}{2}\frac{y}{\delta}\right) \tag{1.32}$$

where Π is **Coles' wake-strength parameter** [Coles and Hirst (1969)] and δ is boundary-layer thickness. It varies with pressure gradient, and for constant pressure, correlation of measurements suggests $\Pi \approx 0.6$. Equation (1.32) is often referred to as the composite law of the wall and **law of the wake** profile.

As demonstrated by Clauser (1956) experimentally and justified with perturbation methods by others analytically [see, for example, Kevorkian and Cole (1981), Van Dyke (1975) or Wilcox (1995a)], the velocity in the defect layer varies in a self-similar manner provided the **equilibrium parameter** defined by

$$\beta_T \equiv \frac{\delta^*}{\tau_w}\frac{dP}{dx} \tag{1.33}$$

is constant. The quantities δ^* and P in Equation (1.33) are displacement thickness and mean pressure, respectively. As demonstrated by Wilcox (1993b), even when β_T is not constant, if it is not changing too rapidly, the value for Π is close

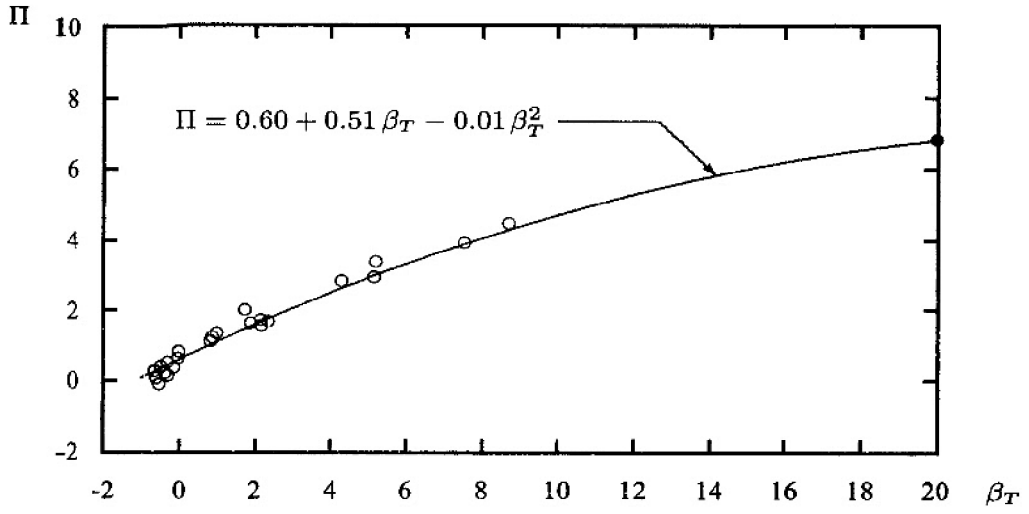

Figure 1.9: *Coles' wake-strength parameter,* Π*, as a function of pressure gradient;* ○ *from data of Coles and Hirst (1969);* • *Skare and Krogstad (1994).*

to the value corresponding to the local value of β_T. Figure 1.9 shows how Π varies with pressure gradient for the so-called **equilibrium turbulent boundary layer**, i.e., a boundary layer for which β_T is constant.

1.3.6 Power Laws

Often, as an approximation, turbulent boundary-layer profiles are represented by a **power-law** relationship. That is, we sometimes say

$$\frac{U}{U_e} = \left(\frac{y}{\delta}\right)^{1/n} \tag{1.34}$$

where n is typically an integer between 6 and 8. A value of $n = 7$, first suggested by Prandtl [Schlichting-Gersten (1999)], yields a good approximation at high Reynolds number for the flat-plate boundary layer. Figure 1.10 compares a 1/7 power-law profile with measurements. The agreement between measured values for a plate-length Reynolds number of $Re_x = 1.09 \cdot 10^7$ and the approximate profile is surprisingly good with differences everywhere less than 3%.

Recently, Barenblatt and others [see, for example, Barenblatt (1991), George, Knecht and Castillo (1992), Barenblatt (1993) and Barenblatt, Chorin and Prostokishin (1997)] have challenged the validity of the law of the wall. Their contention is that a power-law variation of the velocity in the inner layer better correlates pipe-flow measurements and represents a more realistic description of the turbulence in a boundary layer.

The critical assumption that Barenblatt et al. challenge is the existence of a wide separation of scales, i.e., large $\delta/(\nu/u_\tau)$. They maintain that the turbulence

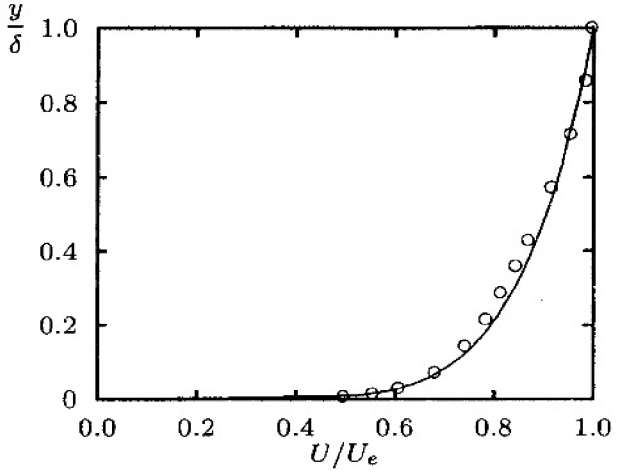

Figure 1.10: *Power-law velocity profile;* — $U/U_e = (y/\delta)^{1/7}$; ∘ *Wieghardt data at* $Re_x = 1.09 \cdot 10^7$ *[Coles and Hirst (1969)].*

in the overlap region is Reynolds-number dependent. If this is true, the law of the wall and defect-law Equations (1.22) and (1.23), respectively, must be replaced by

$$U = u_\tau \tilde{f}\left(y^+, Re\right) \qquad \text{and} \qquad U = U_e - u_o \tilde{g}(\eta, Re) \tag{1.35}$$

where Re is an appropriate Reynolds number, $\tilde{f}$ and $\tilde{g}$ are universal functions, and u_o is a velocity scale that is not necessarily equal to u_τ. Equivalently, the Barenblatt et al. hypothesis replaces Equation (1.18) by

$$\frac{\partial U}{\partial y} = \frac{u_\tau}{y} \Phi\left(y^+, Re\right) \tag{1.36}$$

where the universal function $\Phi(y^+, Re)$ appears in place of $F(y^+)$.

In the Millikan argument, the assumption of a wide separation of scales implies that the boundary layer possesses self-similar solutions both in the defect layer and the sublayer, in the sense that a similarity variable, e.g., $y^+ = u_\tau y/\nu$ and $\eta = y/\Delta$, exists in each region. The assumption that we can regard y^+ and η as distinct independent variables in the overlap region is described as a condition of **complete similarity**. By contrast, the Barenblatt hypothesis corresponds to **incomplete similarity**. Barenblatt (1979) discusses the distinction between complete and incomplete similarity in detail.

Under the assumption of incomplete similarity, there is no a priori reason for the function $\Phi(y^+, Re)$ to approach a constant value in the limit $y^+ \to \infty$, even when $Re \to \infty$. Rather, Barenblatt et al. argue that for large y^+,

$$\Phi\left(y^+, Re\right) = A\left(y^+\right)^\alpha \tag{1.37}$$

where the coefficient A and the exponent α are presumed to be functions of Reynolds number. In the nomenclature of Barenblatt, Chorin and Prostokishin

(1997), they assume "incomplete similarity in the parameter $[y^+]$ and no similarity in the parameter Re." Combining Equations (1.36) and (1.37) yields

$$\frac{\partial U^+}{\partial y^+} = A\left(y^+\right)^{\alpha-1} \quad \Longrightarrow \quad U^+ = \frac{A}{\alpha}\left(y^+\right)^{\alpha} \tag{1.38}$$

Based primarily on experimental data for pipe flow gathered by Nikuradse in the 1930's [Schlichting-Gersten (1999)], Barenblatt, Chorin and Prostokishin conclude that

$$A = 0.577\ell nRe + 2.50 \quad \text{and} \quad \alpha = \frac{1.5}{\ell nRe} \tag{1.39}$$

where Re is Reynolds number based on average velocity and pipe diameter.

To test the Barenblatt et al. alternative to the law of the wall, Zagarola, Perry and Smits (1997) have performed an analysis based on more recent experiments by Zagarola (1996). The advantage of these data lies in the much wider range of Reynolds numbers considered, especially large values, relative to those considered by Nikuradse. They conclude that the classical law of the wall provides closer correlation with measurements than the power law given by combining Equations (1.38) and (1.39), although they recommend a somewhat larger value for κ of 0.44.

To remove the possibility that the 60-year-old data of Nikuradse provide a poor correlation of A and α, Zagarola, Perry and Smits determine their values from the Zagarola data, concluding that

$$A = 0.7053\ell nRe + 0.3055 \quad \text{and} \quad \alpha = \frac{1.085}{\ell nRe} + \frac{6.535}{(\ell nRe)^2} \tag{1.40}$$

Even with these presumably more-accurate values, the logarithmic law of the wall still provides closer correlation with measurements than the power-law form.

This prompted Barenblatt, Chorin and Prostokishin (1997) — with a questionable argument — to demonstrate that at high Reynolds number the Zagarola experiments have significant surface roughness. Zagarola, Perry and Smits (1997) reject this possibility in stating that "the pipe surface was shown to be smooth."

Buschmann and Gad-el-Hak (2003) have offered what may be the final chapter of the power-law saga. They have performed an extensive analysis of mean-velocity profiles to determine if the power-law or the classical law-of-the-wall formulation provides optimum correlation of measurements. Their profiles include five sets of measurements and one data set from a Direct Numerical Simulation. After a detailed statistical analysis, they conclude that "the examined data do not indicate any statistically significant preference toward either law."

1.4 A Brief History of Turbulence Modeling

The primary emphasis in this book is upon the time-averaged Navier-Stokes equation. The origin of this approach dates back to the end of the nineteenth century when Reynolds (1895) published results of his research on turbulence. His pioneering work proved to have such profound importance for all future developments that we refer to the standard time-averaging process as one type of Reynolds averaging.

The earliest attempts at developing a mathematical description of turbulent stresses sought to mimic the molecular gradient-diffusion process. In this spirit, Boussinesq (1877) introduced the concept of a so-called eddy viscosity. As with Reynolds, Boussinesq has been immortalized in turbulence literature. The Boussinesq eddy-viscosity approximation is so widely known that few authors find a need to reference his original paper.

Neither Reynolds nor Boussinesq attempted a solution of the Reynolds-averaged Navier-Stokes equation in any systematic manner. Much of the physics of viscous flows was a mystery in the nineteenth century, and further progress awaited Prandtl's discovery of the boundary layer in 1904. Focusing upon turbulent flows, Prandtl (1925) introduced the mixing length (an analog of the mean-free path of a gas) and a straightforward prescription for computing the eddy viscosity in terms of the mixing length. The mixing-length hypothesis, closely related to the eddy-viscosity concept, formed the basis of virtually all turbulence-modeling research for the next twenty years. Important early contributions were made by several researchers, most notably by von Kármán (1930). In modern terminology, we refer to a model based on the mixing-length hypothesis as an **algebraic model** or a **zero-equation model of turbulence**. By definition, an n-equation model signifies a model that requires solution of n additional differential transport equations in addition to those expressing conservation of mass, momentum and energy for the mean flow.

To improve the ability to predict properties of turbulent flows and to develop a more realistic mathematical description of the turbulent stresses, Prandtl (1945) postulated a model in which the eddy viscosity depends upon the kinetic energy of the turbulent fluctuations, k. He proposed a modeled partial-differential equation approximating the exact equation for k. This improvement, on a conceptual level, takes account of the fact that the turbulent stresses, and thus the eddy viscosity, are affected by where the flow has been, i.e., upon flow history. Thus was born the concept of the so-called **one-equation model of turbulence**.

While having an eddy viscosity that depends upon flow history provides a more physically realistic model, the need to specify a turbulence length scale remains. That is, on dimensional grounds, viscosity has dimensions of velocity times length. Since the length scale can be thought of as a characteristic eddy size and since such scales are different for each flow, turbulence models that do

not provide a length scale are **incomplete**. That is, we must know something about the flow, other than initial and boundary conditions, in advance in order to obtain a solution. Incomplete models are not without merit and, in fact, have proven to be of great value in many engineering applications.

To elaborate a bit further, an incomplete model generally defines a turbulence length scale in a prescribed manner from the mean flow, e.g., the displacement thickness, δ^*, for an attached boundary layer. However, a different length scale in this example would be needed when the boundary layer separates since δ^* may be negative. Yet another length might be needed for free shear flows, etc. In essence, incomplete models usually define quantities that may vary more simply or more slowly than the Reynolds stresses (e.g., eddy viscosity and mixing length). Presumably, such quantities would prove to be easier to correlate than the actual stresses.

A particularly desirable type of turbulence model would be one that can be applied to a given turbulent flow by prescribing at most the appropriate boundary and/or initial conditions. Ideally, no advance knowledge of any property of the turbulence should be required to obtain a solution. We define such a model as being **complete**. Note that our definition implies nothing regarding the accuracy or universality of the model, only that it can be used to determine a flow with no prior knowledge of any flow details.

Kolmogorov (1942) introduced the first **complete** model of turbulence. In addition to having a modeled equation for k, he introduced a second parameter ω that he referred to as "the rate of dissipation of energy in unit volume and time." The reciprocal of ω serves as a turbulence time scale, while $k^{1/2}/\omega$ serves as the analog of the mixing length and $k\omega$ is the analog of the dissipation rate, ϵ. In this model, known as a k-ω model, ω satisfies a differential equation somewhat similar to the equation for k. The model is thus termed a **two-equation model of turbulence**. While this model offered great promise, it went with virtually no applications for the next quarter century because of the unavailability of computers to solve its nonlinear differential equations.

Chou (1945) and Rotta (1951) laid the foundation for turbulence models that obviate use of the Boussinesq approximation. Rotta devised a plausible model for the differential equation governing evolution of the tensor that represents the turbulent stresses, i.e., the Reynolds-stress tensor. Such models are most appropriately described as **stress-transport models**. Many authors refer to this approach as **second-order closure** or **second-moment closure**. The primary conceptual advantage of a stress-transport model is the natural manner in which nonlocal and history effects are incorporated.

Although quantitative accuracy often remains difficult to achieve, such models automatically accommodate complicating effects such as sudden changes in strain rate, streamline curvature, rigid-body rotation, and body forces. This stands in distinct contrast to eddy-viscosity models that account for these effects only if

empirical terms are added. For a three-dimensional flow, a stress-transport model introduces seven equations, one for the turbulence (length or equivalent) scale and six for the components of the Reynolds-stress tensor. As with Kolmogorov's k-ω model, stress-transport models awaited adequate computer resources.

Thus, by the early 1950's, four main categories of turbulence models had evolved, viz.,

1. Algebraic (Zero-Equation) Models
2. One-Equation Models
3. Two-Equation Models
4. Stress-Transport Models

With the coming of the age of computers since the 1960's, further development of all four classes of turbulence models has occurred. The following overview lists a few of the most important modern developments for each of the four classes.

Algebraic Models. Van Driest (1956) devised a viscous damping correction for the mixing-length model that is included in virtually all algebraic models in use today. Cebeci and Smith (1974) refined the eddy-viscosity/mixing-length model to a point that it can be used with great confidence for most attached boundary layers. To remove some of the difficulties in defining the turbulence length scale from the shear-layer thickness, Baldwin and Lomax (1978) proposed an alternative algebraic model that enjoyed widespread use for many years.

Figure 1.11: *A. M. O. Smith (1911-1997), whose pioneering work in CFD and turbulence modeling were routine accomplishments in a brilliant career.*

One-Equation Models. Of the four types of turbulence models described above, the one-equation model has enjoyed the least popularity and success.

Perhaps the most successful early model of this type was formulated by Bradshaw, Ferriss and Atwell (1967). In the 1968 Stanford Conference on Computation of Turbulent Boundary Layers [Coles and Hirst (1969)] the best turbulence models of the day were tested against the best experimental data of the day. In this author's opinion, of all the models used, the Bradshaw-Ferriss-Atwell model most faithfully reproduced measured flow properties.

There has been renewed interest in one-equation models based on a postulated equation for eddy viscosity [c.f. Sekundov (1971), Baldwin and Barth (1990), Goldberg (1991), Spalart and Allmaras (1992) and Menter (1994)]. This work has been motivated primarily by the ease with which such model equations can be solved numerically, relative to two-equation models and stress-transport models. Of these recent one-equation models, that of Spalart and Allmaras appears to be the most accurate for practical turbulent-flow applications.

Two-Equation Models. While Kolmogorov's k-ω model was the first of this type, it remained in obscurity until the coming of the computer. By far the most extensive work on two-equation models has been done by Launder and Spalding (1972) and a continuing succession of students and colleagues. Launder's k-ϵ model is as well known as the mixing-length model and, until the last decade of the twentieth century, was the most widely used two-equation model. Even the model's demonstrable inadequacy for flows with adverse pressure gradient [c.f. Rodi and Scheuerer (1986), Wilcox (1988a, 1993b) and Henkes (1998a)] initially did little to discourage its widespread use.

With no prior knowledge of Kolmogorov's work, Saffman (1970) formulated a k-ω model that enjoys advantages over the k-ϵ model, especially for integrating through the viscous sublayer and for predicting effects of adverse pressure gradient. Wilcox and Alber (1972), Saffman and Wilcox (1974), Wilcox and Traci (1976), Wilcox and Rubesin (1980), Wilcox (1988a, 1998), Menter (1992a), Kok (2000) and Hellsten (2005), for example, have pursued further development and application of k-ω models. This text, in Chapter 4, introduces a new version of the k-ω model, a significant improvement over that described in the first and second editions of this book. Lakshminarayana (1986) observed that k-ω models had become the second most widely used type of two-equation turbulence model even before the k-ϵ model's numerous inadequacies were widely known.

Stress-Transport Models. By the 1970's, sufficient computer resources became available to permit serious development of this class of model. The most noteworthy efforts were those of Donaldson [Donaldson and Rosenbaum (1968)], Daly and Harlow (1970) and Launder, Reece and Rodi (1975). The latter evolved as the baseline stress-transport model despite its dependence on essentially the same flawed equation for ϵ that plagues the k-ϵ model.

Chapter 6 describes a stress-transport model based on the ω equation that greatly improves computational accuracy over that of the Launder-Reece-Rodi model. More recent contributions by Lumley (1978), Speziale (1985, 1987a,

1991) and Reynolds (1987) have added mathematical rigor to the closure process. However, because of the large number of equations and complexity involved in stress-transport models, they have thus far found their way into a relatively small number of applications compared to algebraic and two-equation models.

This book investigates all four classes of turbulence models. The primary emphasis is upon examining the underlying physical foundation and upon developing the mathematical tools for analyzing and testing the models. **The text is not intended to be a catalog of all turbulence models.** Rather, the text approaches each class of models in a generic sense. Detailed information is provided for models that have stood the test of time; additionally, references are given for most models.

As a concluding comment, turbulence models have been created that fall beyond the bounds of the four categories cited above. This is true because model developers have tried unconventional approaches in an attempt to remove deficiencies of existing models of the four basic classes. Given the erratic track record of most turbulence models, new ideas are always welcome.

Problems

1.1 To appreciate why laminar flow is of minimal importance in many engineering applications, compute the percent of the vehicle over which laminar flow exists for the following situations. In each case, let x_t denote arclength measured from the leading stagnation point of the vehicle or wing and assume transition occurs at a (very high) Reynolds number of $Re_{x_t} = 5 \cdot 10^5$.

(a) A 14-foot automobile moving at 75 mph ($\nu = 1.62 \cdot 10^{-4}$ ft^2/sec).

(b) A 14-foot automobile moving at 25 mph ($\nu = 1.62 \cdot 10^{-4}$ ft^2/sec).

(c) A small aircraft with an average wing chord length of 8 feet moving at 150 mph ($\nu = 1.58 \cdot 10^{-4}$ ft^2/sec).

(d) A *Boeing 747* with an average wing chord length of 30 feet moving at 550 mph ($\nu = 4.25 \cdot 10^{-4}$ ft^2/sec).

1.2 To appreciate why laminar flow is of minimal importance in many engineering applications, compute the percent of the vehicle over which laminar flow exists for the following situations. In each case, let x_t denote arclength measured from the leading stagnation point of the vehicle or wing and assume transition occurs at a (very high) Reynolds number of $Re_{x_t} = 2 \cdot 10^6$. Note that 1 knot = 0.514 m/sec.

(a) A 10-meter sailboat moving at 3.5 knots ($\nu = 1.00 \cdot 10^{-6}$ m^2/sec).

(b) A 10-meter sailboat moving at 7.7 knots ($\nu = 1.00 \cdot 10^{-6}$ m^2/sec).

(c) A 30-meter yacht moving at 12 knots ($\nu = 0.90 \cdot 10^{-6}$ m^2/sec).

(d) A 100-meter tanker moving at 16 knots ($\nu = 1.50 \cdot 10^{-6}$ m^2/sec).

1.3 Using dimensional analysis, deduce the Kolmogorov length, time and velocity scales defined in Equation (1.1).

1.4 Using dimensional analysis, deduce the Kolmogorov $-5/3$ law, Equation (1.8), beginning with the assumption that the energy spectral density, $E(\kappa)$, depends only upon wavenumber, κ, and dissipation rate, ϵ.

1.5 As noted in Subsection 1.3.3, for an automobile moving at 65 mph, the Kolmogorov length scale near the driver's window is $\eta \approx 2 \cdot 10^{-4}$ inch. If $\nu = 1.60 \cdot 10^{-4}$ ft^2/sec, what are the Kolmogorov time and velocity scales? Repeat the computations for a point farther from the surface where $\eta = 0.02$ inch.

1.6 The viscous sublayer of a turbulent boundary layer extends from the surface up to $y^+ \approx 30$. To appreciate how thin this layer is, consider the boundary layer on the side of your freshly washed and waxed (and therefore smooth) automobile. When you are moving at $U = 55$ mph, the skin friction coefficient, c_f, just below your rear-view mirror is 0.0028. Using the fact that

$$U/u_\tau = \sqrt{2/c_f}$$

estimate the sublayer thickness and compare it to the diameter of the head of a pin, which is $d_{pin} = 0.05$ inch. Assume $\nu = 1.68 \cdot 10^{-4}$ ft^2/sec.

1.7 The viscous sublayer of a turbulent boundary layer extends from the surface up to $y^+ \approx 30$. To appreciate how thin this layer is, consider the boundary layer on the hull of a large tanker moving at speed U. Assuming the boundary layer has negligible pressure gradient over most of the hull, you can assume the boundary-layer thickness, δ, and skin friction, c_f, are

$$\delta \approx 0.37 x Re_x^{-1/5}$$

$$c_f \approx 0.0576 Re_x^{-1/5}$$

(a) Noting that $U/u_\tau = \sqrt{2/c_f}$, verify that the sublayer thickness, $\delta_{sl} = 30\nu/u_\tau$, is given by

$$\delta_{sl} \approx \frac{478}{Re_x^{7/10}}\,\delta$$

(b) Compute δ_{sl} at points on the hull where $Re_x = 2.8 \cdot 10^7$ and $\delta = 2.5$ in, and where $Re_x = 5.0 \cdot 10^8$ and $\delta = 25$ in. Express your answer in terms of h_δ/δ_{sl}, to the nearest integer, where $h_\delta = 1/10$ inch is the height of the symbol δ_{sl} on this page.

1.8 A surface is called *hydraulically smooth* when the surface roughness height, k_s, is such that

$$k_s^+ \equiv \frac{u_\tau k_s}{\nu} < 5$$

where u_τ is friction velocity and ν is kinematic viscosity. Consider the flow of air over a flat plate of length 1 m. For the following plate materials, what is the maximum freestream velocity, U, at which the surface will be hydraulically smooth? Assume skin friction is given by $c_f \approx 0.0576 Re_x^{-1/5}$ and that $\nu = 1.51 \cdot 10^{-5}$ m^2/sec.

Plate Material	k_s (mm)
Copper	0.0015
Galvanized iron	0.15
Concrete	1.50

1.9 A surface is called *completely rough* when the surface roughness height, k_s, is such that

$$k_s^+ \equiv \frac{u_\tau k_s}{\nu} > 70$$

where u_τ is friction velocity and ν is kinematic viscosity. Consider the flow of water over a flat plate. For the following plate materials, what is the minimum freestream velocity, U, at which the surface will be completely rough at $x = 5$ ft? Assume skin friction is given by $c_f \approx 0.0576 Re_x^{-1/5}$ and that $\nu = 1.08 \cdot 10^{-5}$ ft^2/sec.

Plate Material	k_s (ft)
Steel	$1.5 \cdot 10^{-4}$
Cast iron	$8.5 \cdot 10^{-4}$
Concrete	$5.0 \cdot 10^{-2}$

1.10 The *atmospheric boundary layer* over a smooth beach is a very large scale turbulent, flat-plate boundary layer, and its boundary-layer thickness and skin friction are accurately represented by

$$\delta \approx 0.37 x Re_x^{-1/5} \qquad \text{and} \qquad c_f \approx 0.0576 Re_x^{-1/5}$$

Suppose you are enjoying a day on the beach and the temperature is 85° F so that the kinematic molecular viscosity is $\nu = 1.72 \cdot 10^{-4}$ ft^2/sec. The atmospheric boundary layer is 250 ft thick and the velocity at that altitude is 20 mph. Your forehead is about 6 inches above the ground level. Is your forehead in the sublayer, log layer or defect layer? What is the wind velocity over your forehead?

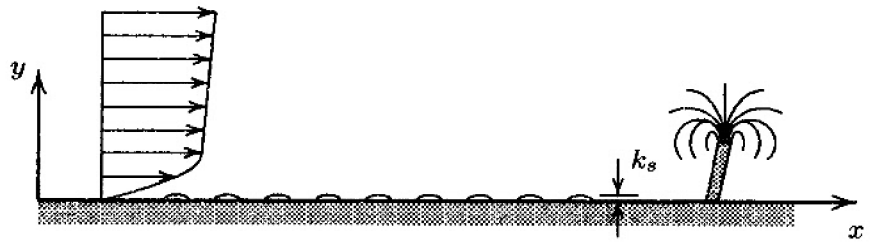

Problems 1.10, 1.11

1.11 Sunbathers are enjoying a day on the beach. They are lying on the sand with essentially uniform spacing, and their bodies resemble sandgrain roughness elements of height $k_s = 30$ cm to the *atmospheric boundary layer*. One of the sunbathers is an eager graduate student who decides to use what he learned in this chapter in a practical situation. First, just downstream of a cluster of sunbathers, he measures the wind velocity at head level, $y_1 \approx 1.8$ m, and finds $u_1 = 2.9$ m/sec. He then climbs a palm tree of height $y_2 \approx 5.0$ m and observes a wind velocity of $u_2 = 3.5$ m/sec. Assuming the beach surface is a *completely-rough* surface, what is the friction velocity according to his measurements? To verify the hypothesis that the surface is completely rough, check to see if $u_\tau k_s/\nu > 70$. Assume that $\nu = 1.60 \cdot 10^{-5}$ m^2/sec.

1.12 Combining Equations (1.25) and (1.28), verify that the function $g(\eta)$ must be

$$g(\eta) = A - \frac{1}{\kappa} \ell n \eta$$

where A is a function of U_e, u_τ, Δ, ν, κ and C. To have a wide separation of scales, A must be a constant, i.e., it must be independent of Reynolds number. Noting that $U_e/u_\tau = \sqrt{2/c_f}$ and using Clauser's thickness, $\Delta = U_e \delta^*/u_\tau$, where δ^* is displacement thickness, determine the skin friction, c_f, as a function of A, C and $Re_{\delta^*} = U_e \delta^*/\nu$.

1.13 For a turbulent boundary layer, the velocity is given by $u^+ = y^+$ in the sublayer and by the law of the wall, Equations (1.20) and (1.21), in the log layer. Determine by trial and error (or Newton's iterations if you are familiar with the method) the value of y^+ (to the nearest 1/10) at which the sublayer and log-layer velocity profiles are equal.

1.14 We would like to determine the values of Reynolds number, Re, for which the Barenblatt exponent, α, is 1/6, 1/7 and 1/8. Compare the values inferred by using the Barenblatt correlation, Equation (1.39), and the Zagarola correlation, Equation (1.40).

1.15 According to Equation (1.32), at the boundary-layer edge we have

$$\frac{U_e}{u_\tau} = \frac{1}{\kappa} \ell n \frac{u_\tau \delta}{\nu} + C + \frac{2\Pi}{\kappa}$$

We would like to determine how skin friction, $c_f = 2u_\tau^2/U_e^2$, is affected by changes in the quantities C and Π.

(a) Assuming only u_τ varies with C, verify that

$$\frac{1}{c_f}\frac{dc_f}{dC} = -\frac{2\kappa\sqrt{c_f/2}}{\kappa + \sqrt{c_f/2}}$$

(b) Assuming $c_f = 0.002$, based on the result of Part (a), how much of a change in C is required to give a 3% change in c_f? Be sure to include a sign in your result.

(c) Derive a similar result for $(dc_f/d\Pi)/c_f$ and determine the approximate change in c_f for a decrease in Π of 1.0. Assume $c_f = 0.002$.

Chapter 2

The Closure Problem

Because turbulence consists of random fluctuations of the various flow properties, we use a statistical approach. Our purposes are best served by the procedure introduced by Reynolds (1895) in which all quantities are expressed as the sum of mean and fluctuating parts. We then form the mean of the continuity and Navier-Stokes equations term by term. As we will see in this chapter, the nonlinearity of the Navier-Stokes equation leads to the appearance of momentum fluxes that act as apparent stresses throughout the flow. These momentum fluxes are unknown a priori. We then derive equations for these stresses, which include additional unknown quantities. This illustrates the issue of closure, i.e., establishing a sufficient number of equations for all of the unknowns. The chapter concludes with a discussion of turbulence scales and more-advanced statistical concepts.

To illustrate the nature of turbulence statistics, it is instructive to observe how the velocity field behaves for a turbulent flow. Figure 2.1 shows measured velocity profiles, $u(y)$, for a flat-plate boundary layer. Plotted with a series

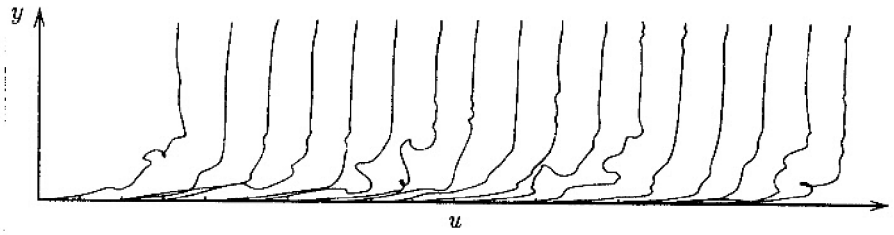

Figure 2.1: *Instantaneous boundary-layer velocity profiles at the same distance from the leading edge of a flat plate at 17 different instants. The profiles are shown with a series of staggered origins. [From Cebeci and Smith (1974) — Copyright © Academic Press 1974 — Used with permission.]*

of staggered origins, all 17 profiles correspond to the same distance from the plate leading edge, and have been measured at several different times using the hydrogen-bubble technique. While the experimental method is a bit crude, e.g., the profiles appear incorrectly multivalued[1] in a few locations, the measured velocity profiles correctly show that the velocity profile changes shape rather dramatically from one instant to the next.

Figure 2.2(a) displays all of the velocity profiles, only this time with a common origin. Clearly, there is a large scatter in the value of the velocity at each distance y from the surface. Figure 2.2(b) shows a standard mean velocity profile for a boundary layer at the same Reynolds number. Comparison of the profiles in (a) and (b) clearly illustrates that the turbulent fluctuations in the velocity cannot be regarded as a small perturbation relative to the mean value. In the following sections, we explore the classical statistical methods used to analyze this inherently complex behavior.

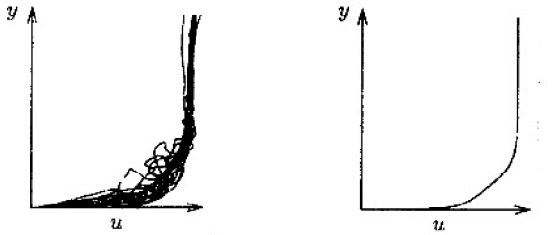

(a) All profiles – one origin (b) Average profile

Figure 2.2: *Instantaneous and average boundary-layer velocity profiles at the same distance from the leading edge of a flat plate. [From Cebeci and Smith (1974) — Copyright © Academic Press 1974 — Used with permission.]*

2.1 Reynolds Averaging

We begin with the averaging concepts introduced by Reynolds (1895). In general, Reynolds averaging assumes a variety of forms involving either an integral or a summation. The three forms most pertinent in turbulence-model research are the **time average**, the **spatial average** and the **ensemble average**: the general term used to describe these averaging processes is "mean."

Time averaging is appropriate for **stationary turbulence**, i.e., a turbulent flow that, on the average, does not vary with time, such as flow in a pipe driven

[1] The hydrogen-bubble technique cannot isolate the velocity component parallel to the surface, so that the profiles include effects of vertical motion as well, and the apparently multivalued profiles are really a kind of velocity-vector plot. This also illustrates that fluctuating velocities are large in all directions.

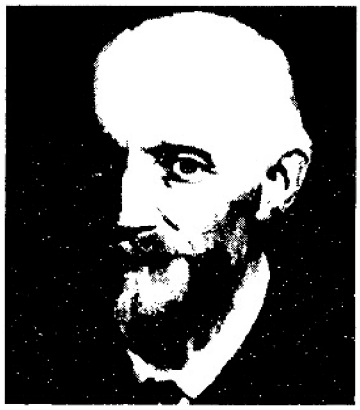

Figure 2.3: *Osborn Reynolds (1842-1912), whose 1895 paper on the dynamics of fluid motion established the averaging techniques that bear his name.*

by a constant-speed blower. For such a flow, we express an instantaneous flow variable as $f(\mathbf{x}, t)$. Its time average, $F_T(\mathbf{x})$, is defined by

$$F_T(\mathbf{x}) = \lim_{T\to\infty} \frac{1}{T} \int_t^{t+T} f(\mathbf{x}, t)\, dt \tag{2.1}$$

The velocity profile depicted in Figure 2.2(b), for example, was obtained using time averaging for accurate measurements of a similar boundary layer. The applicability of Reynolds averaging (of whatever kind) implicitly depends upon this steadiness of mean values. Time averaging is the most commonly used form of Reynolds averaging because most turbulent flows of interest in engineering are stationary. There are important exceptions, of course, such as the motion of the atmosphere.

Spatial averaging can be used for **homogeneous** turbulence, which is a turbulent flow that, on the average, is uniform in all directions. We average over all spatial coordinates by doing a volume integral. Calling the average F_V, we have

$$F_V(t) = \lim_{V\to\infty} \frac{1}{V} \iiint_V f(\mathbf{x}, t)\, dV \tag{2.2}$$

Ensemble averaging is the most general type of Reynolds averaging suitable for, e.g., flows that decay in time. As an idealized example, in terms of measurements from N identical experiments (with initial and boundary conditions that differ by random infinitesimal perturbations) where $f(\mathbf{x}, t) = f_n(\mathbf{x}, t)$ in the n^{th} experiment, the average is F_E, defined by

$$F_E(\mathbf{x}, t) = \lim_{N\to\infty} \frac{1}{N} \sum_{n=1}^{N} f_n(\mathbf{x}, t) \tag{2.3}$$

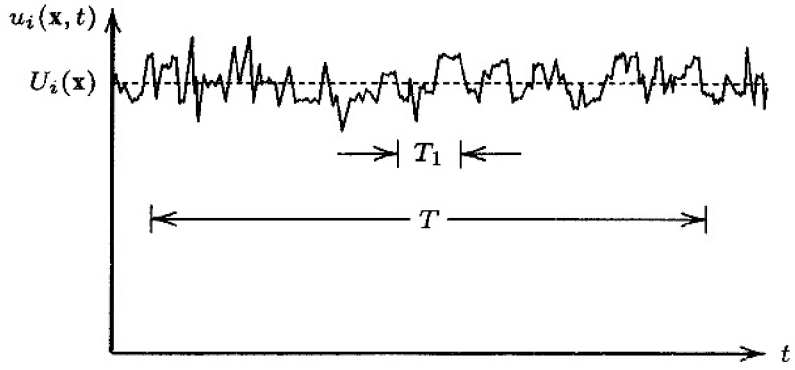

Figure 2.4: *Time averaging for stationary turbulence. Although obscured by the scale of the graph, the instantaneous velocity, $u_i(\mathbf{x},t)$, has continuous derivatives of all order.*

From this point on, we will consider only time averaging. There is no loss of generality however as virtually all of our results are valid for other kinds of Reynolds averaging. Consider a stationary turbulent flow so that Equation (2.1) holds. For such a flow, we express the instantaneous velocity, $u_i(\mathbf{x},t)$, as the sum of a mean, $U_i(\mathbf{x})$, and a fluctuating part, $u_i'(\mathbf{x},t)$, so that[2]

$$u_i(\mathbf{x},t) = U_i(\mathbf{x}) + u_i'(\mathbf{x},t) \tag{2.4}$$

As in Equation (2.1), the quantity $U_i(\mathbf{x})$ is the time-averaged, or mean, velocity defined by

$$U_i(\mathbf{x}) = \lim_{T\to\infty} \frac{1}{T} \int_t^{t+T} u_i(\mathbf{x},t)\, dt \tag{2.5}$$

The time average of the mean velocity is again the same time-averaged value, i.e.,

$$\overline{U_i}(\mathbf{x}) = \lim_{T\to\infty} \frac{1}{T} \int_t^{t+T} U_i(\mathbf{x})\, dt = U_i(\mathbf{x}) \tag{2.6}$$

where an overbar is shorthand for the time average. The time average of the fluctuating part of the velocity is zero. That is, using Equation (2.6),

$$\overline{u_i'} = \lim_{T\to\infty} \frac{1}{T} \int_t^{t+T} [u_i(\mathbf{x},t) - U_i(\mathbf{x})]\, dt = U_i(\mathbf{x}) - \overline{U_i}(\mathbf{x}) = 0 \tag{2.7}$$

While Equation (2.5) is mathematically well defined, we can never truly realize infinite T in any physical flow. This is not a serious problem in practice. In forming our time average, as illustrated in Figure 2.4, we just select a time T

[2] By convention, throughout this text the instantaneous variable is denoted by a lower-case symbol, the mean is denoted by the corresponding upper-case symbol and the fluctuating part is the lower-case symbol with a prime.

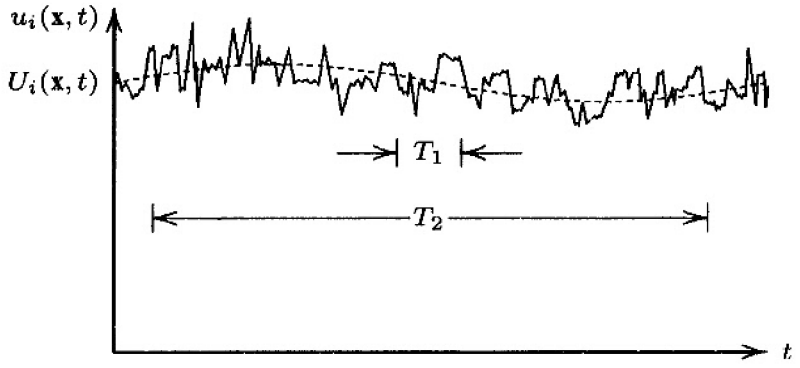

Figure 2.5: *Time averaging for nonstationary turbulence. Although obscured by the scale of the graph, the instantaneous velocity, $u_i(\mathbf{x},t)$, has continuous derivatives of all order.*

that is very long relative to the maximum period of the velocity fluctuations, T_1, which we don't need to define precisely. In other words, rather than formally taking the limit $T \to \infty$, we do the indicated integration in Equation (2.5) with $T \gg T_1$. As an example, for flow at 10 m/sec in a 5 cm diameter pipe, an integration time of 20 seconds would probably be adequate. In this time the flow moves 4000 pipe diameters.

There are some flows for which the mean flow contains very slow variations with time that are not turbulent in nature. For instance, we might impose a slowly varying periodic pressure gradient in a duct or we might wish to compute flow over a helicopter blade or flow through an automobile muffler. Clearly, Equations (2.4) and (2.5) must be modified to accommodate such applications. The simplest, but a bit arbitrary, method is to replace Equations (2.4) and (2.5) with

$$u_i(\mathbf{x},t) = U_i(\mathbf{x},t) + u_i'(\mathbf{x},t) \tag{2.8}$$

and

$$U_i(\mathbf{x},t) = \frac{1}{T}\int_t^{t+T} u_i(\mathbf{x},t)\,dt, \qquad T_1 \ll T \ll T_2 \tag{2.9}$$

where T_2 is the time scale characteristic of the slow variations in the flow that we do not wish to regard as belonging to the turbulence. Figure 2.5 illustrates these concepts.

A word of caution is in order regarding Equation (2.9). We are implicitly assuming that time scales T_1 and T_2 exist that differ by several orders of magnitude. Many unsteady flows of engineering interest do not satisfy this condition. We cannot use Equations (2.8) and (2.9) for such flows because there is no distinct boundary between our imposed unsteadiness and turbulent fluctuations. For such flows, the mean [as defined in Equation (2.9)] and fluctuating components

are correlated, i.e., the time average of their product is non-vanishing. In meteorology, for example, this is known as the **spectral gap problem**. If the flow is periodic, **Phase Averaging** (see problems section) can be used; otherwise, full ensemble averaging is required. Phase averaging is a type of ensemble averaging with phase angle replacing time. For a rigorous approach, an alternative method such as Large Eddy Simulation (Chapter 8) will be required.

Clearly our time-averaging process, involving integrals over time, commutes with spatial differentiation. Thus, for any scalar p and vector u_i,

$$\overline{p_{,i}} = P_{,i} \qquad \text{and} \qquad \overline{u_{i,j}} = U_{i,j} \tag{2.10}$$

Because we are dealing with definite integrals, time averaging is a linear operation. Thus if c_1 and c_2 are constants while a and b denote any two flow properties with mean values A and B, respectively, then

$$\overline{c_1 a + c_2 b} = c_1 A + c_2 B \tag{2.11}$$

The time average of an unsteady term like $\partial u_i/\partial t$ is obviously zero for stationary turbulence. For nonstationary turbulence, we must look a little closer. We know that

$$\frac{1}{T}\int_t^{t+T} \frac{\partial}{\partial t}(U_i + u_i')\, dt = \frac{U_i(\mathbf{x}, t+T) - U_i(\mathbf{x}, t)}{T} + \frac{u_i'(\mathbf{x}, t+T) - u_i'(\mathbf{x}, t)}{T} \tag{2.12}$$

The second term on the right-hand side of Equation (2.12) can be neglected provided $|u_i'|$ is small relative to $|U_i|$. Since we are assuming T is very small relative to the time scale of the mean flow, i.e. that $T \ll T_2$, the first term is the value corresponding to the limit $T \to 0$, i.e., $\partial U_i/\partial t$. Hence,

$$\overline{\frac{\partial u_i}{\partial t}} \approx \frac{\partial U_i}{\partial t} \tag{2.13}$$

The approximation that $|u_i'| \ll |U_i|$ is always questionable, especially for free shear flows and for flows very close to a solid boundary. This is one of the inherent complications of turbulence, namely that the fluctuations cannot be assumed to be small relative to the mean values.

Using time averaging in this manner is nevertheless useful for analysis, especially for time-marching numerical methods implemented for solving steady-flow problems. Because Equation (2.13) depends on the doubtful approximation that $|u_i'| \ll |U_i|$ while fluctuations are often in excess of 10% of the mean, a degree of caution must be exercised when such methods are used for time-varying flows.

2.2 Correlations

Thus far we have considered averages of linear quantities. When we average the product of two properties, say ϕ and ψ, we have the following:

$$\overline{\phi\psi} = \overline{(\Phi + \phi')(\Psi + \psi')} = \overline{\Phi\Psi + \Phi\psi' + \Psi\phi' + \phi'\psi'} = \Phi\Psi + \overline{\phi'\psi'} \quad (2.14)$$

where we take advantage of the fact that the product of a mean quantity and a fluctuating quantity has zero mean because the mean of the latter is zero. There is no a priori reason for the mean of the product of two fluctuating quantities to vanish. Thus, Equation (2.14) tells us that the mean value of a product, $\overline{\phi\psi}$, differs from the product of the mean values, $\Phi\Psi$. The quantities ϕ' and ψ' are said to be **correlated** if $\overline{\phi'\psi'} \neq 0$. They are **uncorrelated** if $\overline{\phi'\psi'} = 0$.

Similarly, for a triple product, we find

$$\overline{\phi\psi\xi} = \Phi\Psi\Xi + \overline{\phi'\psi'}\Xi + \overline{\psi'\xi'}\Phi + \overline{\phi'\xi'}\Psi + \overline{\phi'\psi'\xi'} \quad (2.15)$$

Again, terms linear in ϕ', ψ' or ξ' have zero mean. As with terms quadratic in fluctuating quantities, there is no a priori reason for the cubic term, $\overline{\phi'\psi'\xi'}$, to vanish.

2.3 Reynolds-Averaged Equations

For simplicity we confine our attention to incompressible, constant-property flow. Effects of compressibility will be addressed in Chapter 5. The equations for conservation of mass and momentum are

$$\frac{\partial u_i}{\partial x_i} = 0 \quad (2.16)$$

$$\rho\frac{\partial u_i}{\partial t} + \rho u_j\frac{\partial u_i}{\partial x_j} = -\frac{\partial p}{\partial x_i} + \frac{\partial t_{ji}}{\partial x_j} \quad (2.17)$$

The vectors u_i and x_i are velocity and position, t is time, p is pressure, ρ is density and t_{ij} is the viscous stress tensor defined by

$$t_{ij} = 2\mu s_{ij} \quad (2.18)$$

where μ is molecular viscosity and s_{ij} is the strain-rate tensor,

$$s_{ij} = \frac{1}{2}\left(\frac{\partial u_i}{\partial x_j} + \frac{\partial u_j}{\partial x_i}\right) \quad (2.19)$$

Note that $s_{ji} = s_{ij}$, so that $t_{ji} = t_{ij}$ for simple viscous fluids (but not for some anisotropic liquids).

To simplify the time-averaging process, we rewrite the convective term in "conservation" form, i.e.,

$$u_j \frac{\partial u_i}{\partial x_j} = \frac{\partial}{\partial x_j}(u_j u_i) - u_i \frac{\partial u_j}{\partial x_j} = \frac{\partial}{\partial x_j}(u_j u_i) \tag{2.20}$$

where we take advantage of mass conservation [Equation (2.16)] in order to drop $u_i \partial u_j / \partial x_j$. Combining Equations (2.17) through (2.20) yields the Navier-Stokes equation in conservation form.

$$\rho \frac{\partial u_i}{\partial t} + \rho \frac{\partial}{\partial x_j}(u_j u_i) = -\frac{\partial p}{\partial x_i} + \frac{\partial}{\partial x_j}(2\mu s_{ji}) \tag{2.21}$$

Time (ensemble) averaging Equations (2.16) and (2.21) yields the **Reynolds averaged equations of motion in conservation form**, viz.,

$$\frac{\partial U_i}{\partial x_i} = 0 \tag{2.22}$$

$$\rho \frac{\partial U_i}{\partial t} + \rho \frac{\partial}{\partial x_j}\left(U_j U_i + \overline{u_j' u_i'}\right) = -\frac{\partial P}{\partial x_i} + \frac{\partial}{\partial x_j}(2\mu S_{ji}) \tag{2.23}$$

The time-averaged mass-conservation Equation (2.22) is identical to the instantaneous Equation (2.16) with the mean velocity replacing the instantaneous velocity. Subtracting Equation (2.22) from Equation (2.16) shows that the fluctuating velocity, u_i', also has zero divergence. Aside from replacement of instantaneous variables by mean values, the only difference between the time-averaged and instantaneous momentum equations is the appearance of the correlation $\overline{u_i' u_j'}$. This is a time-averaged rate of momentum transfer due to the turbulence.

Herein lies the fundamental problem of turbulence. *In order to compute all mean-flow properties of the turbulent flow under consideration, we need a prescription for computing* $\overline{u_i' u_j'}$.

Equation (2.23) can be written in its most recognizable form by using Equation (2.20) in reverse. The resulting equation is

$$\rho \frac{\partial U_i}{\partial t} + \rho U_j \frac{\partial U_i}{\partial x_j} = -\frac{\partial P}{\partial x_i} + \frac{\partial}{\partial x_j}\left(2\mu S_{ji} - \rho \overline{u_j' u_i'}\right) \tag{2.24}$$

Equation (2.24) is usually referred to as the **Reynolds-averaged Navier-Stokes equation (RANS)**. The quantity $-\rho \overline{u_i' u_j'}$ is known as the **Reynolds-stress tensor** and we denote it by $\rho \tau_{ij}$, so that τ_{ij} is the **specific Reynolds stress tensor** given by

$$\tau_{ij} = -\overline{u_i' u_j'} \tag{2.25}$$

By inspection, $\tau_{ij} = \tau_{ji}$ so that this is a symmetric tensor, and thus has six independent components. Hence, we have produced six unknown quantities as

a result of Reynolds averaging. Unfortunately, we have gained no additional equations. Now, for general three-dimensional flows, we have four unknown mean-flow properties, viz., pressure and the three velocity components. Along with the six Reynolds-stress components, we thus have ten unknowns. Our equations are mass conservation [Equation (2.22)] and the three components of Equation (2.24) for a grand total of four. This means our system is not yet **closed**. To close the system, we must find enough equations to solve for our unknowns.

2.4 The Reynolds-Stress Equation

In quest of additional equations, we can take moments of the Navier-Stokes equation. That is, we multiply the Navier-Stokes equation by a fluctuating property and time average the product. Using this procedure, we can derive a differential equation for the Reynolds-stress tensor. To illustrate the process, we introduce some special notation. Let $\mathcal{N}(u_i)$ denote the "Navier-Stokes operator," viz.,

$$\mathcal{N}(u_i) = \rho\frac{\partial u_i}{\partial t} + \rho u_k\frac{\partial u_i}{\partial x_k} + \frac{\partial p}{\partial x_i} - \mu\frac{\partial^2 u_i}{\partial x_k \partial x_k} \tag{2.26}$$

The viscous term has been simplified by noting from mass conservation (for incompressible flow) that $s_{ki,k} = u_{i,kk}$. The Navier-Stokes equation can be written symbolically as

$$\mathcal{N}(u_i) = 0 \tag{2.27}$$

In order to derive an equation for the Reynolds stress tensor, we form the following time average.

$$\overline{u_i'\mathcal{N}(u_j) + u_j'\mathcal{N}(u_i)} = 0 \tag{2.28}$$

Note that, consistent with the symmetry of the Reynolds stress tensor, the resulting equation is also symmetric in i and j. For the sake of clarity, we proceed term by term. Also, for economy of space, we use tensor notation for derivatives throughout the time averaging process. Non-obvious results in the following equations usually involve the continuity equation ($\partial u_i/\partial x_i = \partial u_i'/\partial x_i = 0$) in various ways. First, we consider the **unsteady term**.

$$\begin{aligned}
\overline{u_i'(\rho u_j)_{,t} + u_j'(\rho u_i)_{,t}} &= \overline{\rho u_i'(U_j + u_j')_{,t}} + \overline{\rho u_j'(U_i + u_i')_{,t}} \\
&= \overline{\rho u_i' U_{j,t}} + \overline{\rho u_i' u_{j,t}'} + \overline{\rho u_j' U_{i,t}} + \overline{\rho u_j' u_{i,t}'} \\
&= \overline{\rho u_i' u_{j,t}'} + \overline{\rho u_j' u_{i,t}'} \\
&= \overline{\rho(u_i' u_j')_{,t}} \\
&= -\rho\frac{\partial \tau_{ij}}{\partial t}
\end{aligned} \tag{2.29}$$

Turning to the **convective term**, we have

$$\begin{aligned}
\overline{\rho u_i' u_k u_{j,k} + \rho u_j' u_k u_{i,k}} &= \overline{\rho u_i' (U_k + u_k')(U_j + u_j')_{,k}} \\
&+ \overline{\rho u_j' (U_k + u_k')(U_i + u_i')_{,k}} \\
&= \overline{\rho u_i' U_k u_{j,k}'} + \overline{\rho u_i' u_k' (U_j + u_j')_{,k}} \\
&+ \overline{\rho u_j' U_k u_{i,k}'} + \overline{\rho u_j' u_k' (U_i + u_i')_{,k}} \\
&= \rho U_k \overline{(u_i' u_j')_{,k}} + \overline{\rho u_i' u_k'} U_{j,k} \\
&+ \overline{\rho u_j' u_k'} U_{i,k} + \overline{\rho u_k' (u_i' u_j')_{,k}} \\
&= -\rho U_k \frac{\partial \tau_{ij}}{\partial x_k} - \rho \tau_{ik} \frac{\partial U_j}{\partial x_k} - \rho \tau_{jk} \frac{\partial U_i}{\partial x_k} \\
&+ \rho \frac{\partial}{\partial x_k} \overline{(u_i' u_j' u_k')} \qquad (2.30)
\end{aligned}$$

In order to arrive at the final line of Equation (2.30), we use the fact that $\partial u_k'/\partial x_k = 0$. The **pressure gradient** term is straightforward.

$$\begin{aligned}
\overline{u_i' p_{,j} + u_j' p_{,i}} &= \overline{u_i' (P + p')_{,j}} + \overline{u_j' (P + p')_{,i}} \\
&= \overline{u_i' p_{,j}' + u_j' p_{,i}'} \\
&= \overline{u_i' \frac{\partial p'}{\partial x_j}} + \overline{u_j' \frac{\partial p'}{\partial x_i}} \qquad (2.31)
\end{aligned}$$

Finally, the **viscous term** yields

$$\begin{aligned}
\overline{\mu (u_i' u_{j,kk} + u_j' u_{i,kk})} &= \overline{\mu u_i' (U_j + u_j')_{,kk}} + \overline{\mu u_j' (U_i + u_i')_{,kk}} \\
&= \overline{\mu u_i' u_{j,kk}'} + \overline{\mu u_j' u_{i,kk}'} \\
&= \overline{\mu (u_i' u_{j,k}')_{,k}} + \overline{\mu (u_j' u_{i,k}')_{,k}} - 2\overline{\mu u_{i,k}' u_{j,k}'} \\
&= \overline{\mu (u_i' u_j')_{,kk}} - 2\overline{\mu u_{i,k}' u_{j,k}'} \\
&= -\mu \frac{\partial^2 \tau_{ij}}{\partial x_k \partial x_k} - 2\mu \overline{\frac{\partial u_i'}{\partial x_k} \frac{\partial u_j'}{\partial x_k}} \qquad (2.32)
\end{aligned}$$

Collecting terms, we arrive at the equation for the Reynolds stress tensor.

$$\begin{aligned}
\frac{\partial \tau_{ij}}{\partial t} + U_k \frac{\partial \tau_{ij}}{\partial x_k} &= -\tau_{ik} \frac{\partial U_j}{\partial x_k} - \tau_{jk} \frac{\partial U_i}{\partial x_k} + 2\nu \overline{\frac{\partial u_i'}{\partial x_k} \frac{\partial u_j'}{\partial x_k}} + \overline{\frac{u_i'}{\rho} \frac{\partial p'}{\partial x_j}} + \overline{\frac{u_j'}{\rho} \frac{\partial p'}{\partial x_i}} \\
&+ \frac{\partial}{\partial x_k} \left[\nu \frac{\partial \tau_{ij}}{\partial x_k} + \overline{u_i' u_j' u_k'} \right] \qquad (2.33)
\end{aligned}$$

We have gained six new equations, one for each independent component of the Reynolds-stress tensor. However, we have also generated 22 new unknowns! Specifically, accounting for all symmetries, we have the following.

$$\begin{aligned} \overline{u_i' u_j' u_k'} &\rightarrow \text{10 unknowns} \\ 2\nu \overline{\frac{\partial u_i'}{\partial x_k} \frac{\partial u_j'}{\partial x_k}} &\rightarrow \text{6 unknowns} \\ \overline{\frac{u_i'}{\rho} \frac{\partial p'}{\partial x_j}} + \overline{\frac{u_j'}{\rho} \frac{\partial p'}{\partial x_i}} &\rightarrow \text{6 unknowns} \end{aligned}$$

With a little rearrangement of terms, we can cast the **Reynolds-stress equation** in suitably compact form, viz.,

$$\frac{\partial \tau_{ij}}{\partial t} + U_k \frac{\partial \tau_{ij}}{\partial x_k} = -\tau_{ik} \frac{\partial U_j}{\partial x_k} - \tau_{jk} \frac{\partial U_i}{\partial x_k} + \epsilon_{ij} - \Pi_{ij} + \frac{\partial}{\partial x_k} \left[\nu \frac{\partial \tau_{ij}}{\partial x_k} + C_{ijk} \right] \quad (2.34)$$

where

$$\Pi_{ij} = \overline{\frac{p'}{\rho} \left(\frac{\partial u_i'}{\partial x_j} + \frac{\partial u_j'}{\partial x_i} \right)} \quad (2.35)$$

$$\epsilon_{ij} = 2\nu \overline{\frac{\partial u_i'}{\partial x_k} \frac{\partial u_j'}{\partial x_k}} \quad (2.36)$$

$$\rho C_{ijk} = \rho \overline{u_i' u_j' u_k'} + \overline{p' u_i'} \delta_{jk} + \overline{p' u_j'} \delta_{ik} \quad (2.37)$$

This exercise illustrates the closure problem of turbulence. Because of the nonlinearity of the Navier-Stokes equation, as we take higher and higher moments, we generate additional unknowns at each level. At no point will this procedure balance our unknowns/equations ledger. On physical grounds, this is not a particularly surprising situation. After all, such operations are strictly mathematical in nature, and introduce no additional physical principles. *In essence, Reynolds averaging is a brutal simplification that loses much of the information contained in the Navier-Stokes equation.* The function of turbulence modeling is to devise approximations for the unknown correlations in terms of flow properties that are known so that a sufficient number of equations exists. In making such approximations, we close the system.

2.5 The Scales of Turbulence

In Chapter 1, we introduced the **Kolmogorov length, velocity and time scales**, which are characteristic of the smallest eddies. We also discussed the **integral**

length scale, ℓ, which is representative of the energy-bearing eddies. While these are some of the most useful scales for describing turbulence, there are others that are commonly used. The purpose of this section is to further quantify the most commonly used turbulence scales, and briefly introduce the concept of **two-point correlations**.

2.5.1 Turbulence Intensity

The Kolmogorov scales, defined in Equation (1.1), provide an estimate of the length, velocity and time scales for the smallest eddies in a turbulent flow. The integral length scale, whose definition has been deferred to this chapter, is a characteristic size of the energy-bearing eddies. Another important measure of any turbulent flow is how intense the turbulent fluctuations are. We quantify this in terms of the specific normal Reynolds stress components, $\overline{u'^2}$, $\overline{v'^2}$ and $\overline{w'^2}$. These three normal Reynolds stresses can also be regarded as the kinetic energy per unit mass of the fluctuating velocity field in the three coordinate directions. These Reynolds stresses are often normalized relative to the freestream mean-flow velocity, U_e, according to

$$\hat{u} \equiv \frac{\sqrt{\overline{u'^2}}}{U_e}, \quad \hat{v} \equiv \frac{\sqrt{\overline{v'^2}}}{U_e}, \quad \hat{w} \equiv \frac{\sqrt{\overline{w'^2}}}{U_e} \tag{2.38}$$

The quantities $\hat{u}$, $\hat{v}$ and $\hat{w}$ are known as the **relative intensities** in the x, y and z directions, respectively.

Figure 2.6 displays the relative intensities for an incompressible flat-plate boundary layer. As shown, the three intensities have different values throughout most of the boundary layer. This is true because the turbulence is **anisotropic**, i.e., the normal-stress components are unequal. As a rough but useful approximation for a flat-plate boundary layer, we find that

$$\overline{u'^2} : \overline{v'^2} : \overline{w'^2} = 4 : 2 : 3 \tag{2.39}$$

These ratios are of course not constant through the layer; also, they are by no means universal for boundary layers, being strongly influenced by pressure gradient and compressibility.

Note that the streamwise intensity, $\hat{u} = \sqrt{\overline{u'^2}}/U_e$, exceeds 0.10, or 10%, very close to the surface. This is consistent with the instantaneous velocity profiles shown in Figure 2.2, and further reinforces the claim that the turbulent fluctuations cannot be adequately treated as a small perturbation about the mean.

If we sum the three normal Reynolds stresses and multiply by $\frac{1}{2}$, we have the **turbulence kinetic energy**, which we denote by the symbol k. Thus, by definition,

$$k \equiv \frac{1}{2}(\overline{u'^2} + \overline{v'^2} + \overline{w'^2}) = \frac{1}{2}\overline{u_i' u_i'} \tag{2.40}$$

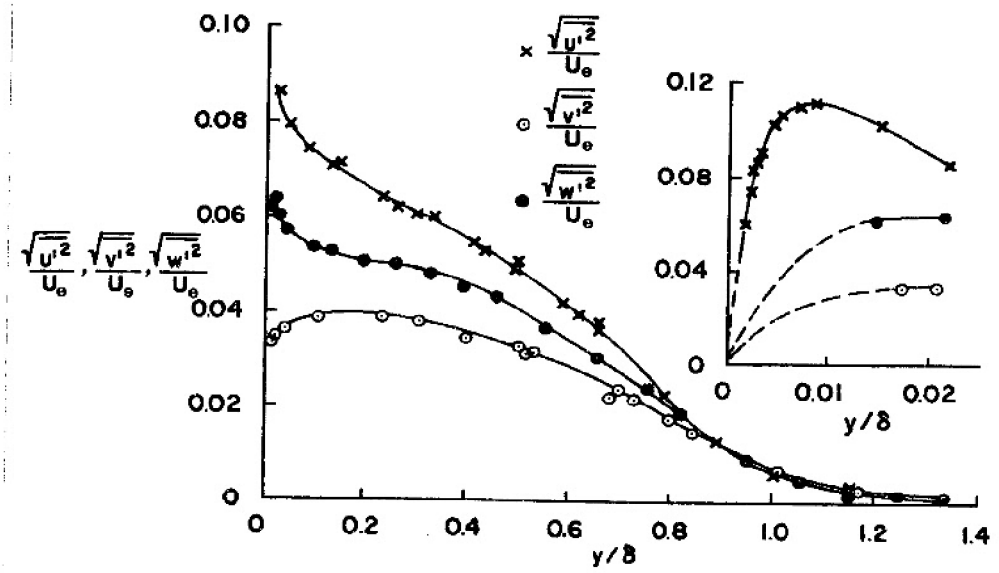

Figure 2.6: *Turbulence intensities for a flat-plate boundary layer of thickness δ. The inset shows values very close to the surface [From Klebanoff (1955)].*

This is the kinetic energy of the turbulent fluctuations per unit mass, and is the same as the quantity defined in Equation (1.3).

As a concluding comment, many turbulence models in current use cannot distinguish the individual normal Reynolds stresses. Rather, only k is provided from the turbulence model. When this is true, we often specify relative turbulence intensity by assuming the fluctuations are more-or-less **isotropic**, i.e., that $\overline{u'^2} \approx \overline{v'^2} \approx \overline{w'^2}$. We then define

$$T' \equiv 100\sqrt{\frac{2}{3}\frac{k}{U_e^2}} \tag{2.41}$$

which gives the relative intensity in percent.

2.5.2 Two-Point Correlation Tensors and Related Scales

All of the discussion in this chapter thus far has dealt with **single-point correlations**. That is, we have been dealing with correlations of turbulent fluctuations at a single point in the flowfield. However, as discussed at the end of Subsection 1.3.2, turbulent eddies are large (and long lived). Consequently, it cannot in general be described entirely in terms of local-flow properties. Townsend (1976) states this succinctly as follows.

Unlike the molecular motion of gases, the motion at any point in a turbulent flow affects the motion at other distant points through the pressure field, and an adequate description cannot be obtained by considering only mean values associated with single fluid particles. This might be put by saying that turbulent motion is less random and more [organized] than molecular motion, and that to describe the [organization] of the flow requires mean values of the functions of the flow variables for two or more particles at two or more positions.

In this subsection, we introduce the notion of **two-point correlations**, and introduce related time and length scales characteristic of turbulent motion.

There are two types of two-point correlations commonly used in experimental and theoretical turbulence studies. One involves a separation in time while the other is based on a spatial separation. The two are related by Taylor's (1935) hypothesis, which assumes temporal and spatial separations are related by

$$\frac{\partial}{\partial t} = -U\frac{\partial}{\partial x} \tag{2.42}$$

This implies the turbulent fluctuations are convected along at the mean-flow speed, U. The Taylor hypothesis is valid provided the turbulent fluctuations are sufficiently weak to avoid inducing significant alterations in the rate at which they are convected. This relationship permits inferring more-relevant two-point space-correlation information from easier-to-measure one-point time-correlation data.

Considering first correlation of velocities at one point and two different times, we define the **autocorrelation tensor**, viz.,

$$\mathcal{R}_{ij}(\mathbf{x}, t; t') = \overline{u_i'(\mathbf{x}, t)u_j'(\mathbf{x}, t + t')} \tag{2.43}$$

That is, we time average the fluctuating quantities at the same point in space but at different times. To see the connection to single-point statistics, note that the turbulence kinetic energy is half the trace of $\mathcal{R}_{ij}$ with $t' = 0$, i.e.,

$$k(\mathbf{x}, t) = \frac{1}{2}\mathcal{R}_{ii}(\mathbf{x}, t; 0) \tag{2.44}$$

A useful time scale characteristic of the energy-bearing eddies can be obtained by integrating $\mathcal{R}_{ii}$ over all possible values of t'. Thus, we arrive at the **integral time scale**,

$$\tau(\mathbf{x}, t) = \int_0^\infty \frac{\mathcal{R}_{ii}(\mathbf{x}, t; t')}{2k(\mathbf{x}, t)} dt' \tag{2.45}$$

In defining $\tau(\mathbf{x}, t)$, we have normalized $\mathcal{R}_{ii}$ relative to k. For experimental work involving stationary turbulence, i.e., turbulence for which mean values are

independent of time, we commonly work with the single streamwise component $\mathcal{R}_{11}(\mathbf{x};t') = \overline{u'(\mathbf{x},t)u'(\mathbf{x},t+t')}$. Normalizing with respect to $\overline{u'^2}$, we arrive at the **Eulerian time-correlation coefficient** defined by

$$\mathcal{R}_E(\mathbf{x};t') \equiv \frac{\overline{u'(\mathbf{x},t)u'(\mathbf{x},t+t')}}{\overline{u'^2}(\mathbf{x})} \tag{2.46}$$

By definition, $\mathcal{R}_E = 1$ when $t' = 0$. For large values of t', we expect the fluctuations to be uncorrelated so that $\mathcal{R}_E \to 0$ as $|t'| \to \infty$. Finally, shifting the time origin shows that $\mathcal{R}_{11}(\mathbf{x};t') = \mathcal{R}_{11}(\mathbf{x};-t')$, so that $\mathcal{R}_E$ is an even function of t'. Figure 2.7 shows a typical Eulerian time-correlation coefficient.

We can determine another time scale by noting the shape of the Eulerian time-correlation coefficient for small time displacement, t'. This is determined, of course, mainly by the small dissipating eddies. That is, expanding in Taylor series about $t' = 0$, we have

$$\mathcal{R}_E(\mathbf{x};t') = 1 + \frac{t'^2}{2}\left(\frac{\partial^2 \mathcal{R}_E}{\partial t'^2}\right)_{t'=0} + \cdots \approx 1 - \left(\frac{t'}{\tau_E}\right)^2 \tag{2.47}$$

where we define the **micro-time scale**, τ_E, as

$$\tau_E \equiv \sqrt{\frac{-2}{(\partial^2 \mathcal{R}_E/\partial t'^2)_{t'=0}}} \tag{2.48}$$

Figure 2.7 shows how Equation (2.47) relates geometrically to the exact time-correlation coefficient. Truncating beyond the term quadratic in t' yields a parabola known as the **osculating parabola**. Its curvature matches that of the exact curve at $t' = 0$. The intercept with the horizontal axis is at $t = \tau_E$.

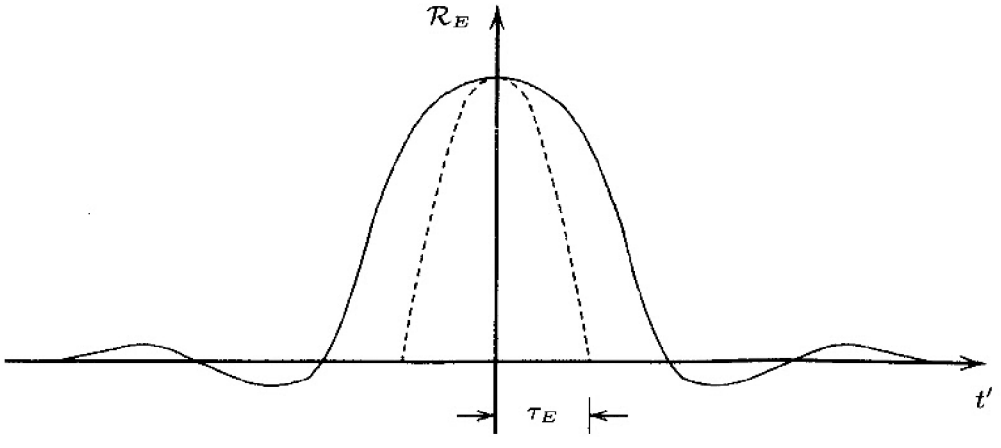

Figure 2.7: *A typical Eulerian time-correlation coefficient (—) with its osculating parabola (- - -).*

Turning now to the two-point space correlation, we consider two points in the flow, say **x** and **x+r**, and do our time average. The **two-point velocity correlation tensor** is defined as

$$R_{ij}(\mathbf{x}, t; \mathbf{r}) = \overline{u_i'(\mathbf{x}, t) u_j'(\mathbf{x} + \mathbf{r}, t)} \tag{2.49}$$

Here, the vector **r** is the displacement vector between the two points in the flow. As with the autocorrelation tensor, the turbulence kinetic energy is simply one half the trace of R_{ij} with zero displacement. viz.,

$$k(\mathbf{x}, t) = \frac{1}{2} R_{ii}(\mathbf{x}, t; \mathbf{0}) \tag{2.50}$$

Normalizing R_{ij} with respect to k, the **integral length scale**, ℓ, is defined as the integral of R_{ii} over all displacements, $r = |\mathbf{r}|$, so that

$$\ell(\mathbf{x}, t) \equiv \frac{3}{16} \int_0^\infty \frac{R_{ii}(\mathbf{x}, t; r)}{k(\mathbf{x}, t)} dr \tag{2.51}$$

where $3/16$ is a scaling factor.

In an entirely analogous manner to our analysis of two-point time correlations, we can determine a length scale corresponding to the smallest eddies. We work with the **longitudinal correlation function** for stationary turbulence defined by

$$f(x; r) \equiv \frac{R_{11}(x; r)}{\overline{u'^2}(x)} \tag{2.52}$$

Constructing the osculating parabola for $f(x)$, we find the **Taylor microscale** given by

$$\lambda \equiv \sqrt{\frac{-2}{\left(\partial^2 f / \partial x^2\right)_{x=0}}} \tag{2.53}$$

Taylor's hypothesis tells us the micro-time scale, τ_E, is related to λ by

$$\lambda = U \tau_E \tag{2.54}$$

As a final comment, when the turbulence is homogeneous and isotropic, the analysis of Taylor (1935) shows that the turbulence kinetic energy decays according to

$$\frac{dk}{dt} = -\frac{10 \nu k}{\lambda^2} \tag{2.55}$$

To see how λ relates to the Kolmogorov length, we note that for homogeneous, isotropic turbulence, the rate of decay of k is simply the dissipation rate, ϵ, so that

$$\frac{dk}{dt} = -\epsilon \qquad \Longrightarrow \qquad \epsilon = \frac{10 \nu k}{\lambda^2} \tag{2.56}$$

Provided the Reynolds number is not too small, Taylor argues that $\epsilon \sim k^{3/2}/\ell$. We can sharpen the estimate by appealing to measurements that indicate

$$\epsilon \approx 0.09\frac{k^{3/2}}{\ell} \qquad \Longrightarrow \qquad k \approx \left(\frac{\epsilon\ell}{0.09}\right)^{2/3} \tag{2.57}$$

Then, using the definition of the Kolmogorov length, $\eta = (\nu^3/\epsilon)^{1/4}$, [see Equation (1.1)] combining Equations (2.56) and (2.57) yields

$$\frac{\lambda}{\eta} \approx 7\left(\frac{\ell}{\eta}\right)^{1/3} \tag{2.58}$$

Since ℓ/η must be at least 10^3 to have a well-defined inertial subrange, the Taylor microscale will be at least 70 times the Kolmogorov length. It will typically lie within the inertial subrange, but well above the range of the very smallest eddies.

Such a hybrid parameter is of questionable value in turbulence modeling research, which, for the sake of simplicity, attempts to separate the physics of the large eddies from that of the small eddies. Recall, for example, how the assumption of a "wide separation of scales" is used to deduce the Kolmogorov $-5/3$ law (Subsection 1.3.4) and the logarithmic law of the wall (Subsection 1.3.5). To understand why the Taylor microscale is a hybrid length scale, observe that we can use Equation (2.56) to solve for λ, viz.,

$$\lambda = \sqrt{\frac{10\nu k}{\epsilon}} \tag{2.59}$$

Hence, this length scale involves a quantity characteristic of the large, energy-bearing eddies, k, as well as quantities characteristic of the small, dissipating eddies, ν and ϵ. Because the Taylor microscale is generally too small to characterize large eddies and too large to characterize small eddies, it has generally been ignored in most turbulence-modeling research. The same comments apply to the micro-time scale, τ_e.

Problems

2.1 Develop the time-averaged form of the equation of state for a perfect gas, $p = \rho RT$, accounting for turbulent fluctuations in the instantaneous pressure, p, density, ρ, and temperature, T.

2.2 Suppose we have a velocity field that consists of: (i) a slowly varying component $U(t) = U_0 e^{-t/\tau}$ where U_0 and τ are constants and (ii) a rapidly varying component $u' = aU_0 \cos(2\pi t/\epsilon^2\tau)$ where a and ϵ are constants with $\epsilon \ll 1$. We want to show that by choosing $T = \epsilon\tau$, the limiting process in Equation (2.9) makes sense.

(a) Compute the exact time average of $u = U + u'$.

(b) Replace T by $\epsilon\tau$ in the slowly varying part of the time average of u and let $t_f = \epsilon^2\tau$ in the fluctuating part of u to show that

$$\overline{U + u'} = U(t) + O(\epsilon)$$

where $O(\epsilon)$ denotes a quantity that goes to zero linearly with ϵ as $\epsilon \to 0$.

(c) Repeat Parts (a) and (b) for du/dt, and verify that in order for Equation (2.13) to hold, necessarily $a \ll \epsilon$.

2.3 For an imposed periodic mean flow, a standard way of decomposing flow properties is to write

$$u(\mathbf{x}, t) = U(\mathbf{x}) + \hat{u}(\mathbf{x}, t) + u'(\mathbf{x}, t)$$

where $U(\mathbf{x})$ is the mean-value, $\hat{u}(\mathbf{x}, t)$ is the organized response component due to the imposed organized unsteadiness, and $u'(\mathbf{x}, t)$ is the turbulent fluctuation. $U(\mathbf{x})$ is defined as in Equation (2.5). We also use the **Phase Average** defined by

$$< u(\mathbf{x}, t) > \equiv \lim_{N \to \infty} \frac{1}{N} \sum_{n=0}^{N-1} u(\mathbf{x}, t + n\tau)$$

where τ is the period of the imposed excitation. Then, by definition,

$$< u(\mathbf{x}, t) > = U(\mathbf{x}) + \hat{u}(\mathbf{x}, t), \quad \overline{< u(\mathbf{x}, t) >} = U(\mathbf{x}), \quad < \hat{u}(\mathbf{x}, t) > = \hat{u}(\mathbf{x}, t)$$

Verify the following. Do not assume that $\hat{u}$ is sinusoidal.

(a) $\overline{\hat{u}} = 0$
(b) $\overline{u'} = 0$
(c) $\overline{\hat{u}v'} = 0$
(d) $< U > = U$
(e) $< u' > = 0$
(f) $< Uv > = U < v >$
(g) $< \hat{u}v > = \hat{u} < v >$
(h) $< \hat{u}v' > = 0$

2.4 Compute the difference between the Reynolds average of a triple product $\lambda\delta\sigma$ and the product of the means, $\Lambda\Delta\Sigma$.

2.5 Compute the difference between the Reynolds average of a quadruple product $\phi\psi\xi\upsilon$ and the product of the means, $\Phi\Psi\Xi\Upsilon$.

2.6 For an incompressible flow, we have an imposed freestream velocity given by

$$u(x,t) = U_o(1 - ax) + U_o ax \sin 2\pi ft$$

where a is a constant of dimension 1/length, U_o is a constant reference velocity, and f is frequency. Integrating over one period, compute the average pressure gradient, dP/dx, for $f = 0$ and $f \neq 0$ in the freestream where the inviscid Euler equation holds, i.e.,

$$\rho \frac{\partial u}{\partial t} + \rho u \frac{\partial u}{\partial x} = -\frac{\partial p}{\partial x}$$

2.7 Consider the Reynolds-stress equation as stated in Equation (2.34).

(a) Show how Equation (2.34) follows from Equation (2.33).

(b) Contract Equation (2.34), i.e., set $i = j$ and perform the indicated summation, to derive a differential equation for the kinetic energy of the turbulence per unit mass defined by $k \equiv \frac{1}{2}\overline{u_i' u_i'}$.

2.8 Consider the third-rank tensor $\overline{u_i' u_j' u_k'}$ appearing in Equation (2.33). In general, third-rank tensors have 27 components. Verify that this tensor has only 10 independent components and list them.

2.9 If we rotate the coordinate system about the z axis by an angle θ, the Reynolds stresses for an incompressible two-dimensional boundary layer transform according to:

$$\begin{aligned}
\tau_{xx}' &= \frac{1}{2}(\tau_{xx} + \tau_{yy}) + \frac{1}{2}(\tau_{xx} - \tau_{yy})\cos 2\theta + \tau_{xy}\sin 2\theta \\
\tau_{yy}' &= \frac{1}{2}(\tau_{xx} + \tau_{yy}) - \frac{1}{2}(\tau_{xx} - \tau_{yy})\cos 2\theta - \tau_{xy}\sin 2\theta \\
\tau_{xy}' &= \tau_{xy}\cos 2\theta - \frac{1}{2}(\tau_{xx} - \tau_{yy})\sin 2\theta \\
\tau_{zz}' &= \tau_{zz}
\end{aligned}$$

Assume the normal Reynolds stresses, $\tau_{xx} = -\overline{u'^2}$, etc. are given by Equation (2.39), and that the Reynolds shear stress is $\tau_{xy} = -\overline{u'v'} \approx \frac{3}{10}k$.

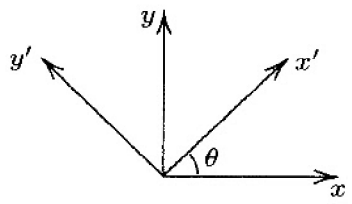

Problem 2.9

(a) Determine the angle the *principal axes* make with the xy axes, i.e., the angle that yields $\tau_{xy}' = 0$.

(b) What is the Reynolds-stress tensor, τ_{ij}', in the *principal axis* system?

2.10 Using Figure 2.6, determine the values of $\overline{u'^2}/k$, $\overline{v'^2}/k$ and $\overline{w'^2}/k$ for dimensionless distances from the surface of $y/\delta = 0.2$, 0.4 and 0.6. Determine the percentage differences between measured values and the following approximations.

(a) Equation (2.39)

(b) $\overline{u'^2} \approx k$, $\overline{v'^2} \approx \frac{2}{5}k$, $\overline{w'^2} \approx \frac{3}{5}k$

2.11 Verify that, for homogeneous-isotropic turbulence, the ratio of the *micro-time scale*, τ_E, to the Kolmogorov time scale varies linearly with the isotropic turbulence-intensity parameter, T'.

Chapter 3

Algebraic Models

The simplest of all turbulence models are described as algebraic. These models use the **Boussinesq eddy-viscosity approximation**[1] to compute the Reynolds stress tensor as the product of an eddy viscosity and the mean strain-rate tensor. For computational simplicity, the eddy viscosity, in turn, is often computed in terms of a mixing length that is analogous to the mean free path in a gas. In contrast to the molecular viscosity, which is an intrinsic property of the fluid, the eddy viscosity (and hence the mixing length) depends upon the flow. Because of this, the eddy viscosity and mixing length must be specified in advance, most simply, by an *algebraic* relation between eddy viscosity and length scales of the mean flow. Thus, algebraic models are, by definition, **incomplete** models of turbulence. This is by no means a pejorative term as incomplete models have proven to be useful in many engineering fields.

We begin this chapter by first discussing molecular transport of momentum. Next we introduce Prandtl's mixing-length hypothesis and discuss its physical implications and limitations. The mixing-length model is then applied to free shear flows for which self-similar solutions hold. We discuss two modern algebraic turbulence models that are based on the mixing-length hypothesis, including applications to attached and separated wall-bounded flows. The latter applications illustrate the limit to the algebraic model's range of applicability. An interesting separated-flow replacement for algebraic models, known as the **Half-Equation Model**, improves agreement between computed and measured flow properties. The chapter concludes with a discussion of the range of applicability of algebraic and half-equation models.

[1] Throughout this text, we use the terminology Boussinesq **approximation** for consistency with general turbulence literature. Strictly speaking, we could more aptly describe it as the Boussinesq **assumption** since it is not an approximation in any useful sense. By contrast, specific formulas for the eddy viscosity are.

3.1 Molecular Transport of Momentum

To understand the motivation for the Boussinesq approximation, it is instructive to discuss momentum transport at the molecular level. However, as a word of caution, **molecules and turbulent eddies are fundamentally different**. They are so different that we will ultimately find, in Section 3.2, that the analogy between turbulent and molecular mixing is false! It is nevertheless fruitful to pursue the analogy to illustrate how important it is to check the premises underlying turbulence closure approximations. At first glance, mimicking the molecular mixing process appears to be a careful exercise in physics. As we will see, the model just cannot stand up under close scrutiny.

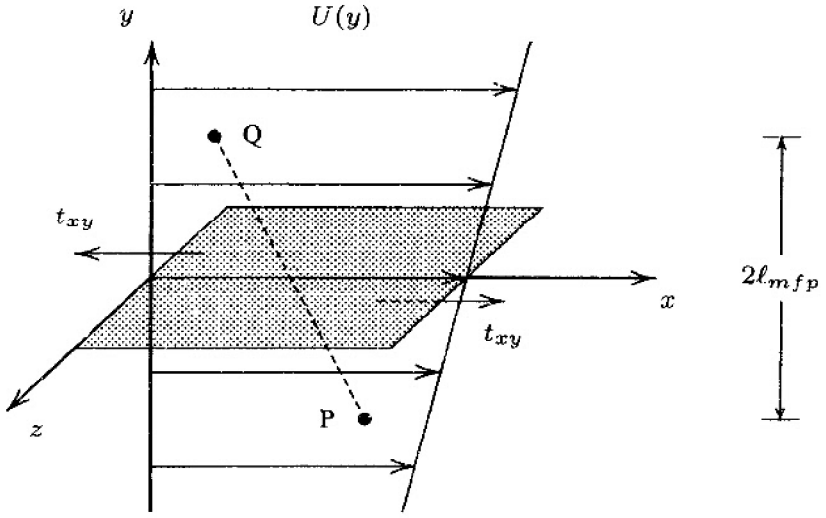

Figure 3.1: *Shear-flow schematic.*

We begin by considering a shear flow in which the velocity is given by

$$\mathbf{U} = U(y)\,\mathbf{i} \tag{3.1}$$

where $\mathbf{i}$ is a unit vector in the x direction. Figure 3.1 depicts such a flow. We consider the flux of momentum across the plane $y = 0$, noting that molecular motion is random in both magnitude and direction. Molecules migrating across $y = 0$ are **typical of where they come from**. That is, molecules moving up bring a momentum deficit and vice versa. This gives rise to a shear stress t_{xy}.

At the molecular level, we decompose the velocity according to

$$\mathbf{u} = \mathbf{U} + \mathbf{u}'' \tag{3.2}$$

where **U** is the average velocity defined in Equation (3.1) and $\mathbf{u}''$ represents the random molecular motion. The instantaneous flux of any property across $y = 0$ is proportional to the velocity normal to the plane which, for this flow, is simply v''. Thus, the instantaneous flux of x-directed momentum, dp_{xy}, across a differential surface area dS normal to the y direction is

$$dp_{xy} = \rho(U + u'')v''dS \tag{3.3}$$

Performing an ensemble average over all molecules, we find

$$dP_{xy} = \overline{\rho u''v''}dS \tag{3.4}$$

The stress acting on $y = 0$ is defined by $\sigma_{xy} = dP_{xy}/dS$. It is customary in fluid mechanics to set $\sigma_{ij} = p\delta_{ij} - t_{ij}$, where p is pressure and t_{ij} is the viscous stress tensor. Thus,

$$t_{xy} = -\overline{\rho u''v''} \tag{3.5}$$

Equation (3.5) bears a strong resemblance to the Reynolds-stress tensor. This is not a coincidence. As pointed out by Tennekes and Lumley (1983), a stress that is generated as a momentum flux can always be written in this form. The only real difference is that, at the macroscopic level, the turbulent fluctuations, u' and v', appear in place of the random molecular fluctuations, u'' and v''. **This similarity is the basis of the Boussinesq eddy-viscosity approximation.**

Referring again to Figure 3.1, we can appeal to arguments from the kinetic theory of gases [e.g., Jeans (1962)] to determine t_{xy} in terms of $U(y)$ and the fluid viscosity, μ. First, consider the average number of molecules moving across unit area in the positive y direction. For a perfect gas, molecular velocities follow the Maxwellian distribution so that all directions are equally probable. The average molecular velocity is the thermal velocity, v_{th}, which is approximately 4/3 times the speed of sound in air. On average, half of the molecules move in the positive y direction while the other half move downward. The average vertical component of the velocity is $v_{th}\cos\phi$ where ϕ is the angle from the vertical. Integrating over a hemispherical shell, the average vertical speed is $v_{th}/2$. Thus, the average number of molecules moving across unit area in the positive y direction is $nv_{th}/4$, where n is the number of molecules per unit volume.

Now consider the transfer of momentum that occurs when molecules starting from point P cross the $y = 0$ plane. As stated earlier, we assume molecules are **typical of where they come from**. On the molecular scale, this is one mean free path away, the mean free path being the average distance a molecule travels between collisions with other molecules. Each molecule starting from a point P below $y = 0$ brings a momentum deficit of $m[U(0) - U(-\ell_{mfp})]$, where m is the molecular mass and ℓ_{mfp} is the mean free path. Hence, the momentum flux from below is

$$\Delta P_{-} = \frac{1}{4}\rho v_{th}[U(0) - U(-\ell_{mfp})] \approx \frac{1}{4}\rho v_{th}\ell_{mfp}\frac{dU}{dy} \tag{3.6}$$

We have replaced $U(-\ell_{mfp})$ by the first two terms of its Taylor-series expansion in Equation (3.6) and used the fact that $\rho = mn$. Similarly, each molecule moving from a point Q above the plane $y = 0$ brings a momentum surplus of $m[U(\ell_{mfp}) - U(0)]$, and the momentum flux from above is

$$\Delta P_+ = \frac{1}{4}\rho v_{th}[U(\ell_{mfp}) - U(0)] \approx \frac{1}{4}\rho v_{th}\ell_{mfp}\frac{dU}{dy} \tag{3.7}$$

Consequently, the net shearing stress is the sum of ΔP_- and ΔP_+, wherefore

$$t_{xy} = \Delta P_- + \Delta P_+ \approx \frac{1}{2}\rho v_{th}\ell_{mfp}\frac{dU}{dy} \tag{3.8}$$

Hence, we conclude that the shear stress resulting from molecular transport of momentum in a perfect gas is given by

$$t_{xy} = \mu\frac{dU}{dy} \tag{3.9}$$

where μ is the molecular viscosity defined by

$$\mu = \frac{1}{2}\rho v_{th}\ell_{mfp} \tag{3.10}$$

The arguments leading to Equations (3.9) and (3.10) are approximate and only roughly represent the true statistical nature of molecular motion. Interestingly, Jeans (1962) indicates that a precise analysis yields $\mu = 0.499\rho v_{th}\ell_{mfp}$, wherefore our approximate analysis is remarkably accurate! However, we have made two implicit assumptions in our analysis that require justification.

First, we have truncated the Taylor series appearing in Equations (3.6) and (3.7) at the linear terms. For this approximation to be valid, we must have $\ell_{mfp}|d^2U/dy^2| \ll |dU/dy|$. The quantity L defined by

$$L \equiv \frac{|dU/dy|}{|d^2U/dy^2|} \tag{3.11}$$

is a length scale characteristic of the mean flow. Thus, the linear relation between stress and strain-rate implied by Equation (3.9) is valid provided the Knudsen number, Kn, is very small, i.e.,

$$Kn = \ell_{mfp}/L \ll 1 \tag{3.12}$$

For most practical flow conditions,[2] the mean free path is several orders of magnitude smaller than any characteristic length scale of the mean flow. Thus, Equation (3.12) is satisfied for virtually all terrestrial engineering problems.

[2]Two noteworthy exceptions are very-high altitude flight and micron-scale flows such as those encountered in micro-machinery.

Second, in computing the rate at which molecules cross $y = 0$, we assumed that $\mathbf{u}''$ remained Maxwellian even in the presence of shear. This will be true if molecules experience many collisions on the time scale of the mean flow for, otherwise, they would have insufficient time to adjust to mean-flow changes. Now, the average time between collisions is ℓ_{mfp}/v_{th}. The characteristic time scale for the mean flow is $|dU/dy|^{-1}$. Thus, we also require that

$$\ell_{mfp} \ll \frac{v_{th}}{|dU/dy|} \tag{3.13}$$

Since v_{th} is of the same order of magnitude as the speed of sound, the right-hand side of Equation (3.13) defines yet another mean-flow length scale. As above, the mean free path is several orders smaller than this length scale for virtually all flows of engineering interest.

3.2 The Mixing-Length Hypothesis

Prandtl (1925) put forth the mixing-length hypothesis. He visualized a simplified model for turbulent motion in which fluid particles coalesce into lumps that cling together and move as a unit. He further visualized that in a shear flow such as that depicted in Figure 3.1, the lumps retain their x-directed momentum for a distance in the y direction, ℓ_{mix}, that he called the mixing length. In analogy to the molecular momentum transport process with Prandtl's lump of fluid replacing the molecule and ℓ_{mix} replacing ℓ_{mfp}, we can say that similar to Equation (3.8),

$$\rho\tau_{xy} = \frac{1}{2}\rho v_{mix}\ell_{mix}\frac{dU}{dy} \quad \Longrightarrow \quad \tau_{xy} = \frac{1}{2}v_{mix}\ell_{mix}\frac{dU}{dy} \tag{3.14}$$

The formulation is not yet complete because the **mixing velocity**, v_{mix}, has not been specified. Prandtl further postulated that

$$v_{mix} = \text{constant} \cdot \ell_{mix}\left|\frac{dU}{dy}\right| \tag{3.15}$$

which makes sense on dimensional grounds. Because ℓ_{mix} is not a physical property of the fluid, we can always absorb the constant in Equation (3.15) and the factor 1/2 in Equation (3.14) in the mixing length. Thus, by analogy to Equations (3.9) and (3.10), Prandtl's mixing-length hypothesis leads to

$$\tau_{xy} = \nu_T\frac{dU}{dy} \tag{3.16}$$

where ν_T is the kinematic **eddy viscosity** given by

$$\nu_T = \ell_{mix}^2\left|\frac{dU}{dy}\right| \tag{3.17}$$

Our formulation still remains incomplete since we have replaced Boussinesq's empirical eddy viscosity, ν_T, with Prandtl's empirical mixing length, ℓ_{mix}. Prandtl postulated further that for flows near solid boundaries the mixing length is proportional to distance from the surface. This turns out to be a reasonably good approximation over a limited portion of a turbulent wall flow. As we will see in Section 3.3, for free shear flows such as jets, wakes and mixing layers, the mixing length is proportional to the width of the layer, δ. However, each of these flows requires a different coefficient of proportionality between ℓ_{mix} and δ. The point is, the mixing length is different for each flow (its ratio to the flow width, for example) and must be known in advance to obtain a solution.

Note that Equation (3.17) can be deduced directly from dimensional analysis. Assuming molecular transport of momentum is unimportant relative to turbulent transport, we expect molecular viscosity to have no significance in a dimensional analysis. The only other dimensional parameters available in a shear flow are the assumed mixing length, ℓ_{mix}, and the velocity gradient, dU/dy. (The eddy viscosity cannot depend upon U since that would violate Galilean invariance.) A straightforward dimensional analysis yields Equation (3.17).

Another interesting observation follows from replacing τ_{xy} by its definition so that

$$-\overline{u'v'} = \ell_{mix}^2 \left|\frac{dU}{dy}\right| \frac{dU}{dy} \tag{3.18}$$

The mixing velocity, v_{mix}, must be proportional to an appropriate average of v' such as the RMS value defined by $v_{rms} = (\overline{v'^2})^{1/2}$. Also, Townsend (1976) states that in most turbulent shear flows, measurements indicate

$$\left|-\overline{u'v'}\right| \approx 0.4 u_{rms} v_{rms} \tag{3.19}$$

Consequently, if $v_{rms} \sim v_{mix}$, comparison of Equations (3.15) and (3.18) shows that the mixing-length model implies v_{rms} and u_{rms} are of the same order of magnitude. This is generally true although u_{rms} is usually 25% to 75% larger than v_{rms} for typical shear flows.

At this point, we need to examine the appropriateness of the mixing-length hypothesis in representing the turbulent transport of momentum. Because we have made a direct analogy to the molecular transport process, we have implicitly made the same two basic assumptions we made for molecular transport. Specifically, we have assumed that the Boussinesq approximation holds and that the turbulence is unaltered by the mean shear. Unfortunately, neither condition is rigorously satisfied in practice!

Concerning the Boussinesq approximation, its applicability depends upon the Knudsen number being small. Close to a solid boundary, for example, the mixing length is approximately linear with distance from the surface, y. Specifically, measurements indicate that $\ell_{mix} \approx 0.41y$. In the same vicinity, the velocity

follows the well-known law of the wall [see Subsection 1.3.5], and the velocity gradient varies inversely with y. Thus, the length L defined in Equation (3.11) is equal to y. Consequently, the Knudsen number is of order one, i.e.,

$$Kn = \ell_{mix}/L \approx 0.41 \tag{3.20}$$

Hence, the linear stress/strain-rate relation of Equation (3.16) is suspect.

Concerning the effect of the mean shear on the turbulence, the assumed lifetime of Prandtl's lumps of fluid is ℓ_{mix}/v_{mix}. Reference to Equation (3.15) shows that this time is proportional to $|dU/dy|^{-1}$. Hence, the analog to Equation (3.13) is

$$\ell_{mix} \sim \frac{v_{mix}}{|dU/dy|} \tag{3.21}$$

Because we do not have $\ell_{mix} \ll v_{mix}/|dU/dy|$, Equation (3.21) tells us that the lumps of fluid will undergo changes as they travel from points P and Q toward $y = 0$. This is indeed consistent with the observed nature of turbulent shear flows. Tennekes and Lumley (1983) describe the situation by saying, "the general conclusion must be that turbulence in a shear flow cannot possibly be in a state of equilibrium which is independent of the flow field involved. The turbulence is continually trying to adjust to its environment, without ever succeeding."

Thus, the theoretical foundation of the mixing-length hypothesis is a bit flimsy to say the least. On the one hand, this is a forewarning that a turbulence model built on this foundation is unlikely to possess a very wide range of applicability. On the other hand, as the entire formulation is empirical in its essence, the usefulness of and justification for any of its approximations ultimately lies in how well the model performs in applications, and we defer to the applications of the following sections as its justification.

As a pleasant surprise, we will see that despite its theoretical shortcomings, the mixing-length model does an excellent job of reproducing measurements. It can be easily calibrated for a specific class of flows, and the model's predictions are consistent with measurements provided we don't depart too far from the established data base used to calibrate the mixing length. Eddy-viscosity models based on the mixing length have been fine tuned for many flows since 1925, most notably by Cebeci and Smith (1974). Strictly speaking, the term **equilibrium** is nonsensical in the context of turbulent shear flows since, as noted above, turbulence is continually attempting to adjust to its environment, without ever succeeding. Nevertheless, most turbulence researchers describe certain flows as **equilibrium turbulent flows**. What they actually mean is a relatively simple flow with slowly-varying properties. Most flows of this type can be accurately described by a mixing-length computation. In this spirit, a fitting definition of equilibrium turbulent flow might be a flow that can be accurately described using a mixing-length model!

3.3 Application to Free Shear Flows

Our first applications will be to incompressible **free shear flows**. A flow is termed free if it is not bounded by solid surfaces. Figure 3.2 illustrates five different types of free shear flows, viz., the **far wake**, the **mixing layer**, the **plane jet**, the **round jet** and the "constrained" **radial jet**. A wake forms downstream of any object placed in a stream of fluid; we will consider only the two-dimensional wake. A mixing layer occurs between two parallel streams moving at different speeds; for the case shown in the figure, the lower stream is at rest. A plane jet (two-dimensional) and a round jet (axisymmetric) occur when fluid is ejected from a nozzle or orifice. A radial jet[3] occurs when two jets of equal strength impinge on one another. We will analyze all three jet configurations, assuming the jet issues into a quiescent fluid.

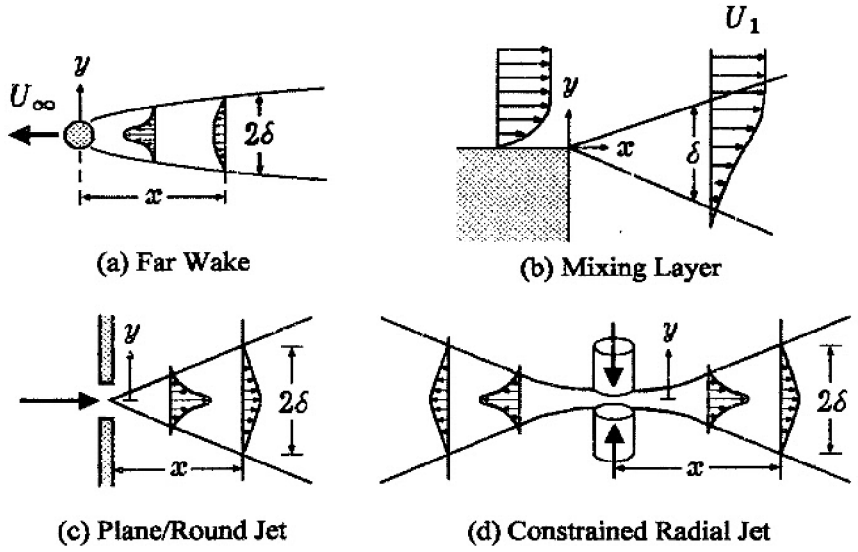

Figure 3.2: *Free shear flows.*

All five of these flows approach what is known as **self similarity** far enough downstream that details of the geometry and flow conditions near $x = 0$ become unimportant. The velocity component $U(x, y)$, for example, can be expressed as

$$U(x, y) = u_o(x)F(y/\delta(x)) \tag{3.22}$$

Similar expressions hold for τ_{xy} and ν_T. This amounts to saying that two velocity profiles located at different x stations have the same shape when plotted in the scaled form $U(x, y)/u_o(x)$ [or $(U_\infty - U(x, y))/u_o(x)$ for the wake] versus $y/\delta(x)$. Flows with this property are also referred to as **self preserving**.

[3]We will confine our analysis to the "constrained" radial jet for which the distance between the opposing jets is small compared to the jet nozzle diameter.

Free shear flows are interesting building-block cases to test a turbulence model on for several reasons. First, there are no solid boundaries so that we avoid the complications boundaries add to the complexity of a turbulent flow. Second, they are mathematically easy to calculate because similarity solutions exist, where the Reynolds-averaged equations of motion can be reduced to ordinary differential equations. This greatly simplifies the task of obtaining a solution. Third, there is a wealth of experimental data available to test model predictions against.

The standard boundary-layer approximations hold for all five of the shear flows considered in this section. Additionally, molecular transport of momentum is negligible compared to turbulent transport. Since all five flows have constant pressure, the equations of motion are (with $m = j = 0$ for the wake, the mixing layer and the plane jet; $m = 0$ and $j = 1$ for the round jet; and $m = 1$ and $j = 0$ for the radial jet):

$$\frac{1}{x^m}\frac{\partial}{\partial x}\left(x^m U\right) + \frac{1}{y^j}\frac{\partial}{\partial y}\left(y^j V\right) = 0 \tag{3.23}$$

$$U\frac{\partial U}{\partial x} + V\frac{\partial U}{\partial y} = \frac{1}{y^j}\frac{\partial}{\partial y}\left(y^j \tau_{xy}\right) \tag{3.24}$$

where y is as shown in Figure 3.2. Of course, while the equations are the same for all five flows, boundary conditions are different. The appropriate boundary conditions will be stated when we discuss each flow.

As a historical note, in addition to the mixing-length model, Prandtl also proposed a simpler eddy-viscosity model specifically for free shear flows, viz.,

$$\nu_T = \chi[U_{max}(x) - U_{min}(x)]\delta(x) \tag{3.25}$$

where U_{max} and U_{min} are the maximum and minimum values of mean velocity in the layer, δ is the half width of the layer, and χ is a dimensionless empirical parameter that we refer to as a **closure coefficient**. This model is very convenient for free shear flows because it is a function only of x by construction, and acceptable results can be obtained if χ is assumed to be constant across the layer. Consequently, laminar-flow solutions can be generalized for turbulent flow with, at most, minor notation changes. We leave application of this model to the problems section. All of the applications in this section will be done using Equations (3.16) and (3.17).

We begin by analyzing the far wake in Subsection 3.3.1. Complete details of the similarity-solution method are given for the benefit of the reader who has not had much experience with this method. The far wake is especially attractive as our first application because a simple closed-form solution can be obtained using the mixing-length model. Then, we proceed to the mixing layer in Subsection 3.3.2. While an analytical solution is possible for the mixing layer, numerical integration of the equations proves to be far simpler. Finally, we study the plane, round and radial jets in Subsection 3.3.3.

3.3.1 The Far Wake

Clearly, the flow in the wake of the body indicated in Figure 3.2(a) is symmetric about the x axis. Thus, we solve for $0 \leq y < \infty$. Boundary conditions follow from symmetry on the axis and the requirement that the velocity approach its freestream value far from the body. Hence,

$$U(x, y) \rightarrow U_\infty \qquad \text{as} \qquad y \rightarrow \infty \tag{3.26}$$

$$\frac{\partial U}{\partial y} = 0 \qquad \text{at} \qquad y = 0 \tag{3.27}$$

The classical approach to this problem is to linearize the momentum equation, an approximation that is strictly valid only in the far wake [Schlichting-Gersten (1999)]. Thus, we say that

$$\mathbf{U}(x, y) = U_\infty \, \mathbf{i} - \hat{\mathbf{u}} \tag{3.28}$$

where $|\hat{\mathbf{u}}| \ll U_\infty$. The linearized momentum equation and boundary conditions become

$$U_\infty \frac{\partial \hat{u}}{\partial x} = -\frac{\partial \tau_{xy}}{\partial y} \tag{3.29}$$

$$\hat{u}(x, y) \rightarrow 0 \qquad \text{as} \qquad y \rightarrow \infty \tag{3.30}$$

$$\frac{\partial \hat{u}}{\partial y} = 0 \qquad \text{at} \qquad y = 0 \tag{3.31}$$

There is also an integral constraint that must be satisfied by the solution. If we consider a control volume surrounding the body and extending to infinity, conservation of momentum leads to the following requirement [see Schlichting-Gersten (1999)],

$$\int_0^\infty \rho U (U_\infty - U) \, dy = \frac{1}{2} D \tag{3.32}$$

where D is the drag of the body per unit width.

We use the mixing-length model to specify the Reynolds shear stress, τ_{xy}, which means we write

$$\tau_{xy} = -\ell_{mix}^2 \left| \frac{\partial \hat{u}}{\partial y} \right| \frac{\partial \hat{u}}{\partial y} \tag{3.33}$$

Finally, to close our set of equations, we assume the mixing length is proportional to the half-width of the wake, $\delta(x)$ [see Figure 3.2(a)]. Thus, we say that

$$\ell_{mix} = \alpha \delta(x) \tag{3.34}$$

where α is a closure coefficient. Our fondest hope would be that the same value of α works for all free shear flows, and is independent of y/δ. Unfortunately, this is not the case, which means the mixing-length model must be recalibrated for each type of shear flow.

To obtain the similarity solution to Equations (3.29) through (3.34), we proceed in a series of interrelated steps. The sequence is as follows.

1. Assume the form of the solution.
2. Transform the equations of motion.
3. Transform the boundary conditions and the integral constraint.
4. Determine the conditions required for existence of the similarity solution.
5. Solve the resulting ordinary differential equation subject to the transformed boundary conditions.

In addition to these 5 steps, we will also determine the value of the closure coefficient α in Equation (3.34) by comparison with experimental data.

Step 1. We begin by assuming the similarity solution can be written in terms of an as yet unknown velocity scale function, $u_o(x)$, and the wake half width, $\delta(x)$. Thus, we assume that the velocity can be written as

$$\hat{u}(x,y) = u_o(x)F(\eta) \tag{3.35}$$

where the **similarity variable**, η, is defined by

$$\eta = y/\delta(x) \tag{3.36}$$

Step 2. In order to transform Equation (3.29), we have to take account of the fact that we are making a formal change of dependent variables. We are transforming from (x,y) space to (x,η) space which means that derivatives must be transformed according to the chain rule of calculus. Thus, derivatives transform according to the following rules. Note that a subscript means that differentiation is done holding the subscripted variable constant.

$$\begin{aligned}\left(\frac{\partial}{\partial x}\right)_y &= \left(\frac{\partial x}{\partial x}\right)_y \left(\frac{\partial}{\partial x}\right)_\eta + \left(\frac{\partial \eta}{\partial x}\right)_y \left(\frac{\partial}{\partial \eta}\right)_x \\ &= \left(\frac{\partial}{\partial x}\right)_\eta + \left(\frac{\partial \eta}{\partial x}\right)_y \left(\frac{\partial}{\partial \eta}\right)_x \\ &= \left(\frac{\partial}{\partial x}\right)_\eta - \frac{\delta'(x)}{\delta(x)}\eta \left(\frac{\partial}{\partial \eta}\right)_x \end{aligned} \tag{3.37}$$

$$\begin{aligned}\left(\frac{\partial}{\partial y}\right)_x &= \left(\frac{\partial x}{\partial y}\right)_x \left(\frac{\partial}{\partial x}\right)_\eta + \left(\frac{\partial \eta}{\partial y}\right)_x \left(\frac{\partial}{\partial \eta}\right)_x \\ &= \left(\frac{\partial \eta}{\partial y}\right)_x \left(\frac{\partial}{\partial \eta}\right)_x \\ &= \frac{1}{\delta(x)} \left(\frac{\partial}{\partial \eta}\right)_x \end{aligned} \tag{3.38}$$

A prime denotes ordinary differentiation so that $\delta'(x) = d\delta/dx$ in Equation (3.37). We now proceed to transform Equation (3.29). For example, the derivatives of $\hat{u}$ are

$$\frac{\partial \hat{u}}{\partial x} = u_o' F(\eta) - \frac{u_o \delta'}{\delta} \eta \frac{dF}{d\eta} \tag{3.39}$$

$$\frac{\partial \hat{u}}{\partial y} = \frac{u_o}{\delta} \frac{dF}{d\eta} \tag{3.40}$$

Proceeding in this manner for all terms in Equation (3.29) and using the mixing-length prescription for the Reynolds stress leads to the transformed momentum equation.

$$\frac{U_\infty \delta u_o'}{u_o^2} F(\eta) - \frac{U_\infty \delta'}{u_o} \eta \frac{dF}{d\eta} = \alpha^2 \frac{d}{d\eta} \left(\left| \frac{dF}{d\eta} \right| \frac{dF}{d\eta} \right) \tag{3.41}$$

Step 3. Clearly, $y \to \infty$ corresponds to $\eta \to \infty$ and $y \to 0$ corresponds to $\eta \to 0$. Thus, the boundary conditions in Equations (3.30) and (3.31) transform to

$$F(\eta) \to 0 \qquad \text{as} \qquad \eta \to \infty \tag{3.42}$$

$$\frac{dF}{d\eta} = 0 \qquad \text{at} \qquad \eta = 0 \tag{3.43}$$

and the integral constraint becomes

$$\int_0^\infty F(\eta)\, d\eta = \frac{D}{2\rho U_\infty u_o \delta} \tag{3.44}$$

Step 4. In seeking a similarity solution, we are attempting to make a separation of variables. The two terms on the left-hand side of Equation (3.41) have coefficients that, in general, vary with x. Also, the right-hand side of Equation (3.44) is a function of x. **The condition for existence of the similarity solution is that these three coefficients be independent of** x. Thus, we require the following three conditions.

$$\frac{U_\infty \delta u_o'}{u_o^2} = a_1, \qquad \frac{U_\infty \delta'}{u_o} = a_2, \qquad \frac{D}{2\rho U_\infty u_o \delta} = 1 \tag{3.45}$$

The quantities a_1 and a_2 must, of course, be constant. Note that we could have introduced a third constant in the integral constraint, but it is unnecessary (we, in effect, absorb the third constant in δ). The solution to these three simultaneous equations is simply

$$\delta(x) = \sqrt{\frac{a_2 D x}{\rho U_\infty^2}} \tag{3.46}$$

$$u_o(x) = \frac{1}{2}\sqrt{\frac{D}{a_2 \rho x}} \tag{3.47}$$

$$a_1 = -a_2 \tag{3.48}$$

Step 5. Finally, we expect that $F(\eta)$ will have its maximum value on the axis, and then fall monotonically to zero approaching the freestream. If this is true, then $F'(\eta)$ will be negative for all values of η and we can replace its absolute value with $-F'(\eta)$. Taking account of Equations (3.45) through (3.48), the momentum equation now simplifies to

$$\alpha^2 \frac{d}{d\eta}\left[(F')^2\right] - a_2(\eta F' + F) = 0 \tag{3.49}$$

The second term is a perfect differential so that Equation (3.49) can be rewritten as

$$\frac{d}{d\eta}\left[\alpha^2 (F')^2 - a_2 \eta F\right] = 0 \tag{3.50}$$

Integrating once and imposing the symmetry condition at $\eta = 0$ [Equation (3.43)] yields

$$\alpha \frac{dF}{d\eta} = -\sqrt{a_2 \eta F} \tag{3.51}$$

where we observe that $F'(\eta)$ is everywhere less than zero. Integrating once more, we find that the solution for $F(\eta)$ is

$$F(\eta) = C^2\left[1 - (\eta/\eta_e)^{3/2}\right]^2 \tag{3.52}$$

where C is a constant of integration and η_e is given by

$$\eta_e = (3\alpha C/\sqrt{a_2}\,)^{2/3} \tag{3.53}$$

This solution has a peak value at $\eta = 0$ and decreases monotonically to zero as $\eta \to \eta_e$. It then increases without limit for $\eta > \eta_e$. The only way we can satisfy the far field boundary condition [Equation (3.42)] is to use Equation (3.52)

for $0 \leq \eta \leq \eta_e$ and to use the trivial solution, $F(\eta) = 0$, for values of η in excess of η_e.

With no loss of generality, we can set $\eta_e = 1$. To understand this, note that $\eta/\eta_e = y/[\eta_e \delta(x)]$. Hence, by setting $\eta_e = 1$ we simply rescale the η coordinate so that $\delta(x)$ is the wake half width as originally planned. Therefore,

$$3\alpha C = \sqrt{a_2} \tag{3.54}$$

Finally, imposing the integral constraint, Equation (3.44), yields an equation for the constant C. Performing the integration, we have

$$\int_0^1 C^2[1 - \eta^{3/2}]^2 \, d\eta = \frac{9}{20} C^2 = 1 \tag{3.55}$$

Therefore,

$$C = \sqrt{20}/3 = 1.491 \tag{3.56}$$

and

$$\alpha = \sqrt{a_2/20} \tag{3.57}$$

If the closure coefficient α were known, our solution would be completely determined at this point with Equation (3.57) specifying a_2. This is the nature of an **incomplete** turbulence model. The coefficient α is unknown because the mixing length [Equation (3.34)] is unknown a priori for this flow. To complete the solution, we appeal to experimental data [c.f. Schlichting-Gersten (1999)], which show that the wake half width grows according to

$$\delta(x) \approx 0.805 \sqrt{\frac{Dx}{\rho U_\infty^2}} \tag{3.58}$$

Comparison of Equations (3.46) and (3.58) shows that the value of a_2 is

$$a_2 = 0.648 \tag{3.59}$$

The value of the coefficient α then follows from Equation (3.57), i.e.,

$$\alpha = 0.18 \tag{3.60}$$

Collecting all of this, the final solution for the far wake, according to the mixing-length model is

$$U(x, y) = U_\infty - 1.38 \sqrt{\frac{D}{\rho x}} \left[1 - (y/\delta)^{3/2}\right]^2 \tag{3.61}$$

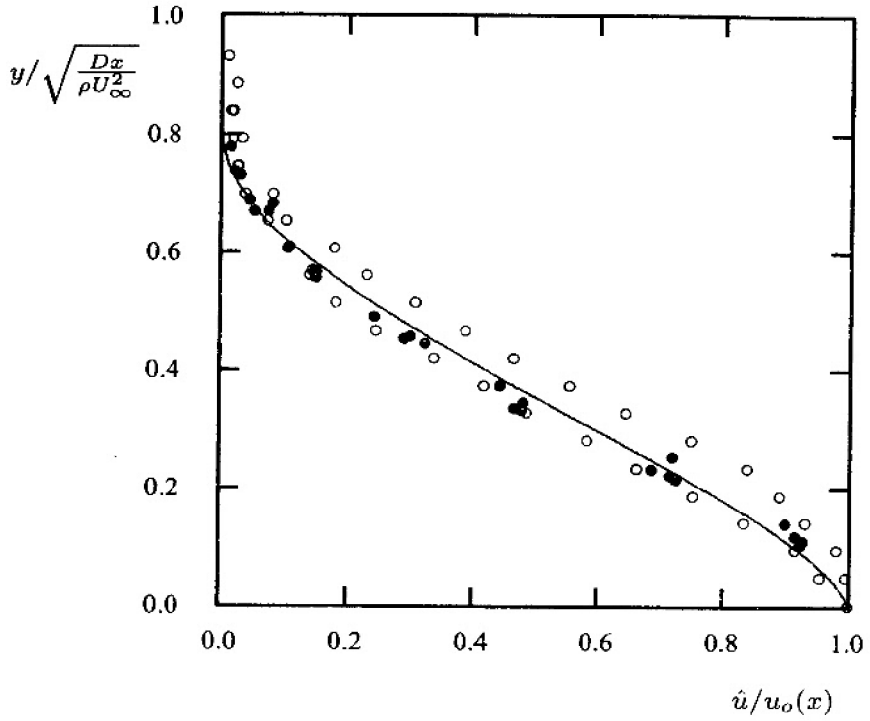

Figure 3.3: *Comparison of computed and measured far-wake velocity profiles:* — *Mixing length;* • *Fage and Falkner (1932);* ○ *Weygandt and Mehta (1995).*

where $\delta(x)$ is given by Equation (3.58). Figure 3.3 compares this profile with data of Fage and Falkner (1932) and the slightly asymmetrical wake data of Weygandt and Mehta (1995). As shown, the mixing-length model, once calibrated, does an excellent job of reproducing measured values. This solution has an interesting feature that we will see in many of our applications. Specifically, we have found a sharp turbulent/nonturbulent interface. This manifests itself in the nonanalytic behavior of the solution at $y/\delta = 1$, i.e., all derivatives of U above $\partial^2 U/\partial y^2$ are discontinuous at $y/\delta = 1$. Measurements confirm existence of such interfaces in all turbulent flows. However, the time-averaged interface is continuous to high order, being subjected to a near-Gaussian jitter. Time averaging would thus smooth out the sharpness of the physical interface. Consistent with this smoothing, we should actually expect analytical behavior approaching the freestream. Hence, the mixing-length model is predicting a nonphysical feature.

3.3.2 The Mixing Layer

For the mixing layer, we consider two parallel streams with velocities U_1 and U_2. By convention, the stream with velocity U_1 lies above $y = 0$ and $U_1 > U_2$.

The boundary conditions are thus

$$U(x,y) \to U_1 \qquad \text{as} \qquad y \to +\infty \tag{3.62}$$

$$U(x,y) \to U_2 \qquad \text{as} \qquad y \to -\infty \tag{3.63}$$

The most convenient way to solve this problem is to introduce the streamfunction, ψ. The velocity components are given in terms of ψ as follows.

$$U = \frac{\partial \psi}{\partial y} \qquad \text{and} \qquad V = -\frac{\partial \psi}{\partial x} \tag{3.64}$$

Equation (3.23) is automatically satisfied and the momentum equation becomes

$$\frac{\partial \psi}{\partial y}\frac{\partial^2 \psi}{\partial x \partial y} - \frac{\partial \psi}{\partial x}\frac{\partial^2 \psi}{\partial y^2} = \frac{\partial}{\partial y}\left[\ell_{mix}^2 \left|\frac{\partial^2 \psi}{\partial y^2}\right| \frac{\partial^2 \psi}{\partial y^2}\right] \tag{3.65}$$

The boundary conditions on ψ are

$$\frac{\partial \psi}{\partial y} \to U_1 \qquad \text{as} \qquad y \to +\infty \tag{3.66}$$

$$\frac{\partial \psi}{\partial y} \to U_2 \qquad \text{as} \qquad y \to -\infty \tag{3.67}$$

Because the velocity is obtained from the streamfunction by differentiation, ψ involves a constant of integration. For the sake of uniqueness, we can specify an additional boundary condition on ψ, although at this point it is unclear where we should impose the extra boundary condition. The choice will become obvious when we set up the similarity solution. As with the far wake, we assume

$$\psi(x,y) = \psi_o(x) F(\eta) \tag{3.68}$$

where the similarity variable, η, is defined by

$$\eta = y/\delta(x) \tag{3.69}$$

As can be verified by substituting Equations (3.68) and (3.69) into Equation (3.65), a similarity solution exists provided we choose

$$\psi_o(x) = AU_1 x \tag{3.70}$$

$$\delta(x) = Ax \tag{3.71}$$

where A is a constant to be determined. Using Equation (3.34) to determine the mixing length, after some algebra Equation (3.65) transforms to

$$\alpha^2 \frac{d}{d\eta}\left[(F'')^2\right] + AFF'' = 0 \tag{3.72}$$

Note that we remove the absolute value sign in Equation (3.65) because we expect a solution with $\partial U/\partial y = \partial^2\psi/\partial y^2 > 0$. As an immediate consequence, we can simplify Equation (3.72). Specifically, expanding the first term leads to the following **linear** equation for the transformed streamfunction, $F(\eta)$.

$$2\alpha^2 \frac{d^3F}{d\eta^3} + AF = 0 \tag{3.73}$$

To determine the constant of integration in the streamfunction, our assumed form for ψ [Equation (3.68)] is consistent with letting $F(\eta)$ vanish at $\eta = 0$. This is known as the dividing streamline. Thus, our boundary conditions are

$$\frac{dF}{d\eta} \to 1 \qquad \text{as} \qquad \eta \to +\infty \tag{3.74}$$

$$\frac{dF}{d\eta} \to U_2/U_1 \qquad \text{as} \qquad \eta \to -\infty \tag{3.75}$$

$$F(0) = 0 \tag{3.76}$$

For simplicity, we consider the limiting case $U_2 = 0$. This problem can be solved in closed form using elementary methods. Unfortunately, the solution is a bit complicated. Furthermore, as with the far-wake solution, the mixing-length model predicts a sharp turbulent/nonturbulent interface and it becomes a rather difficult chore to determine a straightforward relationship between the closure coefficient α and the constant A, the latter being the value of y/x at the interface. The easier way to proceed is to solve the equation numerically for various values of α^2/A and compare with measurements to infer the value of α. Proceeding in this manner with Program **MIXER** (see Appendix C), optimum agreement between computed and measured [Liepmann and Laufer (1947)] velocity profiles occurs if we choose

$$A = 0.247 \qquad \text{and} \qquad \alpha = 0.071 \qquad \text{(Mixing Layer)} \tag{3.77}$$

This value of α is nearly identical to the value (0.070) quoted by Launder and Spalding (1972). Figure 3.4 compares computed and measured velocity profiles. The traditional definition of spreading rate, δ', for the mixing layer is the difference between the values of y/x where $(U - U_2)^2/(U_1 - U_2)^2$ is 9/10 and 1/10. The values of A and α have been selected to give a spreading rate of

$$\delta' = 0.115 \tag{3.78}$$

which is within the range of measured values, i.e., 0.105 to 0.120. While the computed velocity goes to zero more rapidly than measured on the low speed side of the mixing layer, the overall agreement between theory and experiment is remarkably good.

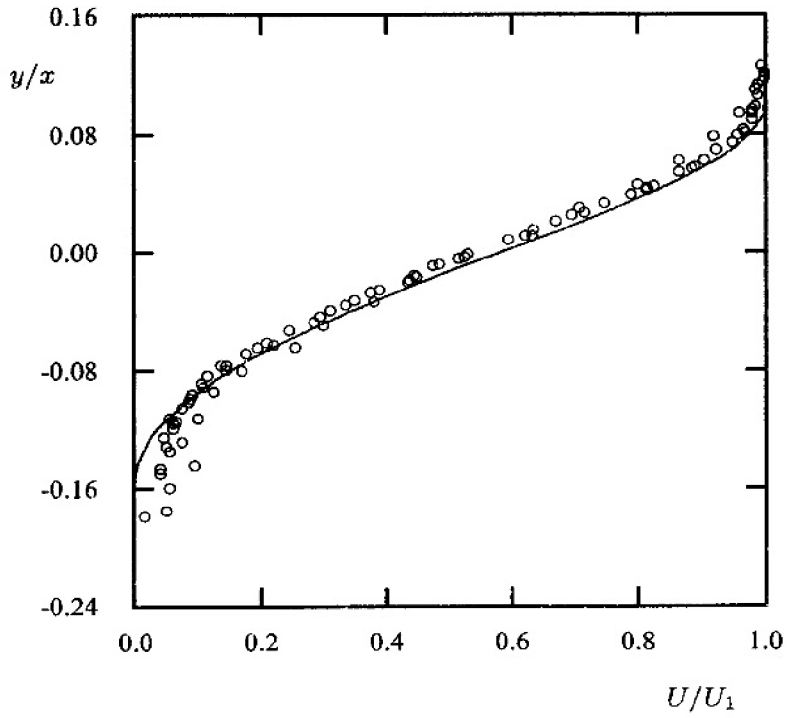

Figure 3.4: *Comparison of computed and measured velocity profiles for a mixing layer: —— Mixing length; ○ Liepmann and Laufer (1947).*

3.3.3 The Jet

We now analyze the **plane jet**, the **round jet** and the **radial jet**. Referring to Figures 3.2(c) and 3.2(d), we assume the jet issues into a stagnant fluid. The jet entrains fluid from the surroundings and grows in width downstream of the origin. Equations (3.23) and (3.24) govern the motion with $m = j = 0$ for the plane jet, $m = 0$, $j = 1$ for the round jet and $m = 1$, $j = 0$ for the radial jet. As with the far wake, we take advantage of the symmetry about the x axis and solve for $0 \leq y < \infty$. The boundary conditions for all three cases are

$$U(x, y) \to 0 \qquad \text{as} \qquad y \to \infty \tag{3.79}$$

$$\frac{\partial U}{\partial y} = 0 \qquad \text{at} \qquad y = 0 \tag{3.80}$$

To insure that the momentum in the jet is conserved, our solution must satisfy the following integral constraint:

$$\pi^{m+j} x^m \int_0^\infty U^2 y^j \, dy = \frac{1}{2} J \tag{3.81}$$

where J is the momentum flux per unit mass, or, **specific momentum flux**.

To solve, we introduce the streamfunction, which can be generalized to account for the axisymmetry of the round and radial jets, i.e.,

$$x^m y^j U = \frac{\partial \psi}{\partial y} \qquad \text{and} \qquad x^m y^j V = -\frac{\partial \psi}{\partial x} \tag{3.82}$$

The momentum equation thus becomes

$$\begin{aligned} & x^m y^{-j} \frac{\partial \psi}{\partial y} \frac{\partial}{\partial x}\left(x^{-m} \frac{\partial \psi}{\partial y}\right) - \frac{\partial \psi}{\partial x} \frac{\partial}{\partial y}\left(y^{-j} \frac{\partial \psi}{\partial y}\right) \\ & = \frac{\partial}{\partial y}\left[y^j \ell_{mix}^2 \left|\frac{\partial}{\partial y}\left(y^{-j} \frac{\partial \psi}{\partial y}\right)\right| \frac{\partial}{\partial y}\left(y^{-j} \frac{\partial \psi}{\partial y}\right)\right] \end{aligned} \tag{3.83}$$

Assuming a similarity solution of the form given in Equations (3.68) and (3.69), the appropriate forms for $\psi_o(x)$ and $\delta(x)$ are

$$\psi_o(x) = \sqrt{\frac{JA^{j+1} x^{m+j+1}}{2\pi^{m+j}}} \tag{3.84}$$

$$\delta(x) = Ax \tag{3.85}$$

As with the mixing layer, A is the value of y/x at the interface between the turbulent and nonturbulent interface. We will select the value of the mixing-length constant α by trial and error to provide as close a match to measurements as possible. For the jet, we expect to have $\partial U/\partial y \leq 0$. Using this fact to replace the absolute value in Equation (3.83) with a minus sign, the following ordinary differential equation for the transformed streamfunction, $F(\eta)$, results.

$$\alpha^2 \eta^j \left[\frac{d}{d\eta}\left(\frac{F'}{\eta^j}\right)\right]^2 = \frac{m+j+1}{2} A F \left(\frac{F'}{\eta^j}\right) \tag{3.86}$$

This equation must be solved subject to the following conditions.

$$F(0) = 0 \tag{3.87}$$

$$\frac{1}{\eta^j}\frac{dF}{d\eta} \to 0 \qquad \text{as} \qquad y \to \infty \tag{3.88}$$

$$\frac{d}{d\eta}\left[\frac{1}{\eta^j}\frac{dF}{d\eta}\right] \qquad \text{as} \qquad y \to 0 \tag{3.89}$$

$$\int_0^\infty \frac{(F')^2}{\eta^j}\, d\eta = 1 \tag{3.90}$$

Doing a numerical solution of Equation (3.86) subject to Equations (3.87) through (3.90), and comparing with experiment yields

$$A = 0.246 \quad \text{and} \quad \alpha = 0.098 \quad \text{(Plane Jet)} \tag{3.91}$$

$$A = 0.233 \quad \text{and} \quad \alpha = 0.080 \quad \text{(Round Jet)} \tag{3.92}$$

$$A = 0.238 \quad \text{and} \quad \alpha = 0.155 \quad \text{(Radial Jet)} \tag{3.93}$$

Values for the mixing-length coefficient, α, are about 8% larger than corresponding values (0.090 and 0.075) quoted by Launder and Spalding (1972) for plane and round jets respectively, which is within the bounds of experimental error. Values quoted in Equations (3.91) – (3.93) have been obtained using Program **JET** (see Appendix C). Figures 3.5, 3.6 and 3.7 compare computed and measured [Bradbury (1965), Heskestad (1965), Wygnanski and Fiedler (1969), Rodi (1975), Witze and Dwyer (1976)] velocity profiles for plane, round and radial jets. Somewhat larger discrepancies between theory and experiment are present for plane and radial jets than for the round jet.

The traditional definition of spreading rate, δ', for the jet is the value of y/x where the velocity is half its peak value. Experimental data indicate δ' is between 0.100 and 0.110 for the plane jet, between 0.086 and 0.095 for the round jet and between 0.096 and 0.110 for the radial jet. The mixing-length computational results shown in Figures 3.5, 3.6 and 3.7 correspond to

$$\delta' = \begin{cases} 0.100 & \text{(Plane Jet)} \\ 0.086 & \text{(Round Jet)} \\ 0.106 & \text{(Radial Jet)} \end{cases} \tag{3.94}$$

This concludes our application of the mixing-length model to free shear flows. A few final comments will help put this model into proper perspective. We postulated in Equation (3.34) that the mixing length is proportional to the width of the shear layer. Our theory thus has a single **closure coefficient**, α, and we have found that it must be changed for each flow. The following values are optimum for the five cases considered. While we have obtained fairly close agreement between computed and measured velocity profiles, we have not predicted the

Flow	α
Far Wake	0.180
Mixing Layer	0.071
Plane Jet	0.098
Round Jet	0.080
Radial Jet	0.155

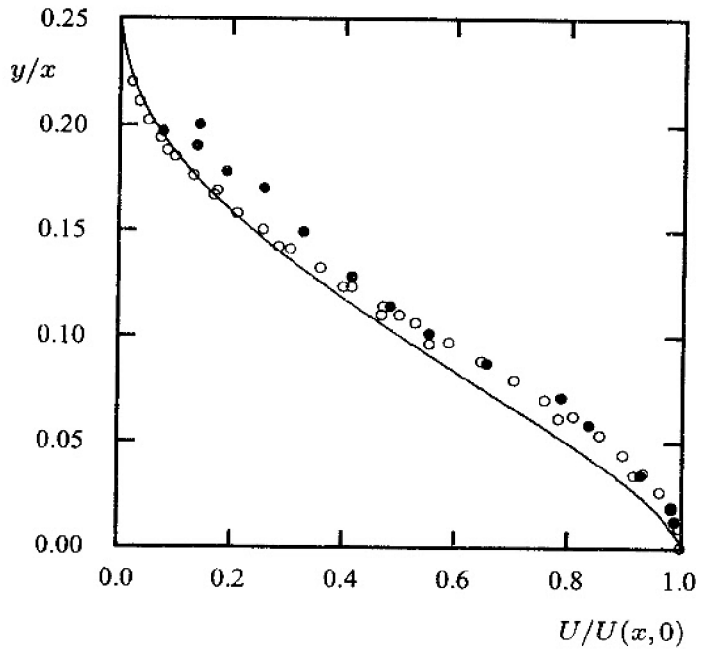

Figure 3.5: *Comparison of computed and measured velocity profiles for the plane jet: —— Mixing length; ○ Bradbury (1965); • Heskestad (1965).*

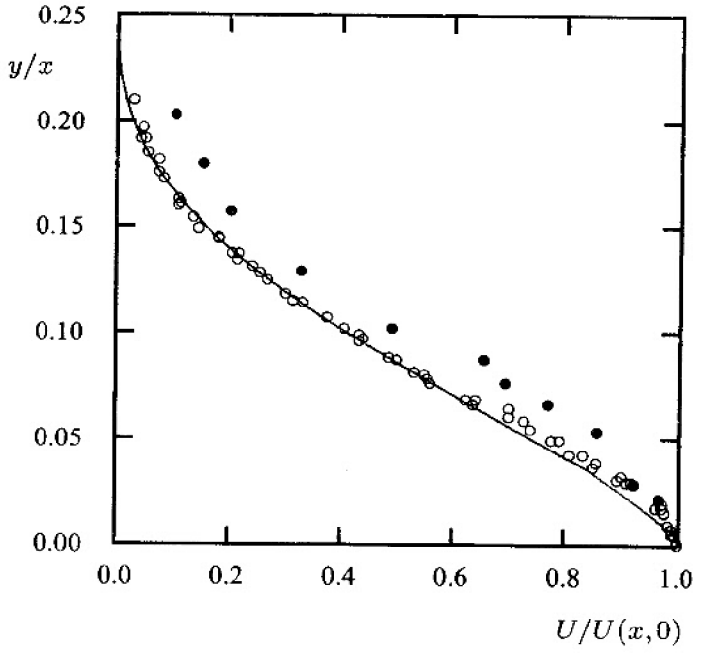

Figure 3.6: *Comparison of computed and measured velocity profiles for the round jet: —— Mixing length; ○ Wygnanski and Fiedler (1969); • Rodi (1975).*

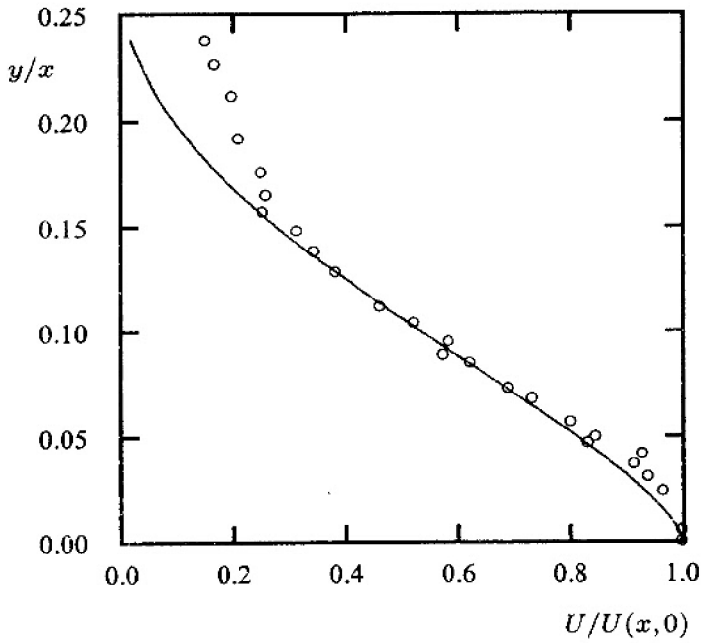

Figure 3.7: *Comparison of computed and measured velocity profiles for the radial jet:* — *Mixing length;* ○ *Witze and Dwyer (1976).*

spreading rate. In fact, we established the value of our closure coefficient by forcing agreement with the measured spreading rate. If we are only interested in far-wake applications or round jets we might use this model with the appropriate closure coefficient for a parametric study in which some flow property might be varied. However, we must proceed with some degree of caution knowing that our formulation lacks universality.

3.4 Modern Variants of the Mixing-Length Model

For free shear flows, we have seen that the mixing length is constant across the layer and proportional to the width of the layer. For flow near a solid boundary, turbulence behaves differently and, not too surprisingly, we must use a different prescription for the mixing length. Prandtl originally postulated that for flows near solid boundaries the mixing length is proportional to the distance from the surface. As we will demonstrate shortly, this postulate is consistent with the well-known **law of the wall**, which has been observed for a wide range of wall-bounded flows over roughly the nearest 10% of the flow width from the surface (see Subsection 1.3.5).

Figure 3.8 shows a typical velocity profile for a turbulent boundary layer. The quantity y^+, defined in Equation (1.21), is dimensionless distance from the

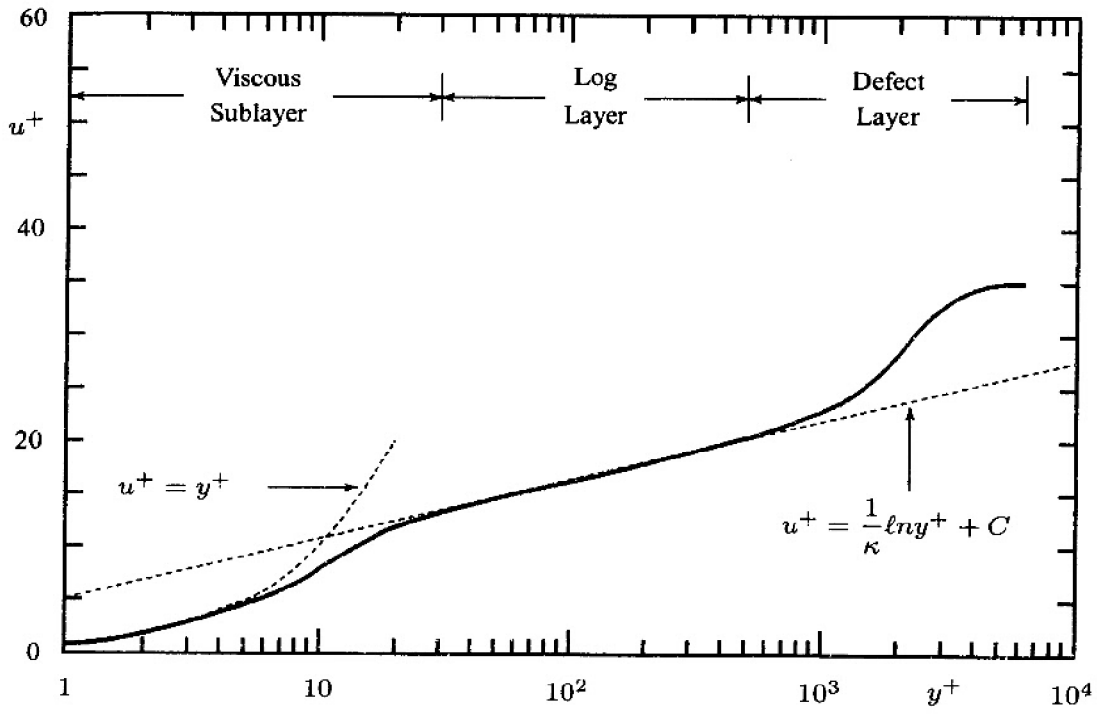

Figure 3.8: *Typical velocity profile for a turbulent boundary layer.*

surface. As discussed in Subsection 1.3.5, three distinct regions are discernible, viz., the **viscous sublayer** (or "viscous wall region"), the **log layer** and the **defect layer**. By definition, the log layer is the portion of the boundary layer sufficiently close to the surface that inertial terms can be neglected yet sufficiently distant that the molecular, or viscous, stress is negligible compared to the Reynolds stress. This region typically lies between $y^+ = 30$ and $y = 0.1\delta$, where the value of y^+ at the upper boundary is dependent upon Reynolds number. Of particular interest to the present discussion, the **law of the wall** holds in the log layer. The viscous sublayer is the region between the surface and the log layer. Close to the surface, the velocity varies approximately linearly with y^+, and gradually asymptotes to the law of the wall for large values of y^+. The defect layer lies between the log layer and the edge of the boundary layer. The velocity asymptotes to the law of the wall as $y/\delta \rightarrow 0$, and makes a noticeable departure from the law of the wall approaching the freestream. Chapter 4 discusses these three layers in great detail.

From a mathematician's point of view, there are actually only two layers, viz., the viscous sublayer and the defect layer, and they overlap. In the parlance of singular-perturbation theory (Appendix B), the defect layer is the region in

which the outer expansion is valid, while the viscous sublayer is the region where the inner expansion holds. In performing the classical matching procedure, we envision the existence of an overlap region, in which both the viscous sublayer and defect-layer solutions are valid. In the present context, matching shows that U varies logarithmically with y in the overlap region, which we choose to call the log layer. Strictly speaking, the log layer is not a distinct layer, but rather the asymptotic limit of the inner and outer layers. Nevertheless, we will find the log layer to be useful because of the simplicity of the equations of motion in the layer.

Consider an incompressible, constant-pressure boundary layer. The flow is governed by the standard boundary-layer equations.

$$\frac{\partial U}{\partial x} + \frac{\partial V}{\partial y} = 0 \tag{3.95}$$

$$U\frac{\partial U}{\partial x} + V\frac{\partial U}{\partial y} = \frac{\partial}{\partial y}\left[\nu\frac{\partial U}{\partial y} - \overline{u'v'}\right] \tag{3.96}$$

Because the convective terms are negligible in the log layer, the sum of the viscous and Reynolds shear stress must be constant. Hence, we can say

$$\nu\frac{\partial U}{\partial y} - \overline{u'v'} \approx \nu\left(\frac{\partial U}{\partial y}\right)_w = \frac{\tau_w}{\rho} = u_\tau^2 \tag{3.97}$$

where subscript w denotes value at the wall and $u_\tau = \sqrt{\tau_w/\rho}$ is known as the **friction velocity**. As noted above, the Reynolds stress is much larger than the viscous stress in the log layer. Consequently, according to the mixing-length model,

$$\ell_{mix}^2\left(\frac{\partial U}{\partial y}\right)^2 \approx u_\tau^2 \tag{3.98}$$

If we say that the mixing length is given by

$$\ell_{mix} = \kappa y \tag{3.99}$$

where κ is a constant, Equation (3.98) can be integrated immediately to yield

$$U \approx \frac{u_\tau}{\kappa}\ell n y + \text{constant} \tag{3.100}$$

Finally, recall the dimensionless velocity and normal distance defined in Equation (1.21), which we repeat here for convenience, viz.,

$$u^+ \equiv \frac{U}{u_\tau} \quad \text{and} \quad y^+ \equiv \frac{u_\tau y}{\nu} \tag{3.101}$$

Introducing Equation (3.101) into Equation (3.100) yields the classical **law of the wall**, viz.,

$$U^+ \approx \frac{1}{\kappa} \ell n y^+ + C \tag{3.102}$$

The coefficient κ is known as the **Kármán constant**, and C is a dimensionless constant. Coles and Hirst (1969) found from correlation of experimental data for a large number of attached, incompressible boundary layers with and without pressure gradient that

$$\kappa \approx 0.41 \tag{3.103}$$

$$C \approx 5.0 \tag{3.104}$$

Note that the mixing-length formula, Equation (3.98) with Equation (3.99), yields the same result as given by dimensional analysis alone [cf. Equations (1.18) and (1.19)].

Using Equation (3.99) all the way from $y = 0$ to $y = \delta$, the mixing-length model fails to provide close agreement with measured skin friction for boundary layers. Of course, not even Prandtl expected that $\ell_{mix} = \kappa y$ throughout the boundary layer. Since the mixing length was first postulated, considerable effort has been made aimed at finding a suitable prescription for boundary-layer computations. Several key modifications to Equation (3.99) have evolved, three of which deserve our immediate attention. See Schlichting-Gersten (1999) or Hinze (1975) for a more-complete history of the mixing-length model's evolution.

The first key modification was devised by Van Driest (1956) who proposed that the mixing length should be multiplied by a damping function. Specifically, Van Driest proposed, with some theoretical support but mainly as a good fit to data, that the mixing length should behave according to

$$\ell_{mix} = \kappa y \left[1 - e^{-y^+/A_o^+}\right] \tag{3.105}$$

where the constant A_o^+ is

$$A_o^+ = 26 \tag{3.106}$$

Aside from the primary need to improve predictive accuracy, the Van Driest modification improves our description of the Reynolds stress in the limit $y \to 0$. With ℓ_{mix} given by Equation (3.99), the asymptotic behavior of the Reynolds shear stress is $\tau_{xy} \sim y^2$ as $y \to 0$. However, the no-slip boundary condition tells us that $u' = 0$ at $y = 0$. Since there is no a priori reason for $\partial u'/\partial y$ to vanish at the surface, we conclude that $u' \sim y$ as $y \to 0$. Since the fluctuating velocity satisfies the continuity equation, we also conclude that $v' \sim y^2$. Hence, the Reynolds shear stress must go to zero as y^3. Results of DNS studies (Chapter 8) indicate that indeed $\tau_{xy} \sim y^3$ as $y \to 0$. However, as noted by Hinze (1975), the coefficient of the y^3 term in a Taylor series expansion for τ_{xy} must be very small as measurements are as close to $\tau_{xy} \sim y^4$ as they are to $\tau_{xy} \sim y^3$ when

$y \to 0$. In the limit of small y the Van Driest mixing length implies τ_{xy} goes to zero as y^4 approaching the surface.

The second key modification was made by Clauser (1956) who addressed the proper form of the eddy viscosity in the defect layer. Similar to Prandtl's special form of the eddy viscosity for wake flows given in Equation (3.25), Clauser specifies that

$$\nu_{T_o} = \alpha U_e \delta^* \tag{3.107}$$

where ν_{T_o} is the kinematic eddy viscosity in the outer part of the layer, δ^* is the displacement thickness, U_e is the velocity at the edge of the layer, and α is a closure coefficient.

In a similar vein, Escudier (1966) found that predictive accuracy is improved by limiting the peak value of the mixing length according to

$$(\ell_{mix})_{max} = 0.09\delta \tag{3.108}$$

where δ is boundary-layer thickness. Escudier's modification is similar to the approximation we used in analyzing free shear flows [Equation (3.34)], although the value 0.09 is half the value we found for the far wake.

Using an eddy viscosity appropriate to wake flow in the outer portion of the boundary layer also improves our physical description of the turbulent boundary layer. Measurements indeed indicate that the turbulent boundary layer exhibits wake-like characteristics in the defect layer. As pointed out by Coles and Hirst (1969), **"a typical boundary layer flow can be viewed as a wake-like structure which is constrained by a wall."** Figure 3.9 illustrates Coles' notion that the defect layer resembles a wake flow while the wall constraint is felt primarily in the sublayer and log layer. Strictly speaking, turbulence structure differs a lot between a boundary layer and a wake. Hence, the terminology "wake component" is misleading from a conceptual point of view. Nevertheless, the mathematical approximations that yield accurate predictions for a wake and for the outer portion of a turbulent boundary layer in zero pressure gradient are remarkably similar.

The third key modification is due to Corrsin and Kistler (1954) and Klebanoff (1954) as a corollary result of their experimental studies of **intermittency**. They found that approaching the freestream from within the boundary layer, the flow is not always turbulent. Rather, it is sometimes laminar and sometimes turbulent, i.e., it is **intermittent**. Their measurements indicate that for smooth walls, the eddy viscosity should be multiplied by

$$F_{Kleb}(y;\delta) = \left[1 + 5.5\left(\frac{y}{\delta}\right)^6\right]^{-1} \tag{3.109}$$

where δ is the boundary-layer thickness. This provides a measure of the effect of intermittency on the flow.

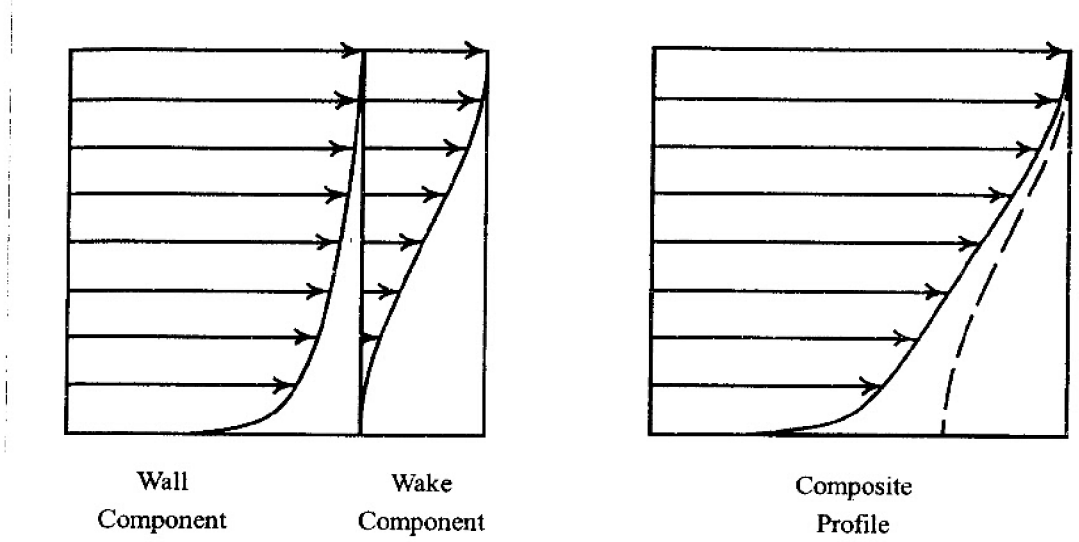

Figure 3.9: *Coles' description of the turbulent boundary layer. [From Coles and Hirst (1969) — Used with permission.]*

All of these modifications have evolved as a result of the great increase in power and accuracy of computing equipment and measurement techniques since the 1940's. The next two subsections introduce the two most noteworthy models in use today that are based on the mixing-length concept. Both include variants of the Van Driest, Clauser, and Klebanoff modifications. Although it is not used in these two models, the Escudier modification has also enjoyed great popularity.

As a final comment, we have introduced two new closure coefficients, A_o^+ and α, and an empirical function, F_{Kleb}. As we continue in our journey through this book, we will find that the number of such coefficients and functions increases as we attempt to describe more and more features of the turbulence.

3.4.1 Cebeci-Smith Model

The Cebeci-Smith model [Smith and Cebeci (1967)] is a two-layer model with ν_T given by separate expressions in each layer. In terms of the normal distance from the nearest solid boundary, y, the eddy viscosity is

$$\nu_T = \begin{cases} \nu_{T_i}, & y \leq y_m \\ \nu_{T_o}, & y > y_m \end{cases} \tag{3.110}$$

where y_m is the smallest value of y for which $\nu_{T_i} = \nu_{T_o}$. The values of ν_T in the inner layer, ν_{T_i}, and the outer layer, ν_{T_o}, are computed as follows.

Inner Layer:

$$\nu_{T_i} = \ell_{mix}^2 \left[\left(\frac{\partial U}{\partial y} \right)^2 + \left(\frac{\partial V}{\partial x} \right)^2 \right]^{1/2} \tag{3.111}$$

$$\ell_{mix} = \kappa y \left[1 - e^{-y^+/A^+} \right] \tag{3.112}$$

Outer layer:

$$\nu_{T_o} = \alpha U_e \delta_v^* F_{Kleb}(y; \delta) \tag{3.113}$$

Closure Coefficients:

$$\kappa = 0.40, \qquad \alpha = 0.0168, \qquad A^+ = 26 \left[1 + y \frac{dP/dx}{\rho u_\tau^2} \right]^{-1/2} \tag{3.114}$$

The function F_{Kleb} is the Klebanoff intermittency function given by Equation (3.109), U_e is boundary-layer edge velocity, and δ_v^* is the **velocity thickness** defined by

$$\delta_v^* = \int_0^\delta (1 - U/U_e)\, dy \tag{3.115}$$

Note that velocity thickness is identical to displacement thickness for incompressible flow. The coefficient A^+ differs from Van Driest's value to improve predictive accuracy for boundary layers with nonzero pressure gradient.[4] The prescription for ν_{T_i} above is appropriate only for two-dimensional flows; for three-dimensional flows, it should be proportional to a quantity such as the magnitude of the vorticity vector. There are many other subtle modifications to this model for specialized applications including surface mass transfer, streamline curvature, surface roughness, low Reynolds number, etc. Cebeci and Smith (1974) give complete details of their model with all of its variations.

The Cebeci-Smith model is especially elegant and easy to implement. Most of the computational effort, relative to a laminar case, goes into computing the velocity thickness. This quantity is readily available in boundary-layer computations so that a laminar-flow program can usually be converted to a turbulent-flow program with just a few extra lines of instructions. Figure 3.10 illustrates a typical eddy viscosity profile using ν_{T_i} between $y = 0$ and $y = y_m$, and ν_{T_o} for the rest of the layer. At Reynolds numbers typical of fully-developed turbulence, matching between inner and outer layers occurs well into the log layer.

[4] However, the Van Driest value should be used in fully-developed pipe flow, for which the dP/dx correction yields imaginary A^+.

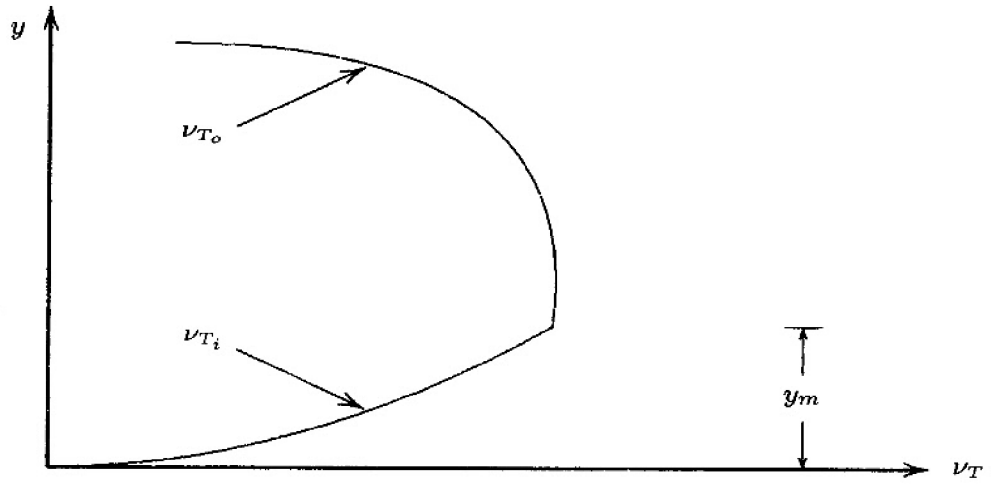

Figure 3.10: *Eddy viscosity for the Cebeci-Smith model.*

We can estimate the value of y_m^+ as follows. Since we expect the matching point to lie in the log layer, the exponential term in the Van Driest damping function will be negligible. Also, the law of the wall [Equation (3.100)] tells us $\partial U/\partial y \approx u_\tau/(\kappa y)$. Thus,

$$\nu_{T_i} \approx \kappa^2 y^2 \frac{u_\tau}{\kappa y} \approx \kappa u_\tau y = \kappa \nu y^+ \tag{3.116}$$

Since the matching point also lies close enough to the surface that we can say $y/\delta \ll 1$, the Klebanoff intermittency function will be close to one so that (with $\delta_v^* = \delta^*$):

$$\nu_{T_o} \approx \alpha U_e \delta^* = \alpha \nu Re_{\delta^*} \tag{3.117}$$

Hence, equating ν_{T_i} and ν_{T_o}, we find

$$y_m^+ \approx \frac{\alpha}{\kappa} Re_{\delta^*} \approx 0.042 Re_{\delta *} \tag{3.118}$$

Assuming a typical turbulent boundary layer for which $Re_{\delta^*} \sim 10^4$, the matching point will lie at $y_m^+ \sim 420$.

3.4.2 Baldwin-Lomax Model

The Baldwin-Lomax model [Baldwin and Lomax (1978)] was formulated for use in computations where boundary-layer properties such as δ, δ_v^* and U_e are difficult to determine. This situation often arises in numerical simulation of separated flows, especially for flows with shock waves. Like the Cebeci-Smith model, this is a two-layer model. The eddy viscosity is given by Equation (3.110), and the inner and outer layer viscosities are as follows.

Inner Layer:

$$\nu_{T_i} = \ell_{mix}^2 |\omega| \tag{3.119}$$

$$\ell_{mix} = \kappa y \left[1 - e^{-y^+/A_o^+}\right] \tag{3.120}$$

Outer Layer:

$$\nu_{T_o} = \alpha C_{cp} F_{wake} F_{Kleb}(y; y_{max}/C_{Kleb}) \tag{3.121}$$

$$F_{wake} = \min\left[y_{max} F_{max}; C_{wk} y_{max} U_{dif}^2 / F_{max}\right] \tag{3.122}$$

$$F_{max} = \frac{1}{\kappa}\left[\max_y(\ell_{mix}|\omega|)\right] \tag{3.123}$$

where y_{max} is the value of y at which $\ell_{mix}|\omega|$ achieves its maximum value.

Closure Coefficients:[5]

$$\left.\begin{array}{lll} \kappa = 0.40, & \alpha = 0.0168, & A_o^+ = 26 \\ C_{cp} = 1.6, & C_{Kleb} = 0.3, & C_{wk} = 1 \end{array}\right\} \tag{3.124}$$

The function F_{Kleb} is Klebanoff's intermittency function [Equation (3.109)] with δ replaced by y_{max}/C_{Kleb}, and ω is the magnitude of the vorticity vector, i.e.,

$$\omega = \left[\left(\frac{\partial V}{\partial x} - \frac{\partial U}{\partial y}\right)^2 + \left(\frac{\partial W}{\partial y} - \frac{\partial V}{\partial z}\right)^2 + \left(\frac{\partial U}{\partial z} - \frac{\partial W}{\partial x}\right)^2\right]^{1/2} \tag{3.125}$$

for fully three-dimensional flows. This simplifies to $\omega = |\partial V/\partial x - \partial U/\partial y|$ in a two-dimensional flow. If the boundary layer approximations are used in a two-dimensional flow, then $\omega = |\partial U/\partial y|$.

U_{dif} is the maximum value of U for boundary layers. For free shear layers, U_{dif} is the difference between the maximum velocity in the layer and the value of U at $y = y_{max}$. For more general flows, it is defined by

$$U_{dif} = \left(\sqrt{U^2 + V^2 + W^2}\right)_{max} - \left(\sqrt{U^2 + V^2 + W^2}\right)_{y=y_{max}} \tag{3.126}$$

The primary difference between the Baldwin-Lomax and Cebeci-Smith models is in the outer layer, where the product $C_{cp}F_{wake}$ replaces $U_e\delta_v^*$. To avoid the

[5]Personal communication between Dr. Lomax and the author of this text has determined that the original Baldwin-Lomax paper inadvertently: (a) assigns a value of $C_{wk} = 0.25$; (b) defines U_{dif} as the difference between the maximum and minimum velocities.

need to locate the boundary-layer edge, the Baldwin-Lomax model establishes the outer-layer length scale in terms of the vorticity in the layer. On the one hand, in using $F_{wake} = y_{max}F_{max}$, we in effect replace δ_v^* by $y_{max}^2\omega/U_e$. On the other hand, using $F_{wake} = C_{wk}y_{max}U_{dif}^2/F_{max}$ effectively replaces the shear layer width, δ, in Prandtl's eddy-viscosity model [Equation (3.25)] by $U_{dif}/|\omega|$.

For boundary-layer flows, there is very little difference between the predictions of the Baldwin-Lomax and Cebeci-Smith models. This indicates that the prescription for determining the outer-layer length scale based on the vorticity and distance from the surface [cf. Equations (3.122) and (3.123)] is entirely equivalent to the velocity thickness, δ_v^*. For more-complicated flows, such as those involving separation, the Baldwin-Lomax model provides an outer length scale that is well defined for most flows. By contrast, δ_v^*, will generally be negative for a separated flow, and thus is an unsuitable length scale.

However, the Baldwin-Lomax model prescription for computing an outer length scale can fail when the vorticity is nonvanishing above the boundary layer. This will occur, for example, on slender bodies at angle of attack, where regions of crossflow separation dominate [e.g., Degani and Schiff (1986) or Gee, Cummings and Schiff (1992)]. In this type of flow, the function $F(y)$ can exhibit more than one relative maximum as illustrated in Figure 3.11. Using a peak beyond the viscous region can lead to nonphysically large eddy viscosity values that lead to gross distortion of the computed flowfield. To eliminate this problem, Degani and Schiff (1986) have devised a procedure that automatically selects the peak value of $F(y)$ within the viscous region. While the Degani-Schiff modification improves model predictions for separated flows, we will see in Section 3.6 that neither the Cebeci-Smith nor the Baldwin-Lomax model embodies a sufficient physical foundation to warrant application to such flows.

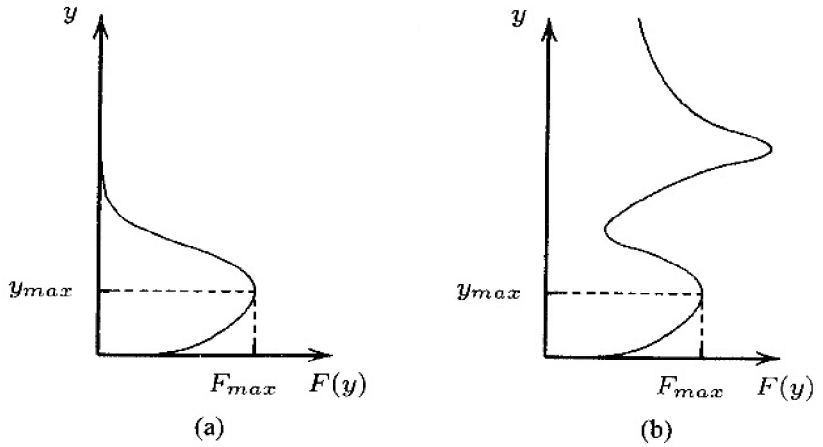

Figure 3.11: *The function $F(y)$ for: (a) a conventional boundary layer; (b) a boundary layer with nonzero freestream vorticity.*

Thus, this type of adjustment to the model reflects no added physical insight, but rather stands as a purely empirical correction.

As a final comment, while Equation (3.124) implies this model has six closure coefficients, there are actually only five. The coefficient C_{cp} appears only in Equation (3.121) where it is multiplied by α, so αC_{cp} is actually a single constant.

3.5 Application to Wall-Bounded Flows

We turn our attention now to application of the Cebeci-Smith and Baldwin-Lomax models to wall-bounded flows, i.e., to flows with a solid boundary. The no-slip boundary condition must be enforced for wall-bounded flows, and we expect to find a viscous layer similar to that depicted in Figure 3.8. This section first examines two internal flows, viz., channel flow and pipe flow. Then, we consider external flows, i.e., boundary layers growing in a semi-infinite medium.

3.5.1 Channel and Pipe Flow

Like the free shear flow applications of Section 3.3, constant cross-section channel and pipe flow are excellent building-block cases for testing a turbulence model. Although we have the added complication of a solid boundary, the motion can be described with ordinary differential equations and is therefore easy to analyze mathematically. Also, experimental data are abundant for these flows.

The classical problems of flow in a channel, or duct, and a pipe are the idealized case of an infinitely long channel or pipe (Figure 3.12). This approximation is appropriate provided we are not too close to the inlet of the channel/pipe so

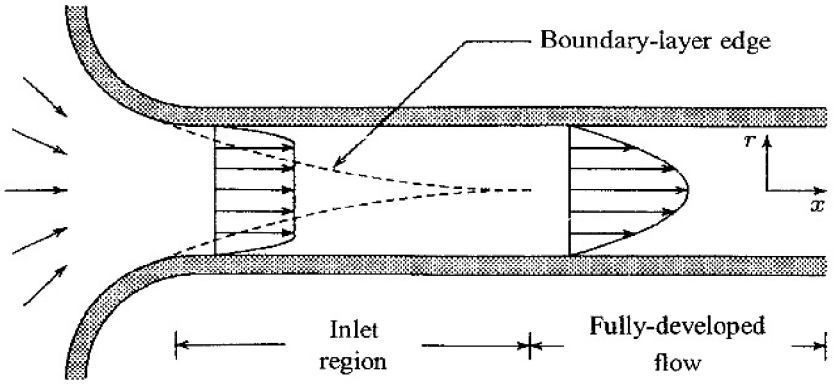

Figure 3.12: *Fully-developed flow in a pipe or channel with the vertical scale magnified.*

that the flow has become **fully-developed**. For turbulent flow in a pipe, flow asymptotes to full development at a distance ℓ_e downstream of the inlet given approximately by [cf. Schlichting-Gersten (1999)]

$$\frac{\ell_e}{D} = 4.4 Re_D^{1/6} \tag{3.127}$$

where Re_D is Reynolds number based on the pipe diameter (or channel half height). Thus, for example, the **entrance length**, ℓ_e, for flow in a pipe with $Re_D = 10^5$ is about 30 pipe diameters. Because, by definition, properties no longer vary with distance along the channel/pipe, we conclude immediately that

$$\frac{\partial \mathbf{U}}{\partial x} = \mathbf{0} \tag{3.128}$$

Denoting distance from the center of the channel or pipe by r, conservation of mass is

$$\frac{\partial U}{\partial x} + \frac{1}{r^j}\frac{\partial}{\partial r}\left[r^j V\right] = 0 \tag{3.129}$$

where $j = 0$ for channel flow and $j = 1$ for pipe flow. In light of Equation (3.128), we see that V does not vary across the channel/pipe. Since V must vanish at the channel/pipe walls, we conclude that $V = 0$ throughout the fully-developed region. Hence, for both channel and pipe flow, the inertial terms are exactly zero, so that the momentum equation simplifies to

$$0 = -\frac{dP}{dx} + \frac{1}{r^j}\frac{d}{dr}\left[r^j\left(\mu\frac{dU}{dr} - \rho\overline{u'v'}\right)\right] \tag{3.130}$$

In fully-developed flow pressure gradient must be independent of x, and if $V = 0$, it is also exactly independent of r. Hence, we can integrate once to obtain

$$\mu\frac{dU}{dr} - \rho\overline{u'v'} = \frac{r}{j+1}\frac{dP}{dx} \tag{3.131}$$

Now, the Reynolds stress vanishes at the channel/pipe walls, and this establishes a direct relationship between the pressure gradient and the shear stress at the walls. If we let R denote the half-height of the channel or the radius of the pipe, applying Equation (3.131) at $r = R$ tells us that

$$\tau_w = -\frac{R}{j+1}\frac{dP}{dx} \tag{3.132}$$

Hence, introducing the friction velocity, u_τ, the momentum equation for channel/pipe flow simplifies to the following first-order, ordinary differential equation.

$$\mu\frac{dU}{dr} - \rho\overline{u'v'} = -\rho u_\tau^2\frac{r}{R} \tag{3.133}$$

Noting that both channel and pipe flow are symmetric about the centerline, we can obtain the complete solution by solving Equation (3.133) with r varying between 0 and R. It is more convenient however to define y as the distance from the wall so that

$$y = R - r \tag{3.134}$$

Hence, representing the Reynolds stress in terms of the eddy viscosity, i.e., $-\rho\overline{u'v'} = \mu_T dU/dy$, we arrive at the following equation for the velocity.

$$(\mu + \mu_T)\frac{dU}{dy} = \rho u_\tau^2 \left(1 - \frac{y}{R}\right) \tag{3.135}$$

Finally, we introduce sublayer-scaled coordinates, U^+ and y^+, from Equation (3.101), as well as $\mu_T^+ = \mu_T/\mu$. This results in the dimensionless form of the momentum equation for channel flow and pipe flow, viz.,

$$(1 + \mu_T^+)\frac{dU^+}{dy^+} = \left(1 - \frac{y^+}{R^+}\right) \tag{3.136}$$

where

$$R^+ = u_\tau R/\nu \tag{3.137}$$

Equation (3.136) must be solved subject to the no-slip boundary condition at the channel/pipe wall. Thus, we require

$$U^+(0) = 0 \tag{3.138}$$

At first glance, this appears to be a standard initial-value problem that can, in principle, be solved using an integration scheme such as the Runge-Kutta method. However, the problem is a bit more difficult, and for both the Cebeci-Smith and Baldwin-Lomax models, the problem must be solved iteratively. That is, for the Cebeci-Smith model, we don't know U_e and δ_v^* a priori. Similarly, with the Baldwin-Lomax model, we don't know the values of U_{dif} and y_{max} until we have determined the entire velocity profile. This is not a serious complication however, and the solution converges after just a few iterations.

The equations for channel and pipe flow can be conveniently solved using a standard over-relaxation iterative procedure. Program **PIPE** (see Appendix C) yields a numerical solution for several turbulence models, including the Cebeci-Smith and Baldwin-Lomax models.

Figure 3.13 compares computed two-dimensional channel-flow profiles with Direct Numerical Simulation (DNS) results of Mansour, Kim and Moin (1988) for Reynolds number based on channel height and average velocity of 13750. As shown, the Cebeci-Smith and Baldwin-Lomax velocity profiles are within 8% and 5%, respectively, of the DNS profiles. Computed Reynolds shear stress profiles for both models differ from the DNS profiles by no more than 2%.

Computed skin friction for both models differs by less than 5% from Halleen and Johnston's (1967) correlation of experimental data, viz.,

$$c_f = 0.0706 Re_H^{-1/4} \tag{3.139}$$

where the skin friction and Reynolds number are based on the average velocity across the channel and the channel height H, i.e., $c_f = \tau_w / (\frac{1}{2}\rho U_{avg}^2)$ and on Reynolds number, $Re_H = U_{avg} H/\nu$.

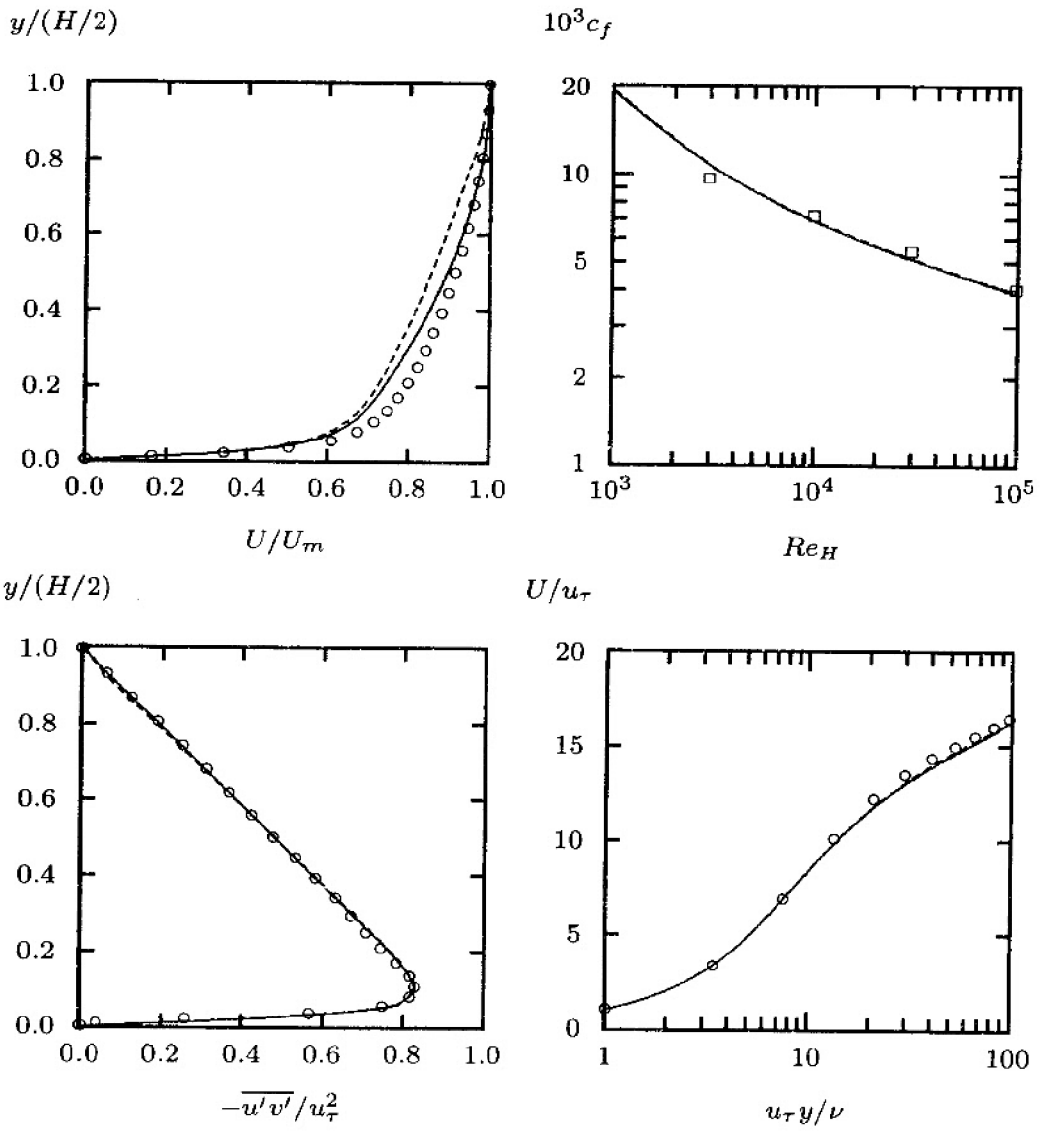

Figure 3.13: *Comparison of computed and measured channel-flow properties, $Re_H = 13750$.* —— *Baldwin-Lomax model;* - - - *Cebeci-Smith model;* ○ *Mansour et al. (DNS);* □ *Halleen-Johnston correlation.*

Figure 3.14 compares model predicted pipe-flow properties with the experimental data of Laufer (1952) for Reynolds number based on pipe diameter and average velocity of 40000. Baldwin-Lomax velocity and Reynolds shear stress differ from measured values by no more than 3%. As with channel flow, the Cebeci-Smith velocity shows greater differences (8%) from the data, while the Reynolds shear stress values are very close to those predicted by the Baldwin-Lomax model.

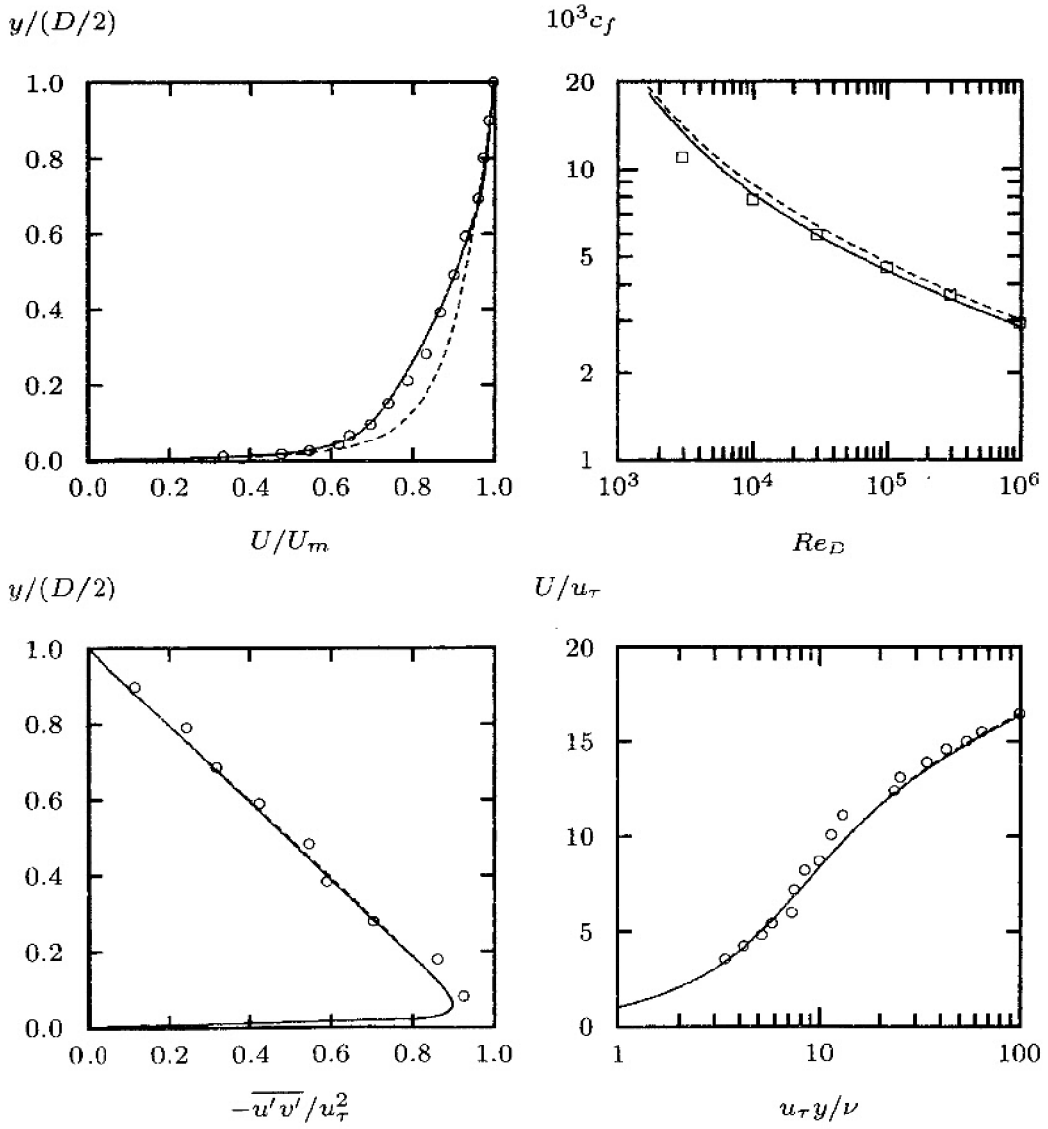

Figure 3.14: *Comparison of computed and measured pipe-flow properties, $Re_D = 40000$.* —— *Baldwin-Lomax model;* - - - *Cebeci-Smith model;* ○ *Laufer;* □ *Prandtl correlation.*

Computed skin friction is within 8% and 1% for the Cebeci-Smith and Baldwin-Lomax models, respectively, of Prandtl's universal law of friction for smooth pipes [see Schlichting-Gersten (1999)] given by

$$\frac{1}{\sqrt{c_f}} = 4\log_{10}\left(2Re_D\sqrt{c_f}\right) - 1.6 \tag{3.140}$$

where c_f and Re_D are based on average velocity across the pipe and pipe diameter, D.

These computations illustrate that subtle differences in the Reynolds shear stress can lead to much larger differences in velocity for pipe and channel flow. This means we must determine the Reynolds shear stress very accurately in order to obtain accurate velocity profiles. To some extent this seems odd. The Reynolds stress is a higher-order correlation while velocity is a simple time average. Our natural expectation is for the mean velocity to be determined with great precision while higher-order quantities such as Reynolds stress are determined with a bit less precision. The dilemma appears to stem from the fact that we need the same precision in τ_{xy} as in $\partial U/\partial y$. As we advance to more complicated turbulence models, we will see this accuracy dilemma repeated, although generally with less severity. As applications go, channel and pipe flow are not very forgiving.

Interestingly, Figure 3.14 shows that for the higher Reynolds number pipe flow, higher velocity is predicted with the Cebeci-Smith model than with the Baldwin-Lomax model. The opposite is true for the lower Reynolds number channel-flow case. Cebeci and Smith (1974) have devised low-Reynolds-number corrections for their model which, presumably, would reduce the differences from the DNS channel-flow results.

3.5.2 Boundary Layers

In general, for a typical boundary layer, we must account for pressure gradient. Ignoring effects of normal Reynolds stresses and introducing the eddy viscosity to determine the Reynolds shear stress, the two-dimensional ($j = 0$) and axisymmetric ($j = 1$) boundary-layer equations are as follows.

$$\frac{\partial U}{\partial x} + \frac{1}{y^j}\frac{\partial}{\partial y}\left(y^j V\right) = 0 \tag{3.141}$$

$$U\frac{\partial U}{\partial x} + V\frac{\partial U}{\partial y} = -\frac{1}{\rho}\frac{dP}{dx} + \frac{1}{y^j}\frac{\partial}{\partial y}\left[y^j(\nu + \nu_T)\frac{\partial U}{\partial y}\right] \tag{3.142}$$

The appropriate boundary conditions follow from the no-slip condition at the surface and from insisting that $U \to U_e$ as we approach the boundary-layer edge.

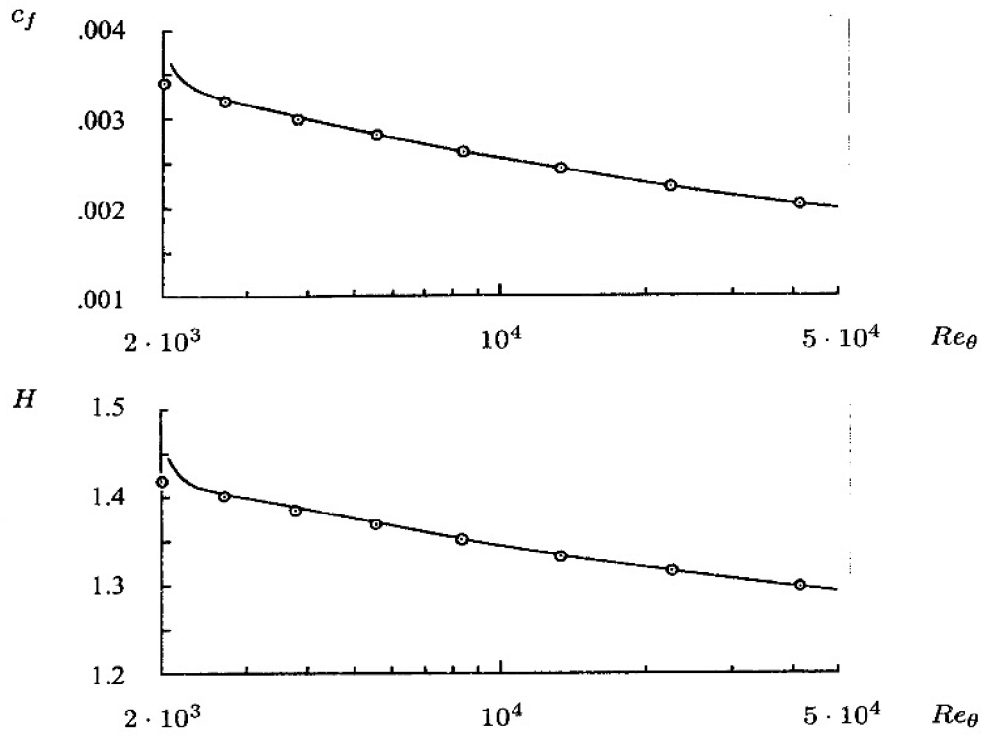

Figure 3.15: *Comparison of computed and correlated shape factor and skin friction for flat-plate boundary layer flow;* ⊙ *Coles;* —— *Cebeci-Smith model. [From Kline et al. (1969) — Used with permission.]*

Consequently, we must solve Equations (3.141) and (3.142) subject to

$$\left.\begin{array}{lcll} U(x,0) & = & 0 & \\ V(x,0) & = & 0 & \\ U(x,y) & \rightarrow & U_e(x) \quad \text{as} \quad & y \rightarrow \delta(x) \end{array}\right\} \tag{3.143}$$

where $\delta(x)$ is the boundary-layer thickness.

The Cebeci-Smith model has been applied to a wide range of boundary-layer flows and has enjoyed a great deal of success. Figure 3.15, for example, compares computed skin friction, c_f, and shape factor, H, for a constant-pressure (flat-plate) boundary layer with Coles' [Coles and Hirst (1969)] correlation of experimental data. Results are expressed as functions of Reynolds number based on momentum thickness, Re_θ. As shown, model predictions virtually duplicate correlated values.

The model remains reasonably accurate for favorable pressure gradient and for mild adverse pressure gradient. Because the model has been fine tuned for boundary-layer flows, differences between computed and measured velocity profiles generally are small. Typically, integral parameters such as momentum thickness and shape factor show less than 10% differences from measured values.

Figure 3.16 compares computed and measured boundary-layer properties for two of the flows considered in the 1968 AFOSR-IFP-Stanford Conference on the Computation of Turbulent Boundary Layers (this conference is often referred to colloquially as Stanford Olympics I). For both cases, computed and measured velocity profiles are nearly identical. Flow 3100 is two dimensional with a mild favorable pressure gradient. Despite the close agreement in velocity profiles overall, differences in shape factor are between 8% and 10%. Flow 3600 is axisymmetric with an adverse pressure gradient. For this flow, shape factors differ by less than 5%. The Baldwin-Lomax model also closely reproduces measured flow properties for these types of boundary layers.

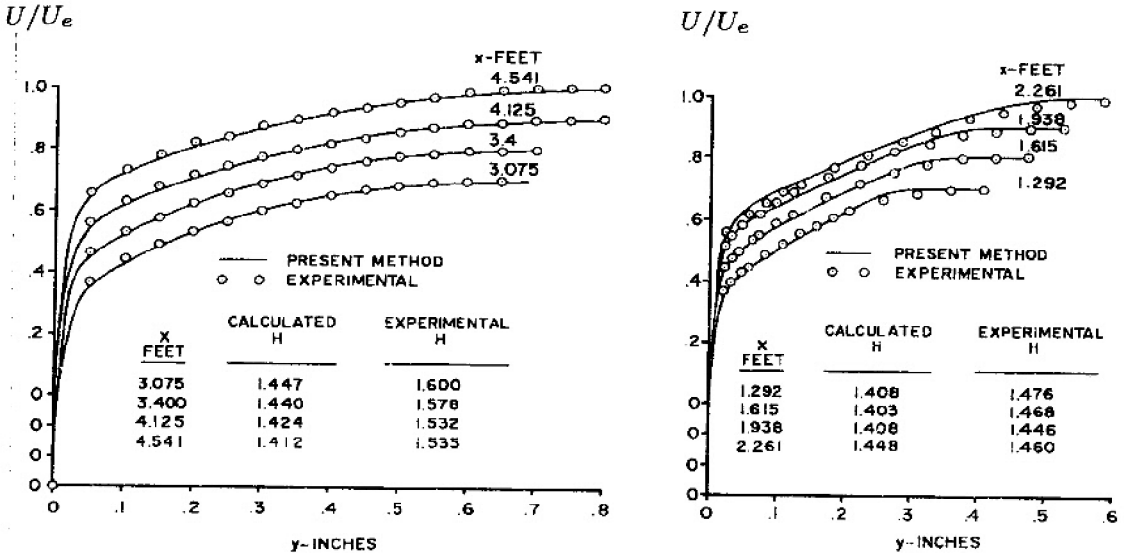

Flow 3100: Favorable ∇p

Flow 3600: Adverse ∇p

Figure 3.16: *Comparison of computed and measured boundary layer velocity profiles and shape factor for flows with nonzero pressure gradient; Cebeci-Smith model. [From Kline et al. (1969) — Used with permission.]*

Figure 3.17 compares computed and measured skin friction for sixteen incompressible boundary layers subjected to favorable, zero and adverse pressure gradients. For both models, computed and measured c_f generally differ by less than 10%. Fifteen of the sixteen cases considered are from Stanford Olympics I. The lone exception is Flow 0141, which corresponds to a boundary layer in an increasingly adverse pressure gradient. This flow has been studied experimentally by Samuel and Joubert [see Kline et al. (1981)]. It was a key boundary-layer case included in the 1980-81 AFOSR-HTTM-Stanford Conference on Complex Turbulent Flows (known colloquially as Stanford Olympics II). Measurements for all cases satisfy the momentum-integral equation, thus assuring their two-dimensionality and accuracy of the experiments.

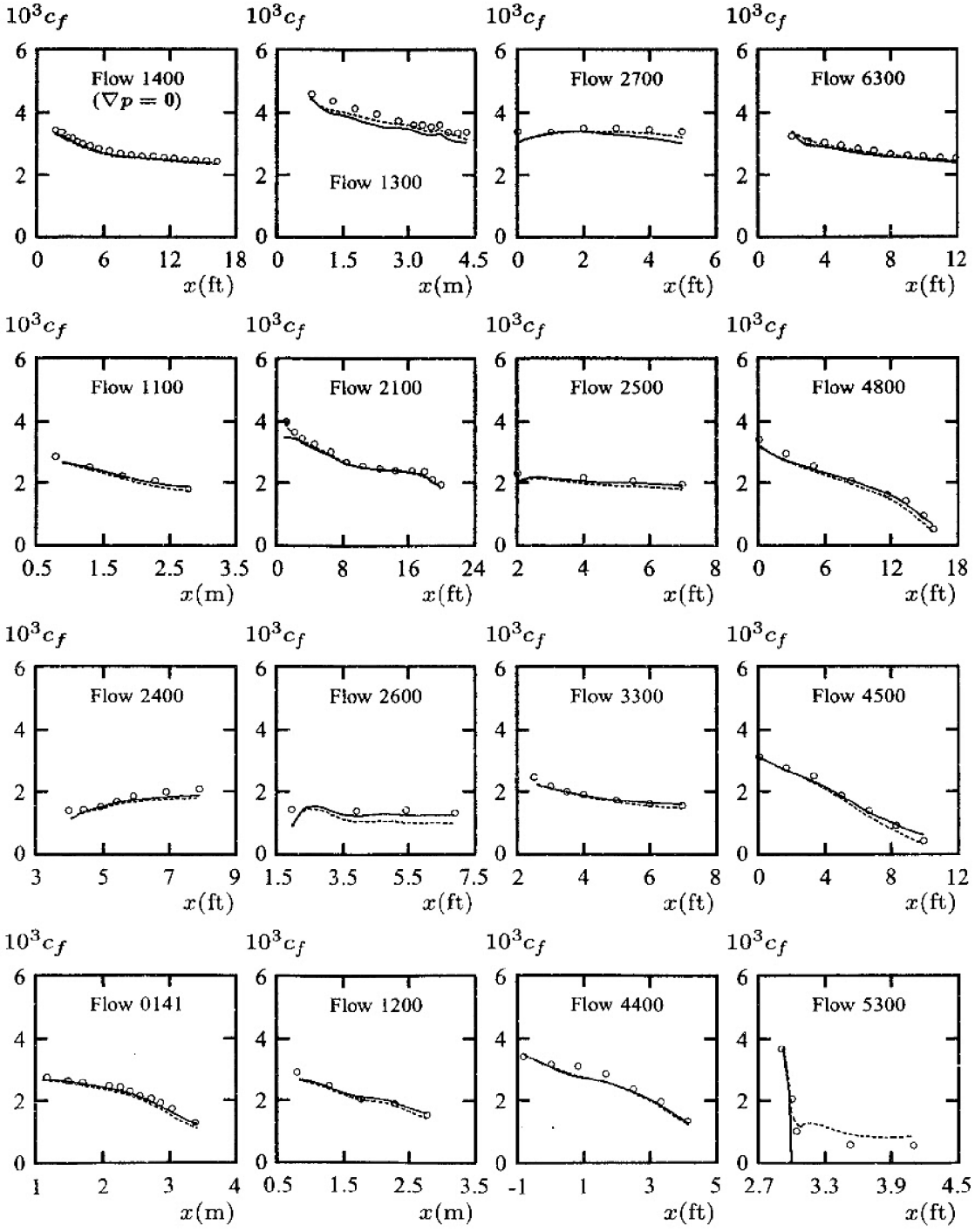

Figure 3.17: *Computed and measured skin friction for boundary layers subjected to a pressure gradient. Top row - favorable ∇p; next to top row - mild adverse ∇p; next to bottom row - moderate adverse ∇p; bottom row - strong adverse ∇p. —— Baldwin-Lomax model; - - - Cebeci-Smith model; ○ measured.*

Table 3.1 summarizes the difference between computed and measured c_f at the final station for the various pressure gradients. This is a sensible measure of the overall accuracy as all transients have settled out, and, with the exception of Flow 2400, the pressure gradient is strongest at the end of the computation. The overall average difference for the 16 cases is 9% for the Baldwin-Lomax model and 11% for the Cebeci-Smith model.

Table 3.1: *Differences Between Computed and Measured Skin Friction.*

Pressure Gradient	Flows	Baldwin-Lomax	Cebeci-Smith
Favorable	1400, 1300, 2700, 6300	7%	5%
Mild Adverse	1100, 2100, 2500, 4800	6%	7%
Moderate Adverse	2400, 2600, 3300, 4500	10%	15%
Strong Adverse	0141, 1200, 4400, 5300	14%	16%
All	–	9%	11%

One noteworthy case is Flow 3300 of the 1968 AFOSR-IFP-Stanford Conference on the Computation of Turbulent Boundary Layers. This flow, also known as Bradshaw Flow C, has a strongly adverse pressure gradient that is gradually relaxed and corresponds to an experiment performed by Bradshaw (1969). It was generally regarded as one of the most difficult to predict of all flows considered in the Conference. As shown, both models predict skin friction very close to the measured value. The Cebeci-Smith value for c_f at the final station ($x = 7$ ft.) is 6% lower than the measured value. The Baldwin-Lomax value exceeds the measured value at $x = 7$ ft. by 3%.

A second case worthy of mention is Flow 0141 of the 1980-81 AFOSR-HTTM-Stanford Conference on Complex Turbulent Flows. The close agreement between theory and experiment for this flow is remarkable. The Cebeci-Smith and Baldwin-Lomax values for c_f at $x \approx 3$ m. are within 14% and 2% of the measured value, respectively. This boundary layer was presumed to be a "simple" flow for Conference participants. However, as we will discuss further in Chapter 4, it proved to be the Achilles heel of the best turbulence models of the day.

The only case the models fail to predict accurately is Flow 5300, which is known as the Stratford (1959) "incipient-separation" flow. The boundary layer experiences an adverse pressure gradient that is of sufficient strength to drive it to the brink of separation. The Cebeci-Smith model's skin friction at the final station ($x = 4.1$ ft.) is 58% higher than measured. The Baldwin-Lomax model predicts boundary-layer separation at $x \approx 3$ ft.

As a final comment, all sixteen computations have been done using Program **EDDYBL**, a boundary-layer program suitable for two-dimensional and axisymmetric flows. The companion CD provided with this book includes the program and detailed user's information (see Appendix C).

3.6 Separated Flows

All of the applications in the preceding section are for attached boundary layers. We turn now to flows having an adverse pressure gradient of sufficient strength to cause the boundary layer to separate. Separation occurs in many practical applications including stalled airfoils, flow near the stern of a ship, flow through a diffuser, etc. Engineering design would be greatly enhanced if our turbulence model were a reliable analytical tool for predicting separation and its effect on surface pressure, skin friction and heat transfer. Unfortunately, algebraic models are quite unreliable for separated flows.

When a boundary layer separates, the streamlines are no longer nearly parallel to the surface as they are for attached boundary layers. We must solve the full Reynolds-averaged Navier-Stokes equation [Equation (2.24)], which includes all components of the Reynolds-stress tensor. In analogy to Stokes hypothesis for laminar flow, we set

$$\tau_{ij} = 2\nu_T S_{ij} \tag{3.144}$$

where S_{ij} is the mean strain-rate tensor defined by

$$S_{ij} = \frac{1}{2}[U_{i,j} + U_{j,i}] \tag{3.145}$$

Figure 3.18 is typical of separated-flow results for an algebraic model. The flow is axisymmetric and has a strong adverse pressure gradient. The experiment was conducted by Driver (1991). The computation was done with Program EDDY2C (see Appendix C). Inspection of the skin friction shows that the Baldwin-Lomax model yields a separation bubble nearly twice as long as the

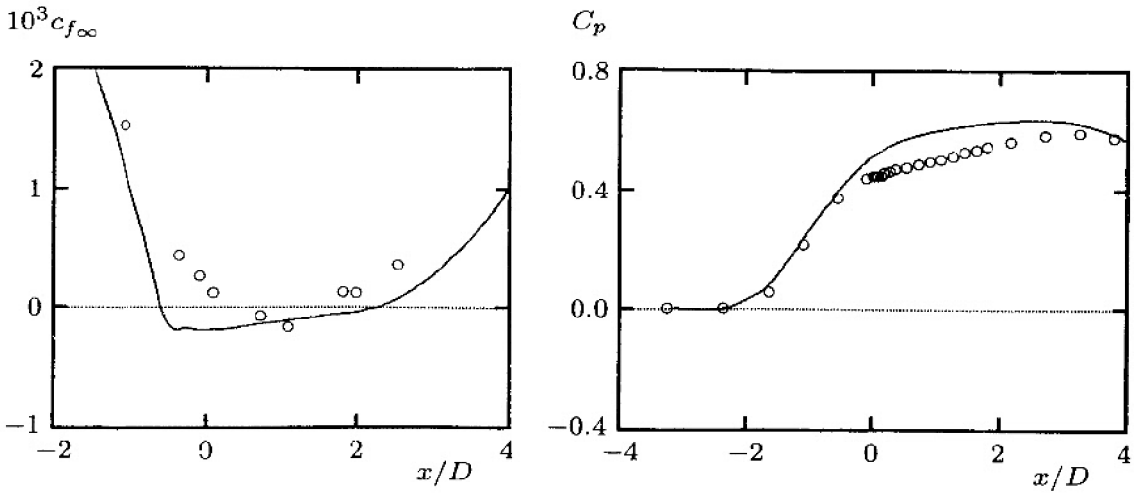

Figure 3.18: *Computed and measured flow properties for Driver's separated flow;* —— *Baldwin-Lomax model;* ○ *Driver.*

experimentally observed bubble. The corresponding rise in pressure over the separation region is 15% to 20% higher than measured. As noted by Menter (1992b), the Cebeci-Smith model yields similar results.

It is not surprising that a turbulence model devoid of any information about flow history will perform poorly for separated flows. On the one hand, the mean strain-rate tensor undergoes rapid changes in a separated flow associated with the curved streamlines over and within the separation bubble. On the other hand, the turbulence adjusts to changes in the flow on a time scale unrelated to the mean rate of strain. Rotta (1962), for example, concludes from analysis of experimental data that when a turbulent boundary layer is perturbed from its equilibrium state, a new equilibrium state is not attained for at least 10 boundary-layer thicknesses downstream of the perturbation. In other words, separated flows are very much out of "equilibrium." The Boussinesq approximation, along with all the "equilibrium" approximations implicit in an algebraic model, can hardly be expected to provide an accurate description for separated flows.

Attempts have been made to remedy the problem of poor separated-flow predictions with the Cebeci-Smith model. Shang and Hankey (1975) introduced the notion of a relaxation length, L, to account for upstream turbulence history effects. They introduced what they called a **relaxation eddy viscosity model** and determined the eddy viscosity as follows.

$$\mu_T = \mu_{T_{eq}} - (\mu_{T_{eq}} - \mu_{T_1})e^{-(x-x_1)/L} \tag{3.146}$$

The quantity $\mu_{T_{eq}} = \rho\nu_{T_{eq}}$ denotes the equilibrium eddy viscosity corresponding to the value given by Equations (3.110) through (3.113), while μ_{T_1} is the value of the eddy viscosity at a reference point, $x = x_1$, upstream of the separation region. Typically, the relaxation length is about $5\delta_1$, where δ_1 is the boundary-layer thickness at $x = x_1$. The principal effect of Equation (3.146) is to reduce the Reynolds stress from the "equilibrium" value predicted by the Cebeci-Smith model. This mimics the experimental observation that the Reynolds stress remains nearly frozen at its initial value while it is being convected along streamlines in the separation region, and approaches a new equilibrium state exponentially.

In a similar vein, Hung (1976) proposed a differential form of Shang and Hankey's Equation (3.146), viz.,

$$\frac{d\mu_T}{dx} = \frac{\mu_{T_{eq}} - \mu_T}{L} \tag{3.147}$$

This equation is very similar to the earlier proposal of Reyhner [Kline et al. (1969)]. Hung (1976) exercised these relaxation models in several supersonic shock-separated flows. He was able to force close agreement between computed and measured locations of the separation point and the surface-pressure distribution. However, he found that these improvements come at the expense

of increased discrepancies between computed and measured skin friction, heat transfer and reattachment-point location.

3.7 The 1/2-Equation Model

Johnson and King (1985) [see also Johnson (1987) and Johnson and Coakley (1990)] have devised a "non-equilibrium" version of the algebraic model. Their starting point is a so-called "equilibrium" algebraic model in which the eddy viscosity is

$$\mu_T = \mu_{T_o} \tanh(\mu_{T_i}/\mu_{T_o}) \tag{3.148}$$

where μ_{T_i} and μ_{T_o} represent inner-layer and outer-layer eddy viscosity, respectively. The hyperbolic tangent is used to eliminate the discontinuity in $\partial\mu_T/\partial y$ attending the use of Equation (3.110).

Inner Layer:

The inner-layer viscosity, μ_{T_i}, is similar to the form used in the Cebeci-Smith and Baldwin-Lomax models. However, the dependence on velocity gradient has been replaced by explicit dependence on distance from the surface, y, and two primary velocity scales, u_τ and u_m, as follows:

$$\mu_{T_i} = \rho\left[1 - \exp\left(-\frac{u_D y/\nu}{A^+}\right)\right]^2 \kappa u_s y \tag{3.149}$$

$$\sqrt{\rho}\, u_s = (1-\gamma_2)\sqrt{\tau_w} + \gamma_2\sqrt{\tau_m} \tag{3.150}$$

$$\gamma_2 = \tanh(y/L_c) \tag{3.151}$$

$$L_c = \frac{\sqrt{\tau_w}}{\sqrt{\tau_w} + \sqrt{\tau_m}} L_m \tag{3.152}$$

$$L_m = \begin{cases} \kappa y_m, & y_m/\delta \le C_1/\kappa \\ C_1\delta, & y_m/\delta > C_1/\kappa \end{cases} \tag{3.153}$$

$$u_m = \sqrt{\tau_m/\rho_m} \tag{3.154}$$

$$u_D = \max[u_m, u_\tau] \tag{3.155}$$

where subscript m denotes the value at the point, $y = y_m$, at which the Reynolds shear stress, $\rho\tau_{xy}$, assumes its maximum value denoted by $\tau_m = (\rho\tau_{xy})_{max}$. Additionally u_τ is the conventional friction velocity and ρ_w is the density at the surface, $y = 0$. In its original form, this model used only the velocity scale u_m in Equation (3.149). This scale proved to provide better predictions of velocity profile shape for separated flows than the velocity-gradient prescription of Prandtl [Equation (3.15)]. Later, the secondary velocity scales u_s and u_D were added to improve predictions for reattaching flows and for flows with nontrivial effects of compressibility.

Outer Layer:

The "non-equilibrium" feature of the model comes in through the appearance of a "nonequilibrium parameter," $\sigma(x)$, so that:

$$\mu_{T_o} = \alpha \rho U_e \delta_v^* F_{Kleb}(y;\delta)\sigma(x) \tag{3.156}$$

Comparison of this equation with Equation (3.113) shows that the outer-layer viscosity, $\mu_{T_o} = \rho \nu_{T_o}$, is equal to that used in the Cebeci-Smith model multiplied by $\sigma(x)$. The Johnson-King model solves the following **ordinary differential equation** for the maximum Reynolds shear stress, τ_m, in terms of $u_m = \sqrt{\tau_m/\rho_m}$.

$$U_m \frac{d}{dx}\left(u_m^2\right) = a_1 \left[\frac{(u_m)_{eq} - u_m}{L_m}\right] u_m^2 - C_{dif}\left[\frac{u_m^3}{C_2\delta - y_m}\right]\left|1 - \sigma^{1/2}(x)\right| \tag{3.157}$$

where U_m is mean velocity and $(u_m)_{eq}$ is the value of u_m according to the "equilibrium" algebraic model [$\sigma(x) = 1$]. The first term on the right-hand side of Equation (3.157) is reminiscent of Hung's relaxation model [Equation (3.147)]. The second term is an estimate of the effect of turbulent diffusion on the Reynolds shear stress. Equation (3.157) is solved along with the Reynolds-averaged equations to determine τ_m. As the solution proceeds, the coefficient $\sigma(x)$ is determined so that the maximum Reynolds shear stress is given by

$$\tau_m = (\mu_T)_m \left(\frac{\partial U}{\partial y} + \frac{\partial V}{\partial x}\right)_m \tag{3.158}$$

That is, the μ_T distribution is adjusted to agree with τ_m. In using this model, computations must be done iteratively since $\sigma(x)$ is unknown a priori, wherefore the value from a previous iteration or an extrapolated value must be used in solving Equation (3.157) for τ_m.

Closure Coefficients:

$$\left.\begin{array}{lll} \kappa = 0.40, & \alpha = 0.0168, & A^+ = 17 \\ a_1 = 0.25, & C_1 = 0.09, & C_2 = 0.70 \\ C_{dif} = 0.50 & \text{for } \sigma(x) \geq 1; & 0 \text{ otherwise} \end{array}\right\} \tag{3.159}$$

The general idea of this model is that the Reynolds shear stress adjusts to departures from "equilibrium" at a rate different from that predicted by the algebraic model. The ordinary differential equation for u_m is used to account for the difference in rates. Because this equation is an **ordinary**, as opposed to a **partial**, differential equation, the turbulence community has chosen the curious terminology **1/2-Equation Model** to describe this model. It is unclear whether this means it has half the number of dimensions (but then, it would have to be a 1/3-Equation Model for three-dimensional applications) or if partial differential equations are twice as hard to solve as ordinary differential equations.

Figure 3.19 compares computed and measured skin friction for the sixteen boundary-layer flows of Stanford Olympics I and II discussed earlier. As with the algebraic models, the computations have been done using Program **EDDYBL** (see Appendix C). Note that predicted c_f for the constant-pressure case (Flow 1400) is 5% less than measured values. This is a direct consequence of using Equation (3.148). As can be readily verified, using Equation (3.110), computed skin friction matches measured values almost exactly.

As summarized in Table 3.2, overall differences between computed and measured c_f are somewhat larger than corresponding differences for the Baldwin-Lomax model. The overall average difference at the final station for the flows is 20% as compared to 9% for the Baldwin-Lomax model (and 11% for the Cebeci-Smith model).

Table 3.2: *Differences Between Computed and Measured Skin Friction.*

Pressure Gradient	Flows	Johnson-King	Baldwin-Lomax
Favorable	1400, 1300, 2700, 6300	7%	7%
Mild Adverse	1100, 2100, 2500, 4800	11%	6%
Moderate Adverse	2400, 2600, 3300, 4500	13%	10%
Strong Adverse	0141, 1200, 4400, 5300	50%	14%
All	–	20%	9%

As noted earlier, Bradshaw Flow C (Flow 3300) was one of the most difficult cases in the 1968 AFOSR-IFP-Stanford Conference on the Computation of Turbulent Boundary Layers. The Johnson-King model fares rather poorly on this case with computed skin friction 19% higher than the measured value at the final station. Recall that the Cebeci-Smith and Baldwin-Lomax model predictions were within 6% and 3% of the measured value, respectively.

Also, for the Samuel-Joubert increasingly adverse pressure gradient case (Flow 0141), the computed skin friction is 13% *higher* than the measured value. By contrast, the Cebeci-Smith and Baldwin-Lomax models predict c_f 14% and 2% *lower*, respectively.

As a bit of a surprise, while the predicted boundary layer remains attached for the Stratford incipient-separation case (Flow 5300), the computed skin friction is more than four times the measured value. Results obtained with the Cebeci-Smith model (see Figure 3.17) are quite a bit closer to measurements.

Although the differences are somewhat larger than those of the algebraic models, inspection of Figure 3.19 shows that, with the exception of Flow 5300, the accuracy is satisfactory for most engineering applications. The differences can probably be reduced to the same levels as for the Baldwin-Lomax and Cebeci-Smith models by either recalibrating the closure coefficients or by using Equation (3.110) instead of Equation (3.148).

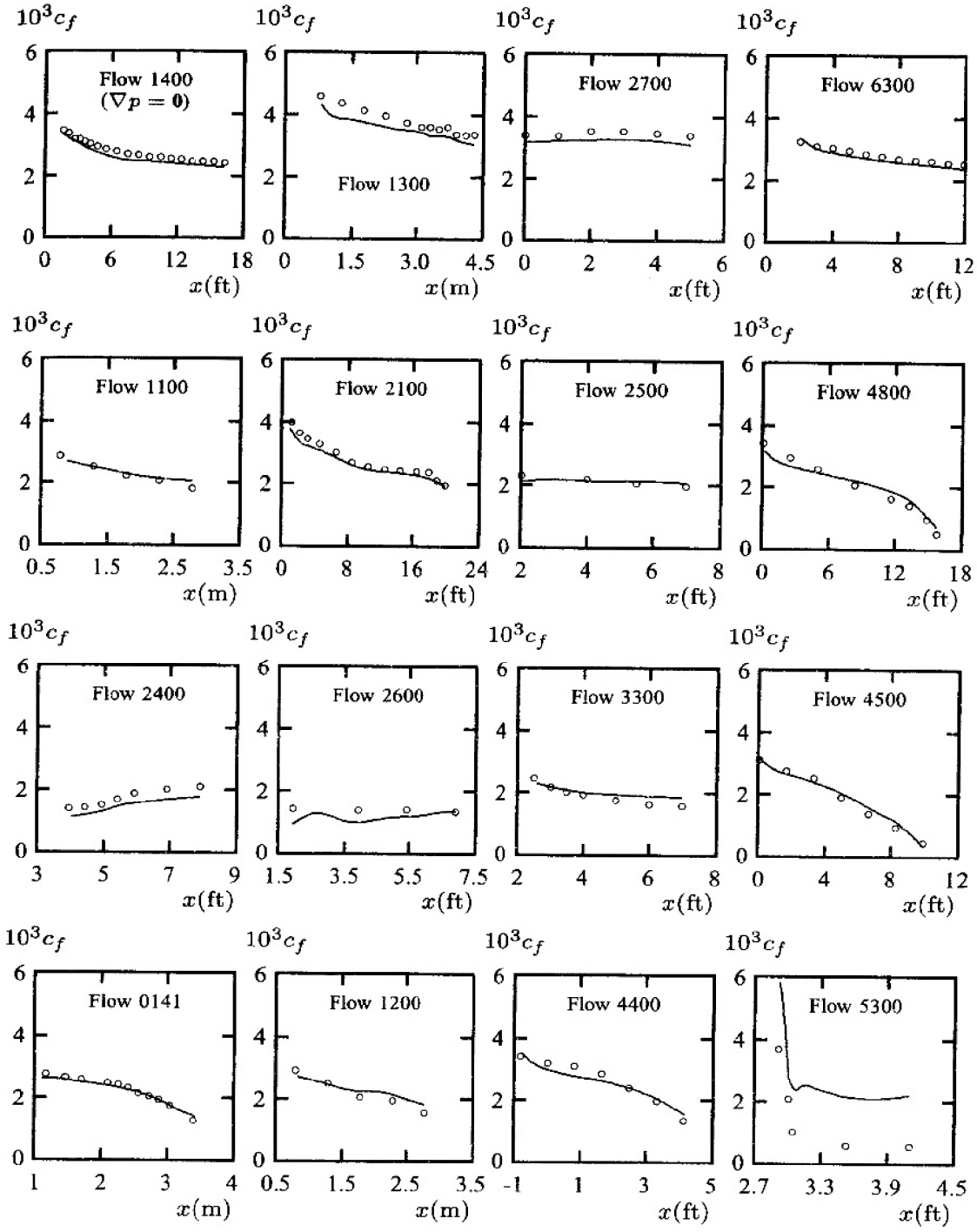

Figure 3.19: *Computed and measured skin friction for boundary layers subjected to a pressure gradient. Top row - favorable ∇p; next to top row - mild adverse ∇p; next to bottom row - moderate adverse ∇p; bottom row - strong adverse ∇p. — Johnson-King model; ○ measured.*

Menter (1992b) has applied the Johnson-King model to Driver's (1991) separated flow. Figure 3.20 compares computed and measured values; results for the Baldwin-Lomax model are also included. As shown, the Johnson-King model predictions are much closer to measurements, most notably in the size of the separation region.

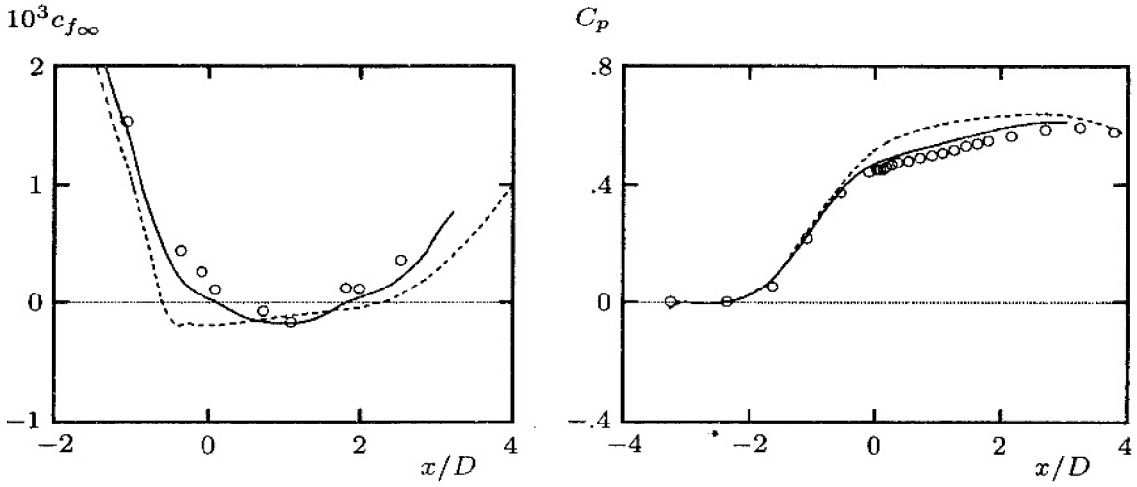

Figure 3.20: *Computed and measured flow properties for Driver's separated flow;* —— *Johnson-King model;* - - - *Baldwin-Lomax;* ○ *Driver.*

3.8 Range of Applicability

Algebraic models are the simplest and easiest to implement of all turbulence models. They are conceptually very simple and rarely cause unexpected numerical difficulties. Because algebraic models are so easy to use, they should be replaced only where demonstrably superior alternatives are available.

The user must always be aware of the issue of **incompleteness**. These models will work well only for the flows for which they have been fine tuned. There is very little hope of extrapolating beyond the established data base for which an algebraic model is calibrated. We need only recall that for the five free shear flows considered in Section 3.3, five different values for the mixing length are needed—and none of these lengths is appropriate for wall-bounded flows!

On balance, both the Cebeci-Smith and Baldwin-Lomax models faithfully reproduce skin friction and velocity profiles for incompressible turbulent boundary layers provided the pressure gradient is not too strong. Neither model is clearly superior to the other: the accuracy level is about the same for both. The chief virtue of the Baldwin-Lomax model over the Cebeci-Smith model is its independence of properties such as δ_v^* that can often be difficult to define accurately in

complex flows. Its other differences from the Cebeci-Smith model are probably accidental. However, neither model is reliable for separated flows. Despite this well-known limitation, many incautious researchers have applied the Baldwin-Lomax model to extraordinarily complex flows where its only virtue is that it doesn't cause the computation to blow up.

The Johnson-King model offers a helpful modification that removes much of the inadequacy of algebraic models for separated flows. However, like algebraic models, the Johnson-King model provides no information about the turbulence length scale and is thus **incomplete**. Consequently, it shares many of the shortcomings of the underlying algebraic model. **On the negative side**, the improved agreement between theory and experiment for separated flows has been gained with a loss of the elegance and simplicity of the Cebeci-Smith model. The number of ad hoc closure coefficients has increased from three to seven, and the model inherently requires an iterative solution procedure. The model is also formulated specifically for wall-bounded flows and is thus restricted to such flows, i.e., the model is highly geometry dependent. **On the positive side**, the Johnson-King model has been applied to many transonic flows that tend to be particularly difficult to predict with modern turbulence models. The model's track record has been quite good with such flows. Its predictions for attached boundary layers could be made even closer to measurements by either using Equation (3.110) instead of Equation (3.148) or simply recalibrating the model's closure coefficients. On balance, this model appears to be a useful engineering design tool, within its verified range of applicability.

Problems

3.1 With the eddy viscosity given by Equation (3.25), generate a similarity solution for the far wake. Obtain the exact closed-form solution, and determine the value of χ by forcing agreement with the corresponding $u_o(x)$ and $\delta(x)$ derived in this chapter. The following integral will be useful when you apply the integral constraint.

$$\int_0^\infty e^{-\xi^2} d\xi = \frac{\sqrt{\pi}}{2}$$

3.2 With the eddy viscosity given by Equation (3.25), generate a similarity solution for the plane jet. Obtain the exact closed-form solution, and determine the value of χ by forcing agreement with the corresponding $u_o(x)$ and $\delta(x)$ derived in this chapter. The following integrals will be useful in deriving the solution.

$$\int \frac{dx}{c^2 - x^2} = \frac{1}{c} \tanh^{-1}\left(\frac{x}{c}\right) + \text{constant}$$

$$\int_0^\infty \left[1 - \tanh^2 \xi\right]^2 d\xi = \frac{2}{3}$$

3.3 Beginning with the integral constraint in Equation (3.81) and assuming the streamwise velocity is $U(x, y) = u_o(x)\mathcal{U}(\eta)$ where $\eta = y/(Ax)$, determine the function $u_o(x)$. Arrange your result so that

$$\int_0^\infty \mathcal{U}^2(\eta)\, \eta^j\, d\eta = 1$$

and verify that your solution is consistent with Equation (3.84).

3.4 Verify that the solution to Equations (3.45) is given by Equations (3.46) – (3.48) for the far wake.

3.5 Beginning with Equation (3.65), introduce Equations (3.68) through (3.71) and derive Equation (3.73) for the mixing layer.

3.6 Beginning with Equation (3.83), derive Equation (3.86) for plane and round jets.

3.7 Beginning with Equation (3.83), derive Equation (3.86) for the radial jet.

3.8 The skin friction and displacement thickness for a constant-pressure turbulent boundary layer are approximately $c_f \approx 0.045 Re_\delta^{-1/4}$ and $\delta^* \approx \frac{1}{8}\delta$, where $Re_\delta = U_e\delta/\nu$ is Reynolds number based on δ. Note also that, by definition, $c_f = 2u_\tau^2/U_e^2$. Assuming the matching point always occurs in the log layer so that $\partial U/\partial y = u_\tau/(\kappa y)$, make a graph of y_m/δ and y_m^+ versus Re_δ for the Cebeci-Smith model. Let Re_δ vary between 10^4 and 10^6. You should first rewrite the equations for ν_{T_i} and ν_{T_o} in terms of y/δ and Re_δ. Then, solve the resulting equation for y_m/δ with an iterative procedure such as Newton's method. Compare your numerical results with Equation (3.118).

3.9 Show that using Equation (3.99) for the mixing length in the viscous sublayer yields a velocity that behaves according to:

$$U^+ \approx y^+ - \frac{\kappa^2}{3}(y^+)^3 + \cdots \qquad \text{as} \qquad y^+ \to 0$$

3.10 Assume the velocity in a boundary layer for $y^+ \gg 1$ is given by

$$U^+ \approx \frac{1}{\kappa}\ell n y^+ + 5.0 + \frac{1}{\kappa}\sin^2\left(\frac{\pi y}{2\delta}\right)$$

Also, assume that $y_{max} \gg 26\nu/u_\tau$ for the Baldwin-Lomax model. Compute the quantities $y_{max}F_{max}$ and $C_{wk}y_{max}U_{dif}^2/F_{max}$ for this boundary layer. Then, noting that skin friction is given by $c_f = 2u_\tau^2/U_e^2$, determine the largest value of c_f for which $F_{wake} = y_{max}F_{max}$. **HINT:** The solution to the transcendental equation $\xi + \tan\xi = 0$ is $\xi \approx 2.03$.

3.11 The momentum equation in the sublayer and log layer for a turbulent boundary layer with surface mass transfer simplifies to:

$$v_w\frac{dU}{dy} = \frac{d}{dy}\left[(\nu + \nu_T)\frac{dU}{dy}\right]$$

where v_w is the (constant) vertical velocity at the surface.

(a) Integrate once using the appropriate surface boundary conditions. Introduce the friction velocity, u_τ, in stating your integrated equation.

(b) Focusing now upon the log layer where $\nu_T \gg \nu$, what is the approximate form of the equation derived in Part (a) if we use the Cebeci-Smith model?

(c) Verify that the solution to the simplified equation of Part (b) is

$$2\frac{u_\tau}{v_w}\sqrt{1 + v_w U/u_\tau^2} = \frac{1}{\kappa}\ell n y + \text{constant}$$

3.12 Determine the constant C in the law of the wall implied by the mixing-length model using a standard numerical integration scheme such as the Runge-Kutta method. That is, solve the following equation for U^+.

$$(1 + \mu_T^+)\frac{dU^+}{dy^+} = 1$$

Integrate from $y^+ = 0$ to $y^+ = 500$ and calculate the limiting value of C as $y^+ \to \infty$ from examination of

$$C = U^+ - \frac{1}{\kappa}\ell n y^+ \qquad \text{at} \qquad y^+ = 250, 300, 350, 400, 450 \text{ and } 500$$

Do the computation with the mixing length given by (i) Equation (3.99) and (ii) Equation (3.105). **NOTE:** To avoid truncation error, verify the following limiting form of the equation for dU^+/dy^+.

$$\frac{dU^+}{dy^+} \approx 1 - \left(\ell_{mix}^+\right)^2 + 2\left(\ell_{mix}^+\right)^4 + \cdots \qquad \text{as} \qquad \ell_{mix}^+ \to 0$$

Use this asymptotic form very close to $y^+ = 0$.

3.13 Generate a solution for channel and pipe flow using a mixing-length model with the mixing length in the inner and outer layers given by

$$\ell_{mix} = \begin{cases} \kappa y \left[1 - e^{-y^+/26}\right] & , \quad \text{Inner Layer} \\ .09R & , \quad \text{Outer Layer} \end{cases}$$

where R is channel half-height or pipe radius. Use a numerical integration scheme such as the Runge-Kutta method, or modify Program **PIPE** (see Appendix C). Compare computed skin friction with Equations (3.139) and (3.140). **See NOTE below.**

NOTE for 3.13 and 3.14: *To assist in presenting your results, verify that skin friction and Reynolds number are given by* $c_f = 2/(U^+_{avg})^2$ *and* $Re_D = 2U^+_{avg}R^+$ *where* $R^+ = u_\tau R/\nu$ *and* U_{avg} *is the average velocity across the channel/pipe. Also, to avoid truncation error, verify the following limiting form of the equation for* dU^+/dy^+ *in the limit* $\ell^+_{mix} \to 0$.

$$\frac{dU^+}{dy^+} \approx \left(1 - \frac{y^+}{R^+}\right)\left[1 - \left(1 - \frac{y^+}{R^+}\right)(\ell^+_{mix})^2 + 2\left(1 - \frac{y^+}{R^+}\right)^2 (\ell^+_{mix})^4\right]$$

Use this asymptotic form very close to $y^+ = 0$.

3.14 Generate a solution for pipe flow using a mixing-length model with the mixing length given by Nikuradse's formula, i.e.,

$$\ell_{mix}/R = 0.14 - 0.08(1 - y/R)^2 - 0.06(1 - y/R)^4$$

where R is pipe radius. Use a numerical integration scheme such as the Runge-Kutta method, or modify Program **PIPE** (see Appendix C). Compare computed skin friction with Equation (3.140). **See NOTE above.**

3.15 Using a standard numerical integration scheme such as the Runge-Kutta method, determine the constant C in the law of the wall implied by the Johnson-King model. That is, solve the following equation for U^+.

$$(1 + \mu^+_T)\frac{dU^+}{dy^+} = 1$$

Integrate from $y^+ = 0$ to $y^+ = 500$ and calculate the limiting value of C as $y^+ \to \infty$ from examination of

$$C = U^+ - \frac{1}{\kappa}\ell n y^+ \qquad \text{at} \qquad y^+ = 250, 300, 350, 400, 450 \text{ and } 500$$

NOTE: To avoid truncation error, verify the following limiting form for dU^+/dy^+.

$$\frac{dU^+}{dy^+} \approx 1 - \left(\ell^+_{mix}\right)^2 + 2\left(\ell^+_{mix}\right)^4 + \cdots \qquad \text{as} \qquad \ell^+_{mix} \to 0$$

Use this asymptotic form very close to $y^+ = 0$.

3.16 Using Program **PIPE** and its menu-driven setup utility, Program **PIPE_DATA** (see Appendix C), compute the skin friction for channel flow according to the Johnson-King model. Compare your results with the Halleen-Johnston correlation [Equation (3.139] for $10^3 \leq Re_H \leq 10^5$. Also, compare the computed velocity profile for $Re_H = 13750$ with the Mansour et al. DNS data, which are as follows.

$y/(H/2)$	U/U_m	$y/(H/2)$	U/U_m	$y/(H/2)$	U/U_m
0.000	0.000	0.404	0.887	0.805	0.984
0.103	0.717	0.500	0.917	0.902	0.995
0.207	0.800	0.602	0.945	1.000	1.000
0.305	0.849	0.710	0.968		

3.17 Using Program **PIPE** and its menu-driven setup utility, Program **PIPE_DATA** (see Appendix C), compute the skin friction for pipe flow according to the Johnson-King model. Compare your numerical results with the Prandtl correlation [Equation (3.140] for $10^3 \leq Re_D \leq 10^6$. Also, compare the computed velocity profile for $Re_D = 40000$ with Laufer's data, which are as follows.

$y/(D/2)$	U/U_m	$y/(D/2)$	U/U_m	$y/(D/2)$	U/U_m
0.010	0.333	0.390	0.868	0.800	0.975
0.095	0.696	0.490	0.902	0.900	0.990
0.210	0.789	0.590	0.931	1.000	1.000
0.280	0.833	0.690	0.961		

3.18 The object of this problem is to compare predictions of algebraic models with measured properties of a turbulent boundary layer with adverse ∇p. The experiment to be simulated was conducted by Ludwieg and Tillman [see Coles and Hirst (1969) – Flow 1200]. Use Program **EDDYBL**, its menu-driven setup utility, Program **EDDYBL_DATA**, and the input data provided on the companion CD (see Appendix C). Do 3 computations using the Cebeci-Smith, Baldwin-Lomax and Johnson-King models and compare computed skin friction with the following measured values.

s (m)	c_f	s (m)	c_f
0.782	$2.92 \cdot 10^{-3}$	2.282	$1.94 \cdot 10^{-3}$
1.282	$2.49 \cdot 10^{-3}$	2.782	$1.55 \cdot 10^{-3}$
1.782	$2.05 \cdot 10^{-3}$		

3.19 The object of this problem is to compare predictions of algebraic models with measured properties of a turbulent boundary layer with adverse ∇p. The experiment to be simulated was conducted by Bradshaw [see Coles and Hirst (1969) – Flow 3300]. Use Program **EDDYBL**, its menu-driven setup utility, Program **EDDYBL_DATA**, and the input data provided on the companion CD (see Appendix C). Do 3 computations using the Cebeci-Smith, Baldwin-Lomax and Johnson-King models and compare computed skin friction with the following measured values.

s (ft)	c_f	s (ft)	c_f	s (ft)	c_f
2.5	$2.45 \cdot 10^{-3}$	4.00	$1.91 \cdot 10^{-3}$	7.00	$1.56 \cdot 10^{-3}$
3.0	$2.17 \cdot 10^{-3}$	5.00	$1.74 \cdot 10^{-3}$		
3.5	$2.00 \cdot 10^{-3}$	6.00	$1.61 \cdot 10^{-3}$		

3.20 The object of this problem is to predict the separation point for flow past a circular cylinder with the boundary-layer equations, using the measured pressure distribution. The experiment to be simulated was conducted by Patel (1968). Use Program **EDDYBL** and its menu-driven setup utility, Program **EDDYBL_DATA**, to do the computations (see Appendix C).

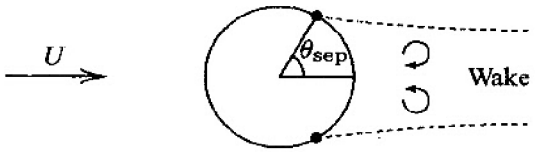

Problem 3.20

(a) Set freestream conditions to $p_{t_\infty} = 2147.7$ lb/ft^2, $T_{t_\infty} = 529.6°$ R, $M_\infty = 0.144$ (PT1, TT1, XMA); use an initial stepsize, initial arclength and final arclength given by $\Delta s = 0.001$ ft, $s_i = 0.262$ ft and $s_f = 0.785$ ft (DS, SI, SSTOP); set the initial boundary-layer properties so that $c_f = 0.00600$, $\delta = 0.006$ ft, $H = 1.40$, $Re_\theta = 929$, (CF, DELTA, H, RETHET); set the maximum number of steps to 500 (IEND1); and set up for $N = 47$ points to define the pressure (NUMBER). Use the following data to define the pressure distribution. The initial and final pressure gradients are zero. Finally, use zero heat flux at the cylinder surface.

s (ft)	p_e (lb/ft^2)	s (ft)	p_e (lb/ft^2)	s (ft)	p_e (lb/ft^2)
0.0000	$2.147540 \cdot 10^3$	0.1500	$2.116199 \cdot 10^3$	0.3500	$2.055516 \cdot 10^3$
0.0025	$2.147528 \cdot 10^3$	0.1625	$2.112205 \cdot 10^3$	0.3625	$2.056591 \cdot 10^3$
0.0050	$2.147491 \cdot 10^3$	0.1750	$2.107903 \cdot 10^3$	0.3750	$2.058435 \cdot 10^3$
0.0075	$2.147429 \cdot 10^3$	0.1875	$2.103448 \cdot 10^3$	0.3875	$2.061661 \cdot 10^3$
0.0100	$2.147343 \cdot 10^3$	0.2000	$2.098378 \cdot 10^3$	0.4000	$2.066423 \cdot 10^3$
0.0125	$2.147233 \cdot 10^3$	0.2125	$2.093155 \cdot 10^3$	0.4125	$2.071954 \cdot 10^3$
0.0250	$2.146314 \cdot 10^3$	0.2250	$2.087317 \cdot 10^3$	0.4250	$2.079021 \cdot 10^3$
0.0375	$2.144796 \cdot 10^3$	0.2375	$2.081325 \cdot 10^3$	0.4375	$2.085473 \cdot 10^3$
0.0500	$2.142688 \cdot 10^3$	0.2500	$2.075334 \cdot 10^3$	0.4500	$2.089161 \cdot 10^3$
0.0625	$2.140018 \cdot 10^3$	0.2625	$2.069189 \cdot 10^3$	0.4625	$2.091004 \cdot 10^3$
0.0750	$2.136807 \cdot 10^3$	0.2750	$2.064580 \cdot 10^3$	0.4750	$2.092080 \cdot 10^3$
0.0875	$2.134021 \cdot 10^3$	0.2875	$2.060893 \cdot 10^3$	0.4875	$2.092230 \cdot 10^3$
0.1000	$2.130641 \cdot 10^3$	0.3000	$2.058588 \cdot 10^3$	0.5000	$2.092230 \cdot 10^3$
0.1125	$2.127261 \cdot 10^3$	0.3125	$2.056898 \cdot 10^3$	0.6500	$2.092230 \cdot 10^3$
0.1250	$2.123881 \cdot 10^3$	0.3250	$2.055823 \cdot 10^3$	0.7850	$2.092230 \cdot 10^3$
0.1375	$2.120194 \cdot 10^3$	0.3375	$2.055362 \cdot 10^3$		

(b) Do three computations using the Cebeci-Smith, Baldwin-Lomax and Johnson-King models. Compare computed separation angle measured from the downstream symmetry axis with the measured value of $\theta_{sep} = 70°$. The radius of the cylinder is $R = 0.25$ ft, so that separation arclength, s_{sep}, is related to this angle by $\theta_{sep} = \pi - s_{sep}/R$.

Chapter 4

One-Equation and Two-Equation Models

As computers have increased in power since the 1960's, turbulence models based upon the equation for the turbulence kinetic energy have become the cornerstone of modern turbulence-modeling research. This chapter discusses two types of eddy-viscosity models, viz., **One-Equation Models** and **Two-Equation Models**, with most of the emphasis on the latter. These models both retain the Boussinesq eddy-viscosity approximation, but differ in one important respect. One-equation models based on the turbulence kinetic energy equation are **incomplete** as they relate the turbulence length scale to some typical flow dimension. These models are rarely used. By contrast, two-equation models and one-equation models based on an equation for the eddy viscosity automatically provide the turbulence length scale or its equivalent and are thus **complete**.

The chapter focuses strictly on incompressible flow and begins with a derivation and discussion of the turbulence kinetic energy equation. We then introduce one-equation models based on this equation and upon a postulated equation for the eddy viscosity. The discussion includes examples of how such models fare for several flows. Next, we introduce two-equation models with specific details of the two most commonly used models. Our first two-equation model applications are to the same free shear flows considered in Chapter 3. Then, we use a powerful tool, singular-perturbation theory, to analyze model-predicted features of the turbulent boundary layer. We apply two-equation models to attached wall-bounded flows and compare to corresponding algebraic-model predictions. We discuss the issue of asymptotic consistency approaching a solid boundary, and the ability of two-equation models to predict transition from laminar to turbulent flow. Our final applications are to separated flows. The concluding section discusses the range of applicability of one- and two-equation models.

4.1 The Turbulence Energy Equation

Turbulence energy equation models have been developed to incorporate nonlocal and flow history effects in the eddy viscosity. Prandtl (1945) postulated computing a characteristic velocity scale for the turbulence, v_{mix}, thus obviating the need for assuming that $v_{mix} \sim \ell_{mix}|\partial U/\partial y|$ [c.f. Equation (3.15)]. He chose the kinetic energy (per unit mass) of the turbulent fluctuations, k, as the basis of his velocity scale, i.e.,

$$k = \frac{1}{2}\overline{u_i' u_i'} = \frac{1}{2}\left(\overline{u'^2} + \overline{v'^2} + \overline{w'^2}\right) \tag{4.1}$$

Thus, in terms of k and a turbulence length scale, ℓ, dimensional arguments dictate that the kinematic eddy viscosity is given by

$$\nu_T = \text{constant} \cdot k^{1/2}\ell \tag{4.2}$$

Note that we drop subscript "mix" in this chapter for convenience, and to avoid confusion with the mixing length used in algebraic models.

The question now arises as to how we determine k. The answer is provided by taking the trace of the Reynolds-stress tensor, which yields the following.

$$\tau_{ii} = -\overline{u_i' u_i'} = -2k \tag{4.3}$$

Thus, the trace of the Reynolds-stress tensor is proportional to the kinetic energy of the turbulent fluctuations per unit volume. The quantity k should strictly be referred to as **specific turbulence kinetic energy** ("specific" meaning "per unit mass"), but is often just called **turbulence kinetic energy**.

In Chapter 2 we derived a differential equation describing the behavior of the Reynolds-stress tensor, τ_{ij}, i.e., Equation (2.34). We can derive a corresponding equation for k by taking the trace of the Reynolds-stress equation. Noting that the trace of the tensor Π_{ij} vanishes for incompressible flow, contracting Equation (2.34) leads to the following **transport equation** for the turbulence kinetic energy.

$$\frac{\partial k}{\partial t} + U_j \frac{\partial k}{\partial x_j} = \tau_{ij}\frac{\partial U_i}{\partial x_j} - \epsilon + \frac{\partial}{\partial x_j}\left[\nu\frac{\partial k}{\partial x_j} - \frac{1}{2}\overline{u_i' u_i' u_j'} - \frac{1}{\rho}\overline{p' u_j'}\right] \tag{4.4}$$

The quantity ϵ is the **dissipation per unit mass** and is defined by the following correlation.

$$\epsilon = \nu\overline{\frac{\partial u_i'}{\partial x_k}\frac{\partial u_i'}{\partial x_k}} \tag{4.5}$$

The various terms appearing in Equation (4.4) represent physical processes occurring as the turbulence moves about in a given flow. The sum of the two

terms on the left-hand side, i.e., the **unsteady term** and the **convection**, is the familiar substantial derivative of k that gives the rate of change of k following a fluid particle. The first term on the right-hand side is known as **Production**, and represents the rate at which kinetic energy is transferred from the mean flow to the turbulence. Rewritten as $\tau_{ij}S_{ij}$ (because τ_{ij} is symmetric), this term is seen to be the rate at which work is done by the mean strain rate against the turbulent stresses. **Dissipation** is the rate at which turbulence kinetic energy is converted into thermal internal energy, equal to the mean rate at which work is done by the fluctuating part of the strain rate against the fluctuating viscous stresses. The term involving $\nu\partial k/\partial x_j$ is called **Molecular Diffusion**, and represents the diffusion of turbulence energy caused by the fluid's natural molecular transport process. We refer to the triple velocity correlation term as **Turbulent Transport**, and regard it as the rate at which turbulence energy is transported through the fluid by turbulent fluctuations. The last term on the right-hand side of the equation is called **Pressure Diffusion**, another form of turbulent transport resulting from correlation of pressure and velocity fluctuations.

The quantity ϵ as defined in Equation (4.5) differs from the classical definition of dissipation given in the preceding paragraph. From the latter, it follows that [cf. Townsend (1976) or Hinze (1975)] the true dissipation, ϵ_{true}, is proportional to the square of the fluctuating strain-rate tensor, s'_{ik}, viz.,

$$\epsilon_{true} = 2\nu\overline{s'_{ik}s'_{ik}}, \qquad s'_{ik} = \frac{1}{2}\left(\frac{\partial u'_i}{\partial x_k} + \frac{\partial u'_k}{\partial x_i}\right) \tag{4.6}$$

Hence, the quantity ϵ is given by (for incompressible flow):

$$\epsilon = \epsilon_{true} - \frac{\partial}{\partial x_k}\left(\overline{\nu u'_i \frac{\partial u'_k}{\partial x_i}}\right) \tag{4.7}$$

In practice, the difference between ϵ and ϵ_{true} is small and should be expected to be significant only in regions of strong gradients, e.g., shock waves or the viscous wall region. In the latter case, Bradshaw and Perot (1993) have shown that the maximum difference is just 2%, and can thus be ignored.

The unsteady term, convection and molecular diffusion are exact while production, dissipation, turbulent transport and pressure diffusion involve unknown correlations. To **close** this equation, we must specify τ_{ij}, dissipation, turbulent transport and pressure diffusion.

The conventional approach to closure of the k equation was initiated by Prandtl (1945) who established arguments for each term in the equation. This term-by-term modeling approach amounts to performing **drastic surgery** on the exact equation, replacing unknown correlations with closure approximations. This process is by no means rigorous. The closure approximations are no better than the turbulence data upon which they are based. Our hope is that we can find

closure approximations that make accurate solutions possible. We will discuss this point in greater detail when we introduce two-equation models.

Reynolds-Stress Tensor: For the class of turbulence models considered in this chapter, we assume the Boussinesq approximation is valid. Thus, we say that the specific Reynolds-stress tensor is given by

$$\tau_{ij} = 2\nu_T S_{ij} - \frac{2}{3}k\delta_{ij} \tag{4.8}$$

where S_{ij} is the mean strain-rate tensor. Note that the second term on the right-hand side of Equation (4.8) is needed to obtain the proper trace of τ_{ij}. That is, since $S_{ii} = 0$ for incompressible flow, contracting Equation (4.8) yields $\tau_{ii} = -2k$ in accord with Equation (4.3).

Strictly, we should regard Equation (4.8) as the definition of ν_T. In this spirit, no approximation is implied, provided we don't explicitly say ν_T is a scalar. However, for the purposes of this chapter, we do in fact assume ν_T is a scalar so that the term "approximation" is appropriate.

Turbulent Transport and Pressure Diffusion: The standard approximation made to represent turbulent transport of scalar quantities in a turbulent flow is that of gradient-diffusion. In analogy to molecular transport processes, we say that $-\overline{u_j'\phi'} \sim \nu_T \partial\Phi/\partial x_j$. Unfortunately, there is no corresponding straightforward analog for the pressure-diffusion term. In the absence of definitive experimental data, the pressure-diffusion term has generally been grouped with the turbulent-transport term, and the sum assumed to behave as a gradient-transport process. Fortunately, DNS results [e.g., Mansour, Kim and Moin (1988)] indicate that the term is quite small for simple flows. Thus, we assume that

$$\frac{1}{2}\overline{u_i'u_i'u_j'} + \frac{1}{\rho}\overline{p'u_j'} = -\frac{\nu_T}{\sigma_k}\frac{\partial k}{\partial x_j} \tag{4.9}$$

where σ_k is a closure coefficient. Assuming the vectors on the left- and right-hand sides of Equation (4.9) are parallel (a somewhat optimistic assumption!), this equation defines σ_k. As stressed by Bradshaw (1994), this statement applies to all turbulence closure coefficients. At this point, no approximation has entered although, of course, we hope the model is realistic enough that σ_k can be chosen to be constant.

Dissipation: The manner in which we determine the dissipation is not unique amongst turbulence energy equation models. It suffices at this point to note that we still have two unknown parameters, which are the turbulence length scale, ℓ, and the dissipation, ϵ. If both properties are assumed to be strictly functions of the turbulence independent of natural fluid properties such as molecular viscosity,

purely dimensional arguments [Taylor (1935)] show that

$$\epsilon \sim k^{3/2}/\ell \tag{4.10}$$

Hence, we still need a prescription for the length scale of the turbulence in order to close our system of equations. In the following sections, we will explore the various methods that have been devised to determine the length scale.

Combining Equations (4.4) and (4.9), we can write the modeled version of the turbulence kinetic energy equation that is used in virtually all turbulence energy equation models. The equation assumes the following form,

$$\frac{\partial k}{\partial t} + U_j \frac{\partial k}{\partial x_j} = \tau_{ij} \frac{\partial U_i}{\partial x_j} - \epsilon + \frac{\partial}{\partial x_j}\left[(\nu + \nu_T/\sigma_k)\frac{\partial k}{\partial x_j}\right] \tag{4.11}$$

where τ_{ij} is given by Equation (4.8).

4.2 One-Equation Models

To complete the closure of the turbulence kinetic energy equation, Prandtl (1945) postulated that the dissipation assumes the form quoted in Equation (4.10). Introducing a closure coefficient that we will call C_D, the dissipation is

$$\epsilon = C_D k^{3/2}/\ell \tag{4.12}$$

and the turbulence length scale remains the only unspecified part of the model. Given twenty years of experience with the mixing-length model, Prandtl had sufficient confidence that he could generalize established prescriptions for the turbulence length scale ℓ. [Of course, $\ell \propto \ell_{mix}$ only if the ratio of production to dissipation is constant. To see this, note that in a thin shear layer, Equation (3.18) gives $\partial U/\partial y = (-\overline{u'v'})^{1/2}/\ell_{mix}$. Hence, balancing production and dissipation means $-\overline{u'v'}\partial U/\partial y = (-\overline{u'v'})^{3/2}/\ell_{mix} = C_D k^{3/2}/\ell$ so that $\ell \propto \ell_{mix}$ if $-\overline{u'v'}/k =$ constant.] As we will discuss further below, measurements show that the constant is about 0.3 for many thin shear layers. Thus, Prandtl's **One-Equation Model** is as follows:

$$\frac{\partial k}{\partial t} + U_j \frac{\partial k}{\partial x_j} = \tau_{ij} \frac{\partial U_i}{\partial x_j} - C_D \frac{k^{3/2}}{\ell} + \frac{\partial}{\partial x_j}\left[(\nu + \nu_T/\sigma_k)\frac{\partial k}{\partial x_j}\right] \tag{4.13}$$

where τ_{ij} is given by Equation (4.8) and the kinematic eddy viscosity is

$$\nu_T = k^{1/2}\ell = C_D k^2/\epsilon \tag{4.14}$$

Note that at this point we make an implicit assumption regarding the "constant" in Equation (4.2), which has been set equal to one in Equation (4.14).

That is, there is no a priori reason why ν_T should depend only upon k and ℓ, i.e., no reason why "constant" should really be constant. In reality, ν_T is the ratio of a turbulence quantity (e.g., $-\overline{u'v'}$) to a mean flow quantity (e.g., $\partial U/\partial y+\partial V/\partial x$). Consequently, ν_T will not, in general, precisely follow mean-flow scales such as U_e and δ^* or turbulence scales such as k and ℓ. Only in **equilibrium flows** for which production and dissipation balance are mean-flow and turbulence scales proportional — and then either can be used for ν_T. Otherwise, an unknown mix of scales is needed.

Emmons (1954) independently proposed essentially the same model. Before the model can be used in applications, the length scale, ℓ, and the closure coefficients σ_k and C_D must be specified. Emmons (1954) and Glushko (1965) applied this model to several flows with some degree of success using Equation (4.14) with $\sigma_k = 1$ and C_D ranging between 0.07 and 0.09. Their length scale distributions were similar to those used for the mixing-length model. Wolfshtein (1967) found that by introducing damping factors in the dissipation and eddy viscosity similar to the Van Driest factor [Equation (3.105)], more satisfactory results can be obtained with this model for low-Reynolds-number flows. More recently, Goldberg (1991) has refined the model even further.

Although it is clearly more complex than an algebraic model, the Prandtl-Emmons-Glushko one-equation model is certainly straightforward and elegant. As originally postulated it involves two closure coefficients and one closure function (the length scale). Even with Wolfshtein's low-Reynolds-number corrections, the number of closure coefficients increases by only two so that the model actually has fewer closure coefficients than the Baldwin-Lomax and Johnson-King models. For attached flows, the Goldberg model has five closure coefficients, two damping functions, and a closure function for the length scale. Goldberg's number of closure coefficients and empirical functions more than doubles for separated flows.

Bradshaw, Ferriss and Atwell (1967) formulated a one-equation model that avoids introducing a gradient-diffusion approximation. Rather than introduce the Boussinesq approximation, they argue that for a wide range of flows, the ratio of the Reynolds shear stress, τ_{xy}, to the turbulence kinetic energy, k, is constant. Measurements [Townsend (1976)] indicate that for boundary layers, wakes and mixing layers the ratio is nearly the same and given by

$$\tau_{xy} \approx \beta_r k, \qquad \beta_r = 0.3 \tag{4.15}$$

The stress/energy ratio, i.e., the constant β_r, is often referred to as **Bradshaw's constant**, and sometimes as **Townsend's constant**.[1] Building upon this presumably universal result, Bradshaw, Ferriss and Atwell formulated a one-equation model based on the turbulence kinetic energy. A novel feature of their formulation is that the equations are hyperbolic for boundary layers rather than parabolic.

[1] The notation $\tau_{xy} = 2a_1 k$ is sometimes used where $a_1 \approx 0.15$.

This is a direct consequence of modeling the k equation's turbulent transport term by a "bulk-convection" process rather than a gradient-diffusion approximation as in Equation (4.11). The resulting equations are thus solved by using the method of characteristics.

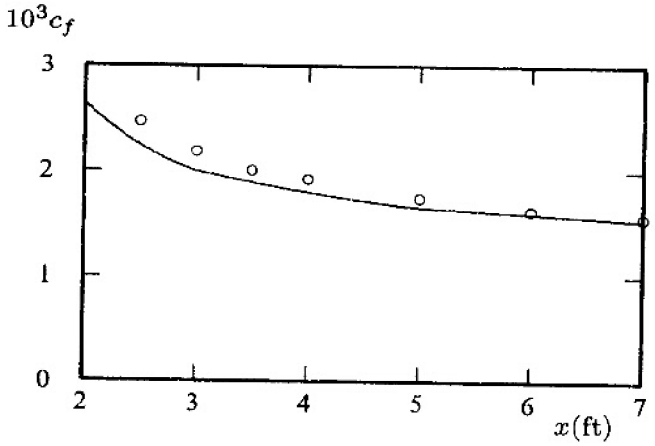

Figure 4.1: *Comparison of computed and measured skin friction for Bradshaw Flow C;* —— *Bradshaw-Ferriss-Atwell model;* ○ *Bradshaw.*

Figure 4.1 compares computed and measured skin friction for Flow 3300 of the 1968 AFOSR-IFP-Stanford Conference on the Computation of Turbulent Boundary Layers. As shown, the differences between theory and experiment are even less than those obtained using the Cebeci-Smith and Baldwin-Lomax models [see Figure 3.17]. Overall, the Bradshaw-Ferriss-Atwell model's skin friction for boundary layers in adverse pressure gradient was closest of the various models tested in the 1968 Conference to measured values.

One-equation models have been formulated that are based on something other than the turbulence energy equation. Nee and Kovasznay (1968), for example, postulated a phenomenological transport equation for the kinematic eddy viscosity, ν_T. The equation involves terms similar to those appearing in Equation (4.13). The model has four closure coefficients and requires prescription of the turbulence length scale. Sekundov (1971) developed a similar model that has generated considerable interest in the Russian research community, but that has rarely been referenced in Western journals. The English-language report of Gulyaev et al. (1993) summarizes work on the Sekundov model in its 1992 version. The paper by Vasiliev et al. (1997) shows that the 1971 version, although very simple, is complete and quite capable.

Baldwin and Barth (1990), Spalart and Allmaras (1992) and Menter (1994) have devised even more elaborate model equations for the eddy viscosity. The Baldwin-Barth model, for example, includes seven closure coefficients and three empirical damping functions. The Baldwin-Barth model is as follows.

Kinematic Eddy Viscosity:

$$\nu_T = C_\mu \nu \tilde{R}_T D_1 D_2 \tag{4.16}$$

Turbulence Reynolds Number:

$$\frac{\partial}{\partial t}\left(\nu\tilde{R}_T\right) + U_j \frac{\partial}{\partial x_j}\left(\nu\tilde{R}_T\right) = (C_{\epsilon 2} f_2 - C_{\epsilon 1})\sqrt{\nu\tilde{R}_T P} + (\nu + \nu_T/\sigma_\epsilon)\frac{\partial^2(\nu\tilde{R}_T)}{\partial x_k \partial x_k} - \frac{1}{\sigma_\epsilon}\frac{\partial \nu_T}{\partial x_k}\frac{\partial(\nu\tilde{R}_T)}{\partial x_k} \tag{4.17}$$

Closure Coefficients and Auxiliary Relations:

$$C_{\epsilon 1} = 1.2, \quad C_{\epsilon 2} = 2.0, \quad C_\mu = 0.09, \quad A_o^+ = 26, \quad A_2^+ = 10 \tag{4.18}$$

$$\frac{1}{\sigma_\epsilon} = (C_{\epsilon 2} - C_{\epsilon 1})\frac{\sqrt{C_\mu}}{\kappa^2}, \qquad \kappa = 0.41 \tag{4.19}$$

$$P = \nu_T \left[\left(\frac{\partial U_i}{\partial x_j} + \frac{\partial U_j}{\partial x_i}\right)\frac{\partial U_i}{\partial x_j} - \frac{2}{3}\frac{\partial U_k}{\partial x_k}\frac{\partial U_k}{\partial x_k}\right] \tag{4.20}$$

$$D_1 = 1 - e^{-y^+/A_o^+} \quad \text{and} \quad D_2 = 1 - e^{-y^+/A_2^+} \tag{4.21}$$

$$f_2 = \frac{C_{\epsilon 1}}{C_{\epsilon 2}} + \left(1 - \frac{C_{\epsilon 1}}{C_{\epsilon 2}}\right)\left(\frac{1}{\kappa y^+} + D_1 D_2\right) \cdot \left[\sqrt{D_1 D_2} + \frac{y^+}{\sqrt{D_1 D_2}}\left(\frac{D_2}{A_o^+}e^{-y^+/A_o^+} + \frac{D_1}{A_2^+}e^{-y^+/A_2^+}\right)\right] \tag{4.22}$$

The Baldwin-Barth model is **complete** as it involves no adjustable functions or coefficients. While this guarantees nothing regarding its suitability for a given application, it does make its implementation convenient. This type of model constitutes the simplest complete model of turbulence.

Note that the Baldwin-Barth model circumvents the need to specify a dissipation length such as the quantity ℓ in Equation (4.13) by expressing the decay, or dissipation, of the eddy viscosity in terms of spatial gradients. That is, the dissipation term in Equation (4.17), ϵ_ν, is

$$\epsilon_\nu = \frac{1}{\sigma_\epsilon}\frac{\partial \nu_T}{\partial x_k}\frac{\partial(\nu\tilde{R}_T)}{\partial x_k} \tag{4.23}$$

As a consequence of this closure approximation, $\epsilon_\nu = 0$ when spatial gradients vanish. Thus, rather than decaying with streamwise distance, the eddy viscosity will remain constant in a uniform stream. This incorrect feature can produce non-physical diffusion in a numerical computation, for example, of a multi-element airfoil.

The Spalart-Allmaras model is also written in terms of the eddy viscosity. The model includes eight closure coefficients and three closure functions. Its defining equations are as follows.

Kinematic Eddy Viscosity:

$$\nu_T = \tilde{\nu} f_{v1} \tag{4.24}$$

Eddy Viscosity Equation:

$$\frac{\partial \tilde{\nu}}{\partial t} + U_j \frac{\partial \tilde{\nu}}{\partial x_j} = c_{b1} \tilde{S} \tilde{\nu} - c_{w1} f_w \left(\frac{\tilde{\nu}}{d} \right)^2 + \frac{1}{\sigma} \frac{\partial}{\partial x_k} \left[(\nu + \tilde{\nu}) \frac{\partial \tilde{\nu}}{\partial x_k} \right] + \frac{c_{b2}}{\sigma} \frac{\partial \tilde{\nu}}{\partial x_k} \frac{\partial \tilde{\nu}}{\partial x_k} \tag{4.25}$$

Closure Coefficients and Auxiliary Relations:

$$c_{b1} = 0.1355, \quad c_{b2} = 0.622, \quad c_{v1} = 7.1, \quad \sigma = 2/3 \tag{4.26}$$

$$c_{w1} = \frac{c_{b1}}{\kappa^2} + \frac{(1 + c_{b2})}{\sigma}, \quad c_{w2} = 0.3, \quad c_{w3} = 2, \quad \kappa = 0.41 \tag{4.27}$$

$$f_{v1} = \frac{\chi^3}{\chi^3 + c_{v1}^3}, \qquad f_{v2} = 1 - \frac{\chi}{1 + \chi f_{v1}}, \qquad f_w = g \left[\frac{1 + c_{w3}^6}{g^6 + c_{w3}^6} \right]^{1/6} \tag{4.28}$$

$$\chi = \frac{\tilde{\nu}}{\nu}, \qquad g = r + c_{w2}(r^6 - r), \qquad r = \frac{\tilde{\nu}}{\tilde{S} \kappa^2 d^2} \tag{4.29}$$

$$\tilde{S} = S + \frac{\tilde{\nu}}{\kappa^2 d^2} f_{v2}, \qquad S = \sqrt{2 \Omega_{ij} \Omega_{ij}} \tag{4.30}$$

The tensor $\Omega_{ij} = \frac{1}{2}(\partial U_i / \partial x_j - \partial U_j / \partial x_i)$ is the rotation tensor and d is distance from the closest surface. Although not listed here, the model even includes a transition correction that introduces four additional closure coefficients and two more empirical functions. Finally, note that the source terms for the eddy viscosity equation depend upon the distance from the closest surface, d, as well as upon the gradient of $\tilde{\nu}$. Since $d \to \infty$ far from solid boundaries, this model also predicts no decay of the eddy viscosity in a uniform stream.

To determine how close one-equation model predictions are to measurements, we turn first to the five free shear flow applications considered in Section 3.3. Since the Baldwin-Barth and Spalart-Allmaras models are complete, the turbulence scales are automatically defined, i.e., neither model involves an adjustable closure coefficient such as α in Equation (3.34). Comparing computed and measured **spreading rate** provides a straightforward, and concise, gauge of how well the models reproduce measured flow properties.

The conventional definition of **spreading rate for the wake** is the value of the similarity variable, $\eta = y\sqrt{\rho U_\infty^2/(Dx)}$ (see Subsection 3.3.1), where the velocity defect is half its maximum value. Similarly **for the plane jet, round jet and radial jet, the spreading rate** is the value of y/x where the velocity is half its centerline value. **For the mixing layer, the spreading rate** is usually defined as the difference between the values of y/x where $(U-U_2)^2/(U_1-U_2)^2$ is 9/10 and 1/10.

Table 4.1: *Free Shear Flow Spreading Rates for One-Equation Models.*

Flow	Baldwin-Barth	Spalart-Allmaras	Measured
Far Wake	0.315	0.341	0.320-0.400
Mixing Layer	–	0.109	0.103-0.120
Plane Jet	–	0.157	0.100-0.110
Round Jet	–	0.248	0.086-0.096
Radial Jet	–	0.166	0.096-0.110

Table 4.1 compares computed and measured spreading rates for the Baldwin-Barth and Spalart-Allmaras models. The numerical results for the Spalart-Allmaras model have been obtained using Programs **WAKE**, **JET** and **MIXER** (see Appendix C). The table includes only the far-wake spreading rate inferred from the computations of Baldwin and Barth (1990) for the Baldwin-Barth model. Figures 4.2 and 4.3 compare computed and measured velocity profiles for the far wake and the mixing layer.

Attempts at incorporating the Baldwin-Barth model in **WAKE**, **JET** and **MIXER** have proven unsuccessful because the tridiagonal matrix corresponding to the discretized form of the equation for $\nu\tilde{R}_T$ is ill conditioned. Contrary to the comments of Baldwin and Barth (1990), who warn of possible numerical difficulties, the problem does not stem from poor grid resolution. Rather, the model predicts a sharp discontinuity in the eddy viscosity just inside the edge of the shear layer that destabilizes the computation, independent of grid size.

The Baldwin-Barth model predicts a far-wake spreading rate 2% below the lower bound of measured values, while the Spalart-Allmaras model's spreading rate is within the range of measurements. The Spalart-Allmaras model's mixing-layer spreading rate is also within the range the measured values. However, its predicted plane-jet and radial-jet spreading rates are more than 40% higher than measured, while the round-jet value is nearly triple the corresponding experimental value. These results are entirely consistent with the fact that these models have been optimized for aerodynamic applications, most notably for flow past a wing. The mixing layer and far wake are salient in this context, while jets are not. These applications do show one of the limitations of the Spalart-Allmaras model, i.e., it is unsuitable for applications involving jet-like free shear regions.

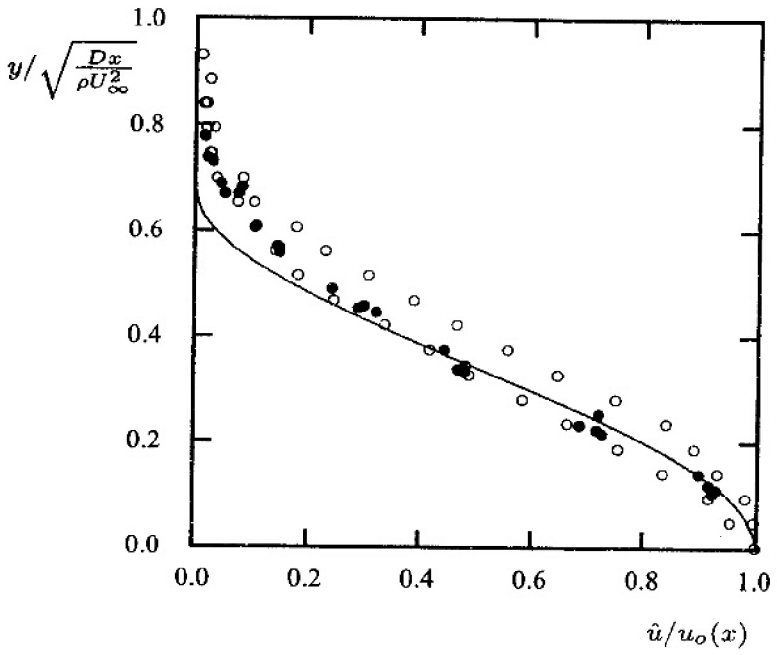

Figure 4.2: *Comparison of computed and measured far-wake velocity profiles:* —— *Spalart-Allmaras model;* • *Fage and Falkner (1932);* ○ *Weygandt and Mehta (1995).*

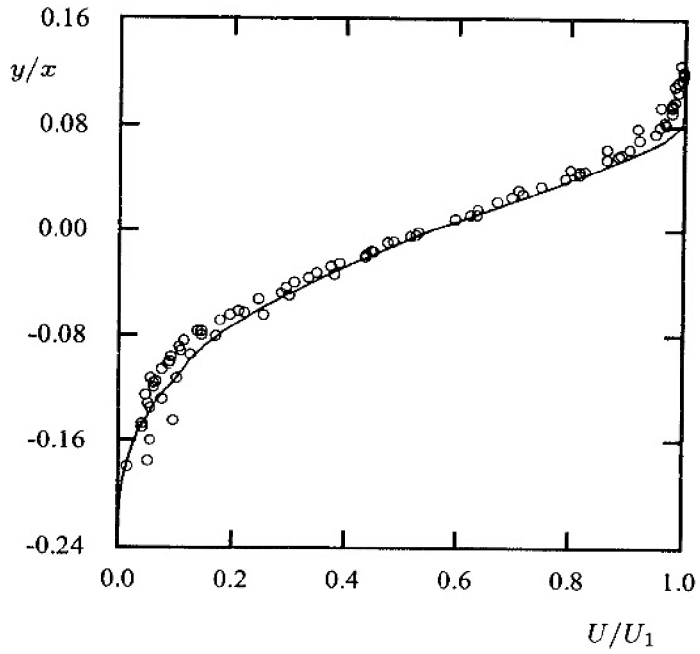

Figure 4.3: *Comparison of computed and measured velocity profiles for a mixing layer:* —— *Spalart-Allmaras model;* ○ *Liepmann and Laufer (1947).*

Figure 4.4 compares computed and measured skin friction for the sixteen boundary layers with pressure gradient used to assess algebraic models in Chapter 3. All computations have been done with Program **EDDYBL** (see Appendix C). Table 4.2 summarizes overall differences between computed and measured c_f for the Baldwin-Barth and Spalart-Allmaras models. The overall average difference at the final station for the flows is 24% for the Baldwin-Barth model and 14% for the Spalart-Allmaras model.

Table 4.2: *Differences Between Computed and Measured Skin Friction.*

Pressure Gradient	Flows	Baldwin-Barth	Spalart-Allmaras
Favorable	1400, 1300, 2700, 6300	2%	1%
Mild Adverse	1100, 2100, 2500, 4800	19%	10%
Moderate Adverse	2400, 2600, 3300, 4500	32%	10%
Strong Adverse	0141, 1200, 4400, 5300	44%	33%
All	--	24%	14%

The Baldwin-Barth model's predicted skin friction is consistently smaller than measured for boundary layers with adverse pressure gradient. As an example, for the Samuel-Joubert increasingly adverse pressure gradient case (Flow 0141), the computed skin friction is 47% lower than the measured value. Although all twelve adverse-pressure-gradient flows are attached, the Baldwin-Barth model predicts separation for three cases, viz., Flows 4800 (mild adverse ∇p), 4500 (moderate adverse ∇p) and 5300 (strong adverse ∇p). This clearly illustrates the model's tendency to respond too strongly to adverse pressure gradient, relative to measurements, in the sense that it always predicts too large of a decrease in skin friction.

As shown by Sai and Lutfy (1995), the Baldwin-Barth model is extremely sensitive to the freestream value of the eddy viscosity. While using nonphysically large values for $\tilde{R}_T$ reduces differences between computed and measured c_f, no freestream values have been found that can prevent separation for Flows 4800, 4500 and 5300.

By contrast, aside from transients near the beginning of several of the computations, the Spalart-Allmaras c_f is as close to corresponding measured values as the Baldwin-Lomax algebraic model. For the Samuel-Joubert case, the computed skin friction is 5% higher than measured. The sole case with large differences between computed and measured flow properties is the "incipient-separation" case of Stratford (1959), i.e., Flow 5300. As shown in Figure 4.4, the predicted value of c_f at the end of the computation is 3.4 times the measured value. Recall that the Johnson-King 1/2-equation model (see Figure 3.19) exhibits similar behavior for this flow, while being much closer to measurements for the other fifteen cases.

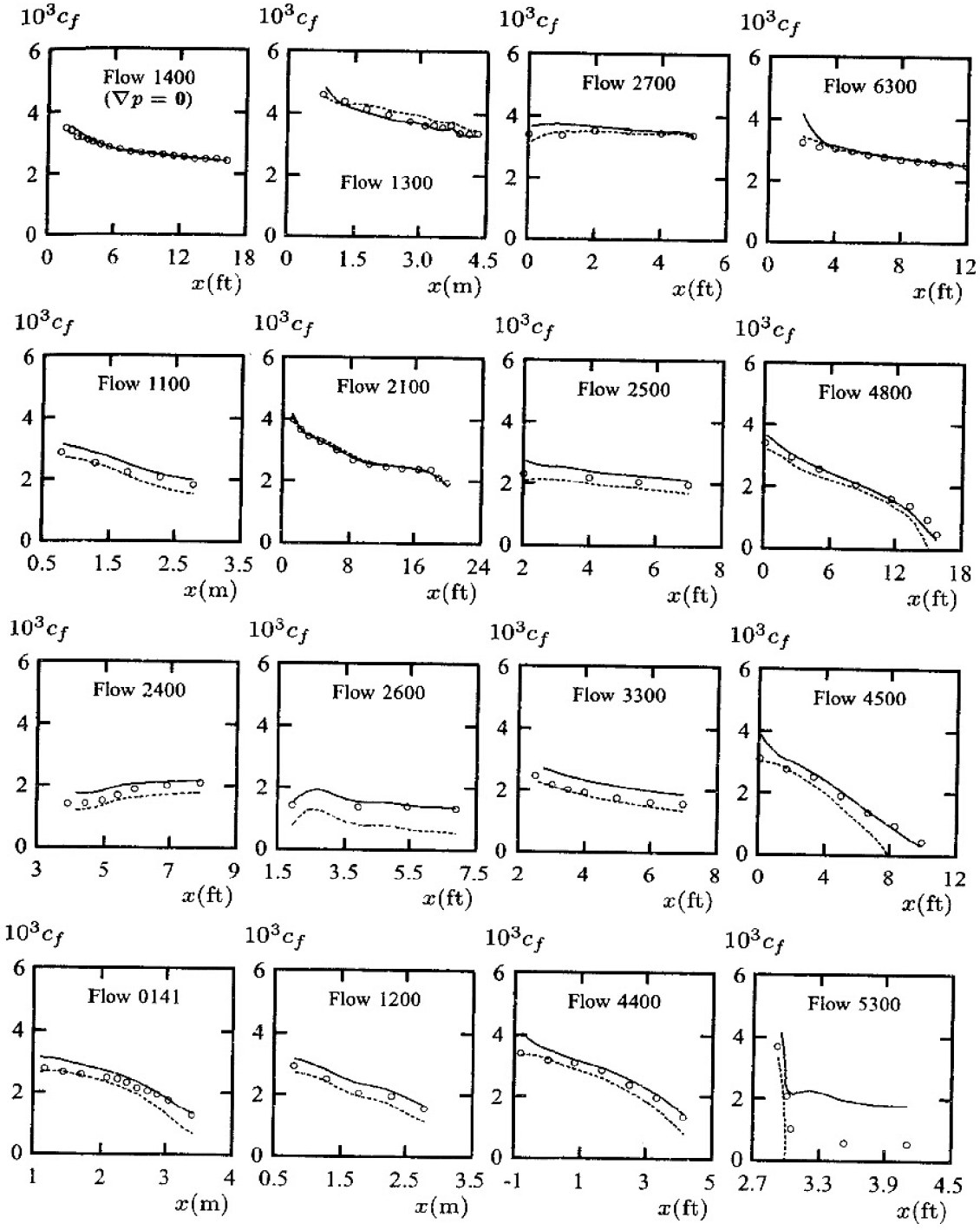

Figure 4.4: *Computed and measured skin friction for boundary layers subjected to a pressure gradient. Top row - favorable ∇p; next to top row - mild adverse ∇p; next to bottom row - moderate adverse ∇p; bottom row - strong adverse ∇p. —— Spalart-Allmaras model; - - - Baldwin-Barth model; ○ measured.*

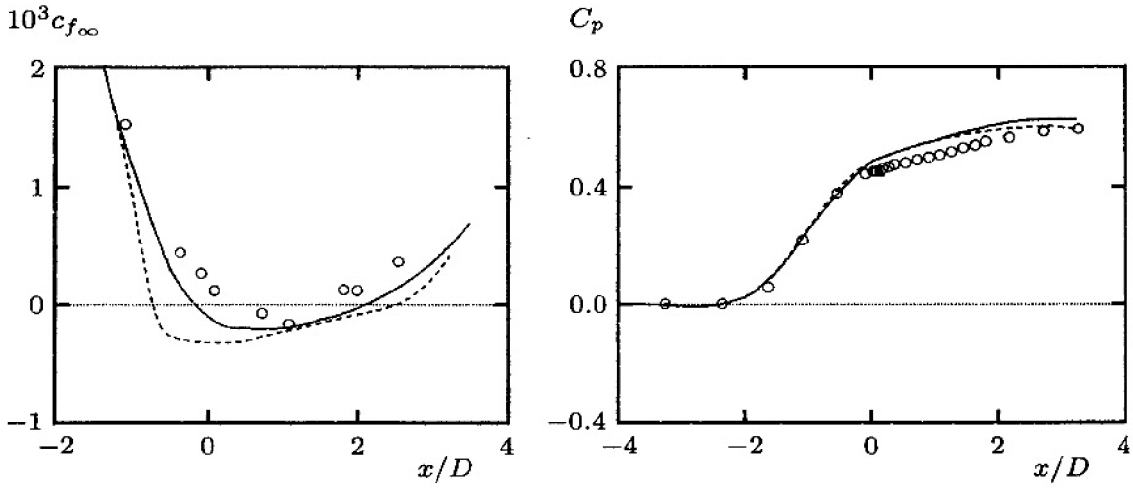

Figure 4.5: *Computed and measured flow properties for Driver's separated flow; —— Spalart-Allmaras model; - - - Baldwin-Barth model; ○ Driver.*

Figure 4.5 shows how the Spalart-Allmaras and Baldwin-Barth models fare for Driver's separated flow as demonstrated by Menter (1992b, 1994). The Spalart-Allmaras model predicts a separation bubble that is about 60% larger than measured. The Baldwin-Barth model skin friction deviates from measured values even more than the Baldwin-Lomax model (see Figure 3.18), with a predicted separation bubble region that is more than twice the size measured by Driver. The results for the Baldwin-Barth model are not surprising in light of how poorly the model fares for attached boundary layers in adverse ∇p.

The backward-facing step (Figure 4.6) is a popular test case for turbulence models because the geometry is simple. Additionally, separation occurs at the

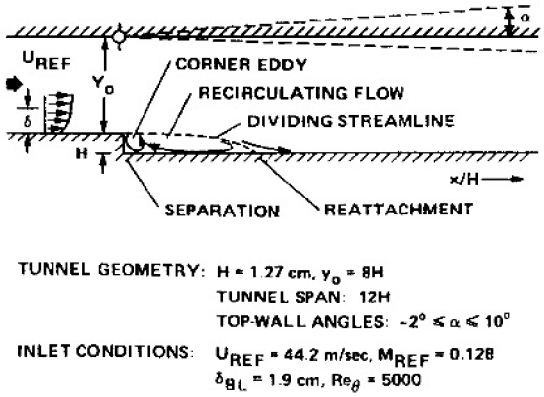

Figure 4.6: *Backward-facing step flow geometry and inlet conditions for the Driver-Seegmiller (1985) experiments. [From Driver and Seegmiller (1985) — Copyright © AIAA 1985 — Used with permission.]*

sharp corner so the flow is easier to predict than a flow for which the separation point is unknown a priori. Figure 4.7 compares computed and measured [Driver and Seegmiller (1985)] skin friction for backstep flow with the upper channel wall inclined to the lower wall at 0°. The Spalart-Allmaras model predicts reattachment at 6.1 step heights, H, downstream of the step. This is within 3% of the measured value of $6.26H$. Although not shown here, the model predicts reattachment at $8.6H$ when the upper wall is inclined at 6°, which is within 6% of the measured value of $8.1H$.

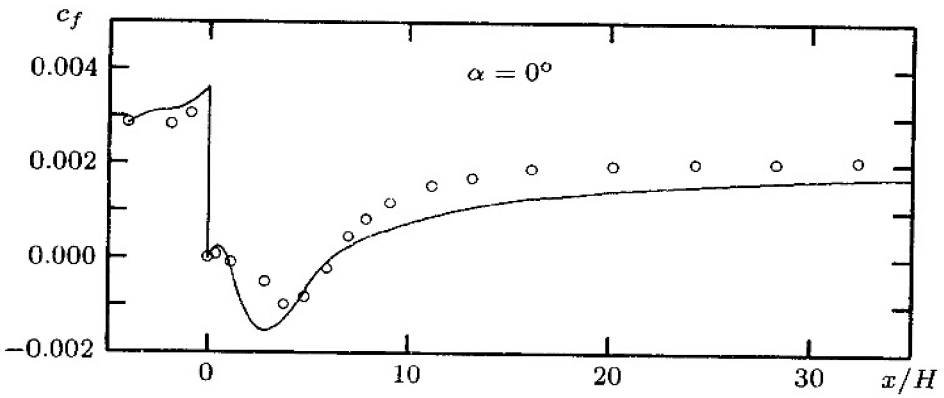

Figure 4.7: *Computed and measured skin friction for flow past a backward-facing step;* —— *Spalart-Allmaras model;* ○ *Driver-Seegmiller.*

Thus, on balance, Spalart-Allmaras predictions are satisfactory for many engineering applications. It is especially attractive for airfoil and wing applications, for which it has been calibrated. Its failure to accurately reproduce jet spreading rates is a cause for concern, and should serve as a warning that the model has some shortcomings. Nevertheless, the model appears to be a valuable engineering tool.

By contrast, the Baldwin-Barth model predicts much larger discrepancies between computed and measured c_f than the Spalart-Allmaras model and the much simpler algebraic models. The discrepancies are so large (an average of 24% for the 16 attached boundary-layer cases) that its use for boundary-layer flows is inadvisable. It is also extremely sensitive to the freestream value of the eddy viscosity and can be very difficult to cast in finite-difference form (e.g., by yielding ill-conditioned matrices). Given all of these flaws, the model should be abandoned in favor of the Spalart-Allmaras model.

In light of these facts, we have not yet arrived at a universal turbulence model. In general, one-equation models share a few of the failures as well as most of the successes of the mixing-length model. While there is a smaller need for adjustment from flow to flow than with the mixing-length model, the Spalart-Allmaras model, as good as it is, is unable to predict spreading rates

for plane, round and radial jets that are consistent with measurements. Also, while the model's predictions for attached boundary layers are usually as close to measurements as those of algebraic models, its skin friction for the Stratford incipient-separation case (Flow 5300) is several times higher than measured. Finally, while it provides close agreement with measured reattachment length for the backward-facing step and airfoils with small separation bubbles, its predicted separation bubble for the Driver flow is significantly larger than measured. This erratic pattern is a bit discomforting, and suggests that something better is needed for general turbulent-flow applications. To reach a more-nearly universal model, especially for separated flows, we must seek a model in which transport effects for the velocity and length scales are accounted for separately. The rest of this chapter is devoted to investigating such models.

4.3 Two-Equation Models

Two-Equation Models of turbulence have served as the foundation for much of the turbulence-model research during the past three decades. For example, almost all of the computations done for the 1980-81 AFOSR-HTTM-Stanford Conference on Complex Turbulent Flows used two-equation turbulence models. These models provide not only for computation of k, but also for the turbulence length scale or equivalent. Consequently, two-equation models are **complete**, i.e., can be used to predict properties of a given turbulent flow with no prior knowledge of turbulence structure.

In the following discussion of two-equation models, arguments are often presented in terms of the k-ω model. This, in no way, constitutes a campaign to popularize the model. Rather, it usually reflects either the author's greater familiarity with the k-ω model (as one of its developers) or its analytical simplicity relative to other models. Except in cases where conclusions are obvious, every attempt has been made to leave the reader to make judgments regarding the superiority of any model described in this book.

The starting point for virtually all two-equation models is the Boussinesq approximation, Equation (4.8), and the turbulence kinetic energy equation in the form of Equation (4.11). As pointed out at the end of Section 4.1, there is an arbitrariness in the way we define the turbulence length scale, ℓ, to go with the velocity scale, $k^{1/2}$.

Kolmogorov (1942), for example, pointed out that a second transport equation is needed to compute the so-called **specific dissipation rate**, ω. This quantity has dimensions of (time)$^{-1}$. On dimensional grounds, the eddy viscosity, turbulence length scale and dissipation can be determined from

$$\nu_T \sim k/\omega, \qquad \ell \sim k^{1/2}/\omega, \qquad \epsilon \sim \omega k \tag{4.31}$$